MINERALS AND METASTASIS: HYDROXYAPATITE PROMOTES BREAST CANCER COLONIZATION OF BONE

A Dissertation
presented to the Faculty of the Graduate School
of Cornell University
in Partial Fulfillment of the Requirement for the Degree of
Doctor of Philosophy

by

Siddharth Preston Pathi

May 2013

Minerals and metastasis: hydroxyapatite promotes breast cancer colonization of bone

Siddharth Pathi, Ph.D.
Cornell University 2013

Bone metastasis commonly causes morbidity and mortality in patients with advanced breast cancer. Despite, better prognoses for breast cancer patients in general, the outlook for those with bone metastasis remains grim, with less than one quarter of those afflicted surviving past five years. Fundamental insights into how microenvironmental cues drive bone metastasis may help to fight the disease. Hydroxyapatite (HA) is a calcium-phosphate mineral that is found both in the bone, to which breast cancer spreads during metastasis, and in the breast tissue of many cancer patients in the form of microcalcifications. Despite the consistent presence of this bioactive mineral in the breast tumor microenvironment, little evidence currently exists to implicate it in cancer pathogenesis. Using a tissue engineering-inspired scaffold that incorporates HA in conjunction with hydrothermal techniques to synthesize well-defined mineral, tumor cell-HA interactions were investigated. Soluble factors from these scaffold cultures were collected, analyzed, and used on other cells to study cell-cell interactions pertinent to bone metastasis. Xenograft models were used to understand how exposure to mineral might affect metastasis *in vivo,* and human patient samples were analyzed to validate findings with our scaffold models. The results suggest that the presence of hydroxyapatite promotes tumor cell growth and adhesion, as well as production of factors such as interleukin-8 (IL-8) that drive bone degradation, a cause of bone pain and pathological fracture in metastasis. Furthermore, tumor cell interactions with hydroxyapatite change gene expression patterns and promote the activation of a migratory axis by enriching levels of stromal-derived factor-1 (SDF-1), possibly dictating the propensity of breast cancer to metastasize to bone. Exposure to mineral promoted bone colonization by tumor cells in mice, and preliminary results indicate that IL-8and the receptor for SDF-1 are elevated in human patients with microcalcifications. The data also suggest that

material properties of HA affect cell behavior, as larger, more crystalline particles stimulate the most IL-8 production, while smaller, less crystalline particles promote adhesion and growth. Integrin interactions are potentially involved in controlling cell-HA interactions, as it was found that blocking integrin binding to HA-adsorbed proteins such as osteopontin and fibronectin attenuated many of the observed behaviors stimulated by HA. Hydrothermal synthesis of HA and mineral-containing scaffolds emerged as excellent tools to study breast cancer biology, revealing that microenvironmental HA may play an important role in driving bone metastasis.

BIOGRAPHICAL SKETCH

Siddharth Pathi was born in Calcutta, India on November 29, 1985. He soon came to the United States, growing up in Ohio and graduating from Tiffin Columbian High School in 2003. Following that, he spent 4 years at Rensselaer Polytechnic Institute majoring in Materials Science and Engineering, graduating Summa cum Laude and receiving the Matthew A. Hunter award as the top student in his field. Siddharth performed research in electronic materials and thin film deposition while at Rensselaer, earning regional and university awards for excellent undergraduate work. In August of 2007, Siddharth enrolled at Cornell University in the Department of Biomedical Engineering as a doctoral student. He elected to work with Dr. Claudia Fischbach to use biomaterials to develop cancer models that could provide fundamental insight into breast cancer metastasis to bone. In his first year at Cornell, Siddharth was awarded the prestigious GAANN (graduate assistance in areas of national need) fellowship based on his previous academic achievements and his potential to impact biomedical science and technology. In 2008, Siddharth additionally succeeded in attaining a National Science Foundation graduate research fellowship based on his first year of research work. He attended and presented at conferences each year during his doctoral work, published a review article, published a book chapter, and was primary author on two manuscripts. Siddharth also mentored many undergraduates and master's students during his doctoral research. Beyond research, Siddharth was very dedicated to teaching responsibilities. He taught three semesters at Cornell, always receiving excellent student reviews, and he was recognized as the department's teaching assistant of the year in 2009. Siddharth's future plans are focused on cancer research, and he is devoted to building a career that will greatly impact human healthcare.

I lovingly dedicate this to my mother and father, who made me realize that anything less than true greatness was selling myself short

ACKNOWLEDGMENTS

This work was made possible by funding from the Nanobiotechnology Center at Cornell (Agreement No. ECS-9876771), the Cornell Center for Materials Research (cooperative agreement DMR 0520404), the National Institute of Health (Grant AR046121), and the National Science Foundation (Graduate Research Fellowship).

This dissertation represents the culmination a five-plus long, but rewarding, years of my work. In these long years, there has been a substantial list of people in my life who helped make this work possible. I must first thank my committee, who provided invaluable insights that helped me refine my research. Primary among my committee of course, I must express my gratitude to my advisor, Dr. Claudia Fischbach, who provided the means for my research. As a mentor, she allowed me freedom as a researcher, and helped me to realize my potential. She taught me the ins-and-outs of research while allowing me to drive the project definition, and for this I am incredibly grateful. Dr. Lara Estroff, was an excellent collaborator and truly like a second mentor. Intellectually, Lara really helped shape the way that I attack problems and go about experiments. She was always available to me, and she provided a significant amount of technical expertise that was used in my research. I would also like to thank Dr. Alex Nikitin, who as a committee member pushed me to look hard and consider the physiological relevance of my work. While he provided me the most challenges during my candidacy exam and defense, his input forced me to think very critically and greatly benefitted my project. His takes forced me to consider factors that most engineers would not, and they helped me to develop as a better-rounded scientist.

Biomedical engineering is an interdisciplinary field, so appropriately my dissertation is the result of numerous collaborations. It was a great opportunity to work with Dr. John Healey

from Memorial-Sloan Kettering Cancer Center in 2008. Spending time in his lab, I learned so much about how oncologists and medical professionals view cancer, and that outlook has enabled me to approach research in a larger context. Drs. Cliff Hudis and Patrick Morris were also excellent contributors who provided expertise, thoughtful conversations, and valuable human samples for my work. Perhaps my most successful collaboration was with Dr. Debra Lin, who provided synthetic mineral for my studies. Debra and I worked as true partners, and I am thankful that I had the opportunity to put together a publication with her.

Of course, I must also acknowledge those that worked alongside me in the Fischbach Lab and directly helped my project. Christine Kowalczewski spent countless hours working with me to help get out my first publication. Her time in front of the microscope now stands as a major part of my career! Chris Patuwo was another dedicated student who devoted a lot of time to the progress of this project. There were no hours too long or too late for Chris, and I am thankful that I had the chance to work with him and become his friend. Angela Du was the most recent student that I had a chance to work with. She spent a lot of time perfecting her skills with working with frozen human tissue, and without her work, an entire chapter of this thesis would not exist. But, above all, in my final two semesters at Cornell, Angela was fun to work with. No matter the stress level or the pressure from deadlines, when Angela and I worked in the lab we laughed and had a good time. This was a huge help for me as I wrapped up my thesis work.

Balance was an important component of my life during my thesis work. My friends - Cameron Bardliving, Spencer Park, Russ Gould, Nathan Cornelius, and Andrew Hughes – made this possible. For nights of fun, I hardly think I could find a better set of guys. There is no way I can quantify how important hanging out with all of them was to keeping my sanity through the most difficult stretches. Thanks guys.

Finally, I have to acknowledge my family. My inspiration to do PhD work was my father. He taught me the importance of intelligence and the constant hunger for knowledge. He made me understand how vital maximizing my potential was. And he ultimately played the most pivotal role in shaping the man I am today. Thank you, dad, for giving me the foundation that enabled me to do this work. My mother has always been my confidante. I cannot imagine a more nurturing person. There is literally nothing that she would not do for me, and knowing that allows me to always feel safe. She taught me everything I know about being caring and showing empathy for other people. Thank you, mom, for inspiring me to enter a field that could directly improve people's lives. My girlfriend Tricia is the most adaptable person I know. She has reshaped her life around me and around the stress of my thesis work. She has experienced the bitterness and the sweetness of time at Cornell as if it were her own. Thank you, Tricia, for being on my team.

To everyone on this list – you have played a massive role in the design, development, or execution of this dissertation. Thank you so much.

TABLE OF CONTENTS

TABLE OF FIGURES

CHAPTER 1: INTRODUCTION

1.1 Breast Cancer Metastasis to Bone

Of the nearly 40,000 estimated annual deaths that result from breast cancer, roughly 70% will be associated with patients afflicted with bone metastasis (1-3). Including facing severely decreased survival odds, patients with bone metastasis will suffer from further complications such as pathological incidence of fracture, nerve compression, severe bone pain, hypercalcaemia, and an overall decrease in quality of life (4). Metastasis involves cells from the initial tumor breaking free and disseminating to distant organs and tissues via lymphatic and blood vessels, and subsequently colonizing and forming secondary tumors (Fig. 1.1). It is considered a hallmark of malignancy, and in the case of breast cancer, it is known to occur with high frequency in the skeletal system (5). While previous research has revealed specific alterations in genetic expression patterns that are correlated with the predilection for breast cancer to metastasize to bone, the potentially instructive influence of the tumor microenvironment in this respect remains unclear.

Breast cancer generally affects the lining of ducts or lobules in the mammary tree. The disease itself is heterogeneous, and it is diagnosed based on a formalized semiquantitative staging system used by oncologists and approved by the American Joint Committee on Cancer. Masses in breast tissue range from totally benign (stage 0) to highly metastatic (stage IV) (6). Along this continuous spectrum, tumors may be roughly divided into two forms: invasive carcinomas that are infiltrating and malignant and ductal carcinomas in situ (DCIS) that may later become invasive. Invasive tumors that spread to lymph nodes and are highly vascularized are prone to metastasis. Around 30% of breast tumor diagnoses are invasive and associated with

metastatic disease (7). Researchers suspect that in the vast majority of these cases, skeletal metastases are present (1, 3, 8).

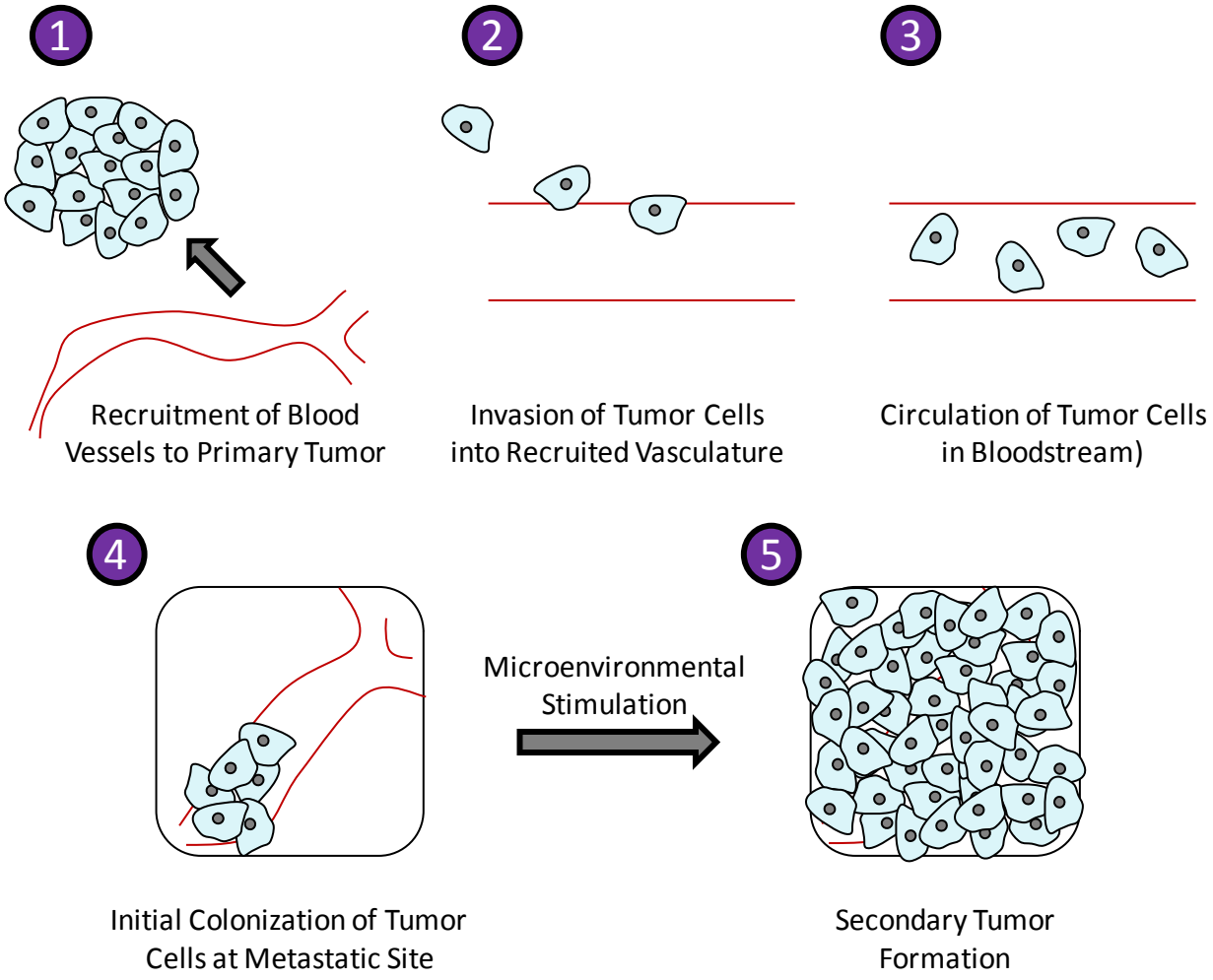

Figure 1.1: Tumor Metastasis
Tumor metastasis is a stepwise process. (1) Angiogenesis: Tumor cells first recruit blood vessel and generate tumor vasculature. (2) Intravasation: Following vascularization, cancer cells must adhere to and invade through the basement membrane of vessels. (3) Embolism: After penetrating vasculature, cells are dislodged from lumen walls and circulate through the blood. (4) Colonization: Once cells reach the site of metastasis, they are arrested in the capillary bed of the tissue. (5) Secondary Growth: In response to microenvironmental cues (soluble factors, cell-cell interactions, etc.), colonized cells proliferate and establish a secondary tumor.

While breast cancer remains the second leading cause of cancer related death among American women, significant improvements have been made through better diagnosis and treatment options in the past decade (9). In fact, 34% of the overall decline in female cancer deaths over the last 10 years are due to better available care options for breast cancer victims (2). Many of these have emerged due to advances in basic research. For instance, investigations into gene expression have shown the importance of estrogen receptor (ER), progesterone receptor (PR), and human epidermal growth factor receptor 2 (HER2) for many cancers (10, 11). These discoveries have led to the development and therapeutic use of receptor inhibitors such as trastuzumab (for HER2) and tamoxifen (for ER), which have been very effective in combating certain subtypes of breast cancer (12, 13). Diagnosis and increased breast cancer awareness are also viewed as having a positive effect, as monthly self breast exams and regular clinical breast exams aid in early detection, which greatly increases survival rates (7, 9).

Despite the positive developments in breast cancer survival, significant challenges remain. In particular, most of the developments in molecular-based therapies are targeted against breast cancer subtypes with high expression of ER, PR, or HER2. Unfortunately, so-called "triple negative" breast cancers that grow aggressively in the absence of these receptors remain impervious to these treatment options, and are known to generate metastases (14). Similarly, while early detection is effective in increasing survival rates, many tumors are not or cannot be detected in early stages, and the five-year survival rate for these patients, many of whom are afflicted with bone metastases, is just 23% (9). There is also evidence that bone metastases are resistant to conventional chemotherapeutics, further highlighting the need for fundamental insight into this devastating disease (15).

Stephen Paget is credited with formalizing the "seed and soil" concept for metastasis in the late 19th century (16), and many researchers have pursued this line of thinking in investigating why metastatic breast cancer has such a strong avidity for bone (8, 17, 18). Recent studies have demonstrated that within breast tumors, heterogeneous expression of specific genes predisposes a certain subset of cells to metastasize to bone (18). Still, no concrete evidence on how this "bone metastasis signature" emerges or is regulated exists. In recent times, the critical nature of the tumor microenvironment in dictating cancer cell behavior has come to light, and it seems likely that microenvironmental control through cues such as cell-cell interactions, cell-ECM interactions, and biomechanical stimuli plays a role in metastasis as well (19-21) (Fig. 1.2). The bone matrix is uniquely defined the presence of the inorganic mineral hydroxyapatite (HA), a material known to bioactively affect cell behavior (22, 23). Thus, for the specific context of bone metastasis, the interaction between breast cancer cells and mineral should be investigated. This interaction occurs both within the bone, due to the presence of the skeletal mineral hydroxyapatite (HA), and at the primary site in the breast where microcalcifications are known to form (24, 25). Thus far, correlation has been shown between breast cancer cell mitogenesis and the presence of HA (24). Additionally, studies of both animal and human samples have shown a correlation between the presence of HA and general malignancy (26, 27). These findings suggest that HA may play a significant role in tumor development and driving bone metastasis.

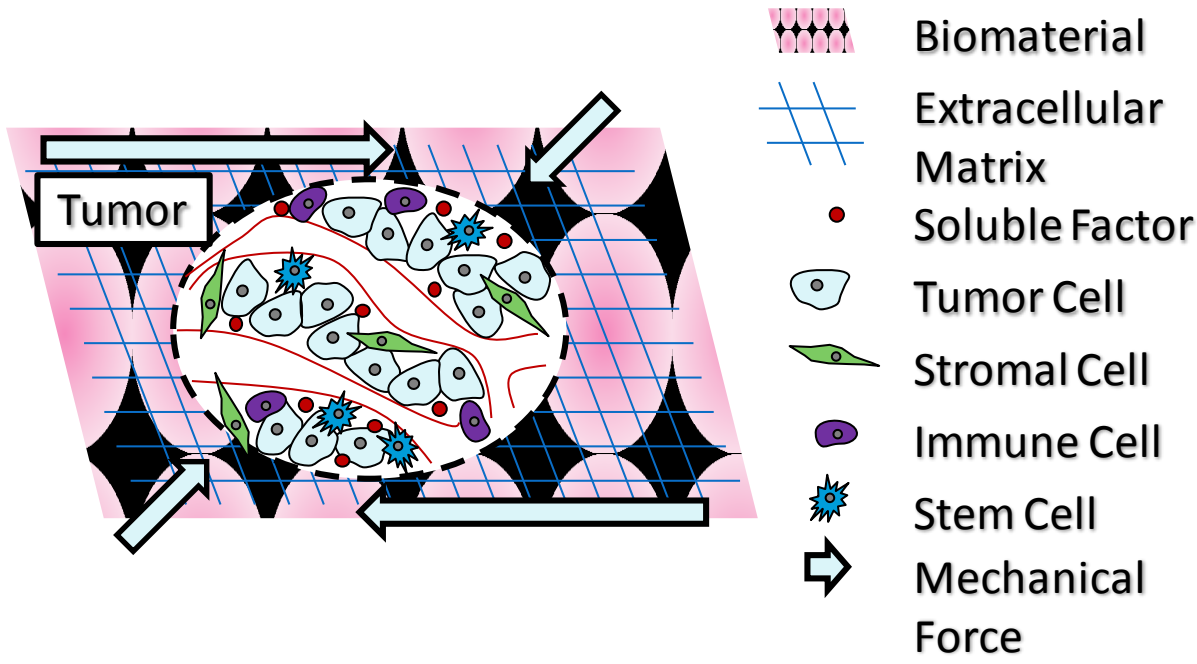

Figure 1.2: Tumor Microenvironment
The tumor microenvironment comprises the local area around a tumor and the various cellular inputs contained in this space. The inputs are a diverse set of physicochemical cues that enable tumors to survive and advance. Study of the microenvironment will help in understanding how external influences on tumor cells permit and promote metastatic disease.

1.2 Mineralization in the body

Tissue mineralization is a fundamental and critical process for vertebrates, helping to imbue bone and teeth with their structural integrity (25). For humans, the normal mineral that is found in the skeleton is chemically similar to geological HA ($Ca_{10}(PO_4)_6)(OH)_2$), though it is generally highly substituted, less crystalline, and more soluble (28). The material and microstructural properties of bone HA are also dynamic, being observed to change as a function of aging and various skeletal pathologies (26, 29). In bone, HA is organized along collagen fibrils, and it makes up the majority of the dry weight of the tissue (30). It is known to associate and interact strongly with a variety of noncollagenous proteins, such as osteopontin and fibronectin, that are capable of supporting cell adhesion, and could be implicated in promoting the colonization of metastatic breast cancer cells (31, 32).

While mineral is predominantly found in normal tissue such as bone and teeth, calcium-based mineral is also observed ectopically through soft tissues in a variety of pathologies. Kidney stones, atherosclerosis, and various skin disorders are all associated with pathological calcification (33, 34). Small degrees of ectopic calcification are not unusual, but radiological studies have shown that the presence of microcalcifications in breast tissue can be a precursor to malignant disease (24, 27). Currently, mammograms, which can reveal flecks of mineral in the breast, are one of the most important diagnostic tools for mammary tumors (9). There is evidence to suggest that tumor cell interactions with microcalcifications are connected to subsequent bone metastasis. Firstly, breast tumor cells in tumors with microcalcifications have been found to produce elevated levels of bone matrix proteins such as bone sialoprotein (BSP) and osteopontin (OPN) (18, 35, 36). Secondly, there is evidence to suggest that breast tumors that tend to display microcalcifications are also more likely to metastasize to bone relative to visceral targets (15, 35,

37). Unfortunately, despite these observations, there is still no predictive power that can be ascribed to mammogram-based diagnoses because an overwhelming majority of patients that have microcalcifications remain disease free (>99%) according to the American Cancer Society. Additionally, there is a lack of mechanistic understanding on how breast cancer cells are affected by mineral due a dearth of appropriate culture systems with which to probe this type of interaction. For these reasons, the presence of microcalcifications has largely been regarded until now as simply a primary diagnostic marker, albeit a crucial one. However, recent work with improved spectral analysis has revealed that breast microcalcifications can be divided into two distinct subgroups: type I, which are composed of calcium oxalate dihydrate, the mineral found in kidney stones; and type II, which are composed of HA as in bone. Interestingly, type I microcalcifications have been found to be associated strictly with benign, non-invasive growths, while type II microcalcifications seem to strongly promote malignancy and metastasis (27). It is certainly notable that breast cancer that is exposed to HA mineral at the primary site is more likely to metastasize to HA-rich bone, and these recent findings demonstrate the need to study the interaction between biological mineral and breast cancer cells carefully.

1.3 Tumor Microenvironment

Advances in genetics have yielded an enormous amount of insight into tumor biology. Common mutations underlying malignant transformation and genes that serve as risk factors for cancer susceptibility have been identified (38). Nonetheless, it is increasingly evident that a comprehensive understanding of cancer and metastasis will require an understanding of how external factors drive tumor cell behavior. In this regard, investigation of pertinent microenvironmental cues is being undertaken. Already, microenvironmental control of cancer

has been implicated in tumor progression and multidrug resistance, and a number of compounds targeted at the tumor microenvironment are in clinical trials (19, 39).

1.3.1 Soluble Factors and Paracrine Signaling

Whenever and wherever tumors develop, they secrete a slew of soluble factors including growth factors, hormones, and cytokines. Numerous findings show that they also deregulate the secretory activity of neighboring cells, causing further perturbation of normal physiology (40). Paracrine signaling is the most common method of cell-cell communication, and it occurs when secreted molecules from tumor cells activate intracellular signaling cascades in other cells via specific receptors, and vice versa. Inception of tumor angiogenesis and cancer-activated inflammation, both hallmarks of cancer, are mediated by soluble factors in the tumor paracrine signaling network (5, 41, 42). The complete list of soluble factors that are involved in tumor paracrine signaling is innumerable, but molecules such as vascular endothelial growth factor (VEGF) and interleukin-8 (IL-8) are known to be important players in breast cancer progression (43, 44). Perhaps one of the most widely-publicized anticancer therapies of all time, Avastin (bevacizumab), is a monoclonal antibody against VEGF that was targeted against the soluble factor to inhibit tumor angiogenesis (45). Despite its associated controversy and limited clinical success, the hype surrounding Avastin reflects the realization of the paramount importance of paracrine signaling in the tumor microenvironment.

1.3.2 Tumor-Extracellular Matrix (ECM) Interactions

Tumor invasion and cancer cell colonization are both fundamentally dependent on interaction with the ECM to provide anchorage and insoluble signaling cues. Even in mineralized tissue, cancer cells only interface directly with adhesive proteins that are intimately associated with HA. Common ECM proteins such as collagen, fibronectin, and laminin provide structural

binding and can initiate intracellular signaling cascades via integrin receptors on cancer cells (44, 46). Additionally, in the case of metastatic breast cancer, there is a high prevalence of other adhesive proteins such as BSP and OPN, which can also induce signals that may promote bone metastasis via integrins and other surface receptors (36). BSP and OPN both contain long negatively-charged amino acid sequences that facilitate their binding to HA, and they possess RGD sequences that enable cell attachment (47, 48). Tumor-ECM interactions are extremely dynamic: not only do tumor cells vary their integrin surface presentation in a spatiotemporally-dependent manner, they also pathologically remodel ECM relative to normal tissue (21).

1.4 Cellular compartment of the bone microenvironment

For breast cancer metastases, interacting with native bone cells represents a critical step in priming the bone microenvironment to establish a pre-metastatic niche that can be colonized. The bone microenvironment is primarily composed of two major specialized cell types: the bone-forming osteoblasts, and the bone-resorbing osteoclasts. Within the trabecular bone, the initial site of metastatic colonization, marrow is also rich in mesenchymal stem cells (MSCs), which are multipotent and capable of differentiating into various connective tissue lineages (49) and hematopoietic stem cells (HSCs), which give rise to all blood cells and osteoclasts themselves (49, 50).(Fig. 1.3). Many investigations have focused on the relationship between cancer cells and osteoclasts, as metastatic lesions from mammary tumors tend to be characterized by bone loss and an overall osteolytic phenotype. Indeed, several studies have convincingly shown that breast cancer cells promote excessive osteoclast activity (4, 51). It has been suggested that osteolysis is a means through which breast cancer can access the growth factor depots within bone, and that this enhanced osteoclast activation is part of a vicious positive feedback cycle by which breast cancer maintains itself in bone (1, 52).

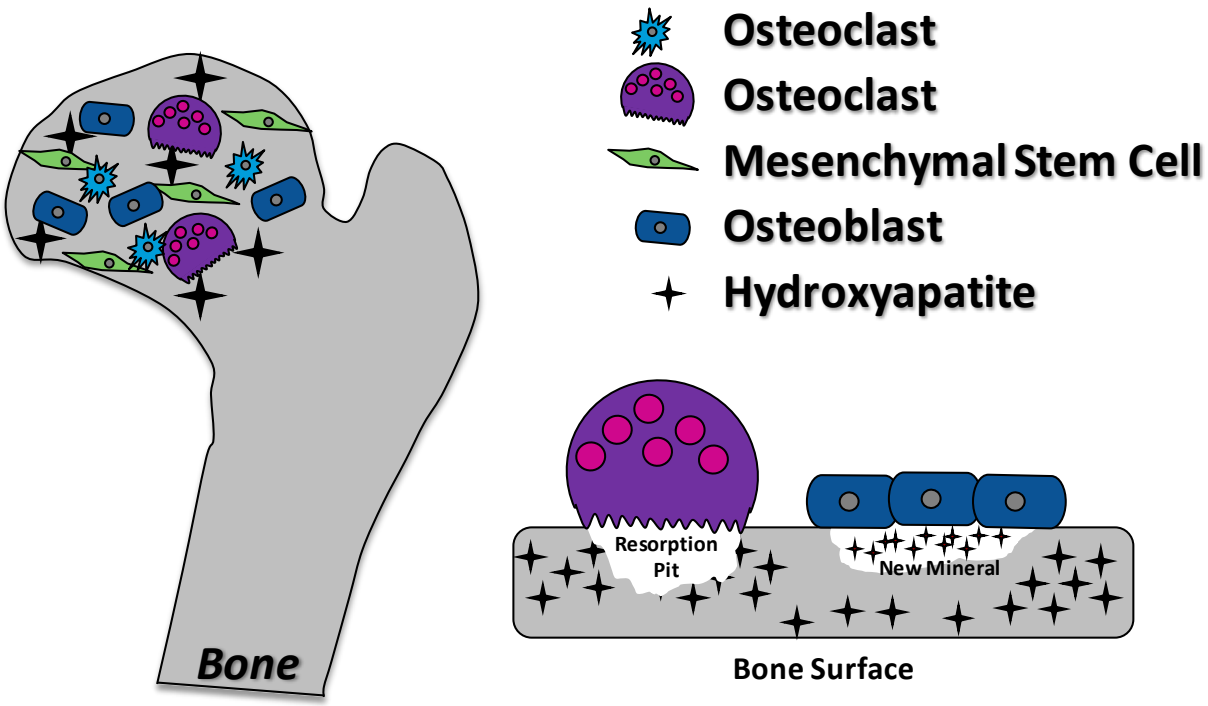

Figure 1.3: Bone Microenvironment
Skeletal metastasis exposes mammary tumor cells to the unique combination of cues found in the bone microenvironment. Cell-cell interactions via endocrine or paracrine signaling take place between tumor cells and native bone cells: osteoclasts, which resorb bone, and osteoblasts, which help in laying down new bone. Undifferentiated mesenchymal stem cells are also present and can interact metastasizing cells. Finally, mammary tumor cells are exposed to hydroxyapatite, the bone mineral.

The role of MSCs in breast cancer metastasis has been more difficult to resolve, due to their highly multifunctional nature. For example, past studies have shown that MSCs contribute to tumor angiogenesis by upregulating their expression of vascular endothelial growth factor (VEGF) (41). Other work has suggested that MSCs may secrete many pro-inflammatory cytokines that aid in tumor development and survival (53). In the specific context of metastasis, some studies indicate that MSCs mobilize tumor cells in a paracrine fashion by directly enhancing motility, while others suggest MSCs as the main stromal cell supporting metastatic recruitment (54, 55). Furthermore, observations that metastatic priming may require endocrine signaling suggest that tumor cells and MSCs may interact even at distant sites (56) to establish a pre-metastatic niche. It is known that the bone marrow is rich in stromal-derived factor 1 (SDF-1), a molecule that is also suspected to drive bone metastases. MSCs are a cell type that produce high levels of SDF-1 (57), suggesting a potential role for MSCs in tumor cell recruitment. However, there is still a lack of work on how SDF-1 levels are regulated during incipient stages of metastatic bone disease. It would seem that work is needed to determine whether or not MSC expression of SDF-1 is altered to promote pre-metastatic niche formation and mammary tumor cell recruitment. Still, the overall breadth of results suggesting a connection between MSCs and breast cancer progression illustrate how understanding this cell-cell interaction will provide fundamental insight into bone metastasis.

1.5 Synthetic HA and mineral-containing model systems

The lack of existing mineral-containing tissue culture systems severely limits the ability to study cancer cell-mineral interactions *in vitro*. Additionally, clinical studies, illustrate the need to carefully control HA properties such as crystallinity, particle size, and substitution for *in vitro* experiments (27). Significant work in the field of biomineralization has revealed much insight

into how to make mineralized films and gels, but few of these systems are suitable for cell culture, due to limitations in oxygen transport and temperature control (25, 32). A multitude of techniques for the creation of synthetic HA have been employed, but as particles alone, they also cannot easily be presented to cells (58). Moreover, few studies have truly utilized technique for the synthesis of physiologically relevant crystal characteristics. There is evidence to suggest that crystal properties affect cellular behavior (59), but few systematic studies that model changing mineral properties that are associated with effects observed in pathologies have been performed. Scaffold systems designed by tissue engineering principles can serve as a vehicle to present mineral particles to cells. Originally designed for bone tissue engineering, scaffold systems are biocompatible and support cell adhesion (60). Based on the current state of the field, it is apparent that to recapitulate tumor cell-mineral interactions, application of controlled mineral synthesis, biomaterials science, and tissue engineering design will be required for the creation of a functional model.

1.6 Research Objectives

Hydroxyapatite mineral is a strikingly unique component of both the metastatic and primary tumor environment for breast cancer. With increasing evidence suggesting that mineral plays an active role in affecting tumor cell behavior, exploring how it may drive breast cancer metastasis to bone is a natural pursuit. More broadly, investigating the complex interplay of tumor cells with mineral, bone and stromal cells, and matrix proteins and determining how these microenvironmental cues affect the paracrine signaling network and drive disease progression may provide insights that aid in revealing novel points for therapeutic intervention.

I hypothesize that the interaction between mineral and breast cancer cells promotes malignancy and underlies the observed affinity of resulting metastases for bone and the subsequent osteolytic phenotype. I have investigated this hypothesis by systematically exploring the following three sub-hypotheses:

1. **Mineral promotes osteoclastogenesis by enhancing tumor cell secretion of osteolytic factors**
2. **Exposure to microcalcifications/mineral primes mammary tumor cells for colonization of bone by stimulating MSC-driven recruitment**
3. **Crystal properties affect tumor cell-mineral interactions and regulation of malignant phenotype**

In the search for innovative ways to fight breast cancer, it is logical to target bone metastases, which remain difficult to deal with currently. Understanding the influence of the microenvironment in driving this process will contribute to the elucidation of the molecular mechanisms of bone metastasis, helping to reveal the potential susceptibilities of metastases for treatment option. Since mineral is a salient feature in the stepwise metastasis cascade, and

because it is already used as a diagnostic marker, it is sensible to study its role as a microenvironmental controller.

1) Mineral promotes osteoclastogenesis by enhancing tumor cell secretion of osteolytic factors

A mineral-containing three-dimensional (3-D) scaffold system was engineered to present HA to a metastatic human breast cancer cell line (MDA-MB231) to monitor changes in secretory behavior in response to the mineral. The system was evaluated to confirm that mineral is reliably exposed to cells, and baseline parameters such as adhesion and tumor cell growth were measured. Changes in the secretion levels of IL-8 were also specifically assessed, as previous studies suggested that this molecule could independently induce osteoclast differentiation and activity (51). Furthermore, clinical studies have indicated that IL-8 expression is associated with increased malignancy (61). Conditioned media was collected from mineral-containing culture models, and this media was used to culture murine osteoclast precursor cells (RAW 264.7) to evaluate the effects of tumor-derived soluble factors on differentiation and resorptive activity. Inhibitory antibodies were used to definitively show the mechanistic role of IL-8 in driving osteolysis.

2) Crystal properties modulate cell-ECM interaction to alter tumor cell behavior and regulate the malignant phenotype

A hydrothermal aging approach was used to create synthetic HA with varying particle size and crystallinity. This novel process involved two steps: first precipitating calcium phosphate through standard solution-based techniques, and subsequently drying and aging them with well-defined heating schedules in a non-stirred pressure vessel. In this manner, homogeneous populations of HA crystals were synthesized before being incorporated into a 3-D scaffold for probing interactions with cancer cells. Basic bioactivity parameters were tested in

the scaffolds as a function of crystal properties, including protein adsorption, cellular growth, and cellular adhesion. The specific capacity of various crystals to adsorb adhesive peptides was measured and correlated with adhesion of MDA-MB231 cells. IL-8 expression was also tested to see how it varied with crystal characteristics.

3) *Exposure to microcalcifications/mineral primes mammary tumor cells for colonization of bone by stimulating MSC-driven recruitment*

To understand how cell-mineral interactions might mediate actual recruitment of breast cancer cells to the bone, the comprehensive effects of the mineral-containing scaffolds were determined. Expression of bone metastasis genes in mineral-containing scaffolds were investigated to see whether these genes may be activated by microenvironmental-HA. Trends observed with MDA-MB231 cells were reassessed with MCF10A.DCIS cells (62). The effect of tumor-derived IL-8 on MSCs was explored, and transwell systems were used to observe migration patterns of cancer cells that were preconditioned in mineral-containing scaffolds and then exposed to MSC secretions. Generally, the potential role of MSCs in recruiting mineral-exposed breast cancer cells was studied. This was done to recapitulate the effect of microcalcifications that may drive bone metastasis physiologically.

MDA-MB231 subpopulations with differential tissue tropism were previously developed via *in vivo* serial passaging and generously provided by Dr. Joan Massague (18). Though it has been thought that these subpopulations inherently possess different gene expression profile relative to one another, the ability of HA to "re-program" these cells was assessed by expression analysis. Subsequently, pre-exposure to mineral in scaffolds was tested for the capacity to affect tissue tropism through a colonization mouse model via intracardiac injection. Finally, a clinical exploration was completed in collaboration with Memorial Sloan Kettering Cancer Center

(MSKCC). Pathological reports, histological analysis, mammography, and immunostaining for IL-8, were blindly performed in conjunction with a team of clinicians, and the correlation between patient outcome, appearance of microcalcifications, and IL-8 levels was determined.

CHAPTER 2: A NOVEL 3-D MINERAL-CONTAINING TUMOR MODEL TO STUDY BREAST CANCER BONE METASTASIS

PUBLISHED IN PLOS ONE (63)

2.1 Contributors

Christine Kowalczweski contributed to this chapter by maintaining cultures of RAW 264.7 cells and performing differentiation studies. Christine also performed image analysis to quantify TRAP staining of differentiation RAW 265. 7 cells. Ramya Tadipatri conducted experiments with Ibandronate, including viability assessment. Both Ramya and Christine fabricated scaffolds that were used in this study. I performed all other experiments and designed the study with Dr. Claudia Fischbach.

2.2 Introduction

Bone metastasis, the spread of tumor cells to the skeleton, is a frequent cause of morbidity and mortality in patients with advanced cancers. Seventy-percent of breast cancer patients with advanced disease develop bone metastases (3), which lead to severe bone pain, pathological fractures, hypercalcemia, and nerve compression (1, 4, 64). These debilitating skeletal events are a consequence of secondary tumor formation and pathological bone remodeling of predominantly osteolytic character (1).

While organ-specific patterns of metastatic colonization are often mediated by site-specific metastasis signatures (65), microenvironmental conditions in the bone are implicated in the pathogenesis of metastatic breast cancer. More specifically, mammary tumor cells located within bone up-regulate expression of growth factors and cytokines that stimulate osteoclastogenesis and inhibit osteoblast differentiation relative to the same cells located in soft

tissue sites (52, 66, 67). This process not only promotes pathological bone resorption, but also leads to the release of morphogens that further stimulate metastatic tumor growth and exacerbate the imbalance between bone formation and resorption.

A variety of growth factors and cytokines drive the vicious cycle of bone metastasis by dually playing roles in tumor progression and bone remodeling. For example, vascular endothelial growth factor (VEGF) promotes bone metastasis by stimulating the formation of new blood vessels necessary for tumor growth and by regulating apoptosis and differentiation of tumor cells and osteoblasts (68, 69). Parathyroid hormone related protein (PTHrP), an osteoclast-activating factor, is widely investigated for its role in metastasis mediated osteolysis, but interleukin-8 (IL-8) may be equally important because of its pro-angiogenic, pro-migratory, and osteoclastogenic activities (51, 66, 70-75). Whether or not specific bone microenvironmental conditions play a role in regulating the signaling by these pro-metastatic factors, however, remains unclear.

The bone extracellular matrix (ECM) is a composite material that consists of an inorganic mineral phase dispersed throughout an organic matrix of collagen. The inorganic component of bone is primarily composed of the mineral hydroxyapatite (HA), a crystalline calcium phosphate phase with the molecular formula Ca5(PO4)3(OH) (76). While HA is noted for its role in imbuing bone with exceptional tissue stiffness and serving as a reservoir of ions (i.e., Ca2+ and PO43-), it also represents a bioactive material that modulates the behavior of both normal and transformed cells (24, 76, 77). For the specific case of bone metastasis, however, it remains an open question as to whether the presence of HA in the bone ECM affects the cellular and molecular interplay intrinsic to bone metastasis.

Three-dimensional (3-D) polymeric scaffolds represent highly innovative tools for recreating tumor microenvironmental conditions in culture (44, 78-80). In relation to conventional 2-D cultures, tumor cells maintained in 3-D scaffold-based, tissue-engineered tumor models exhibit characteristics that are more representative of their malignant behavior in vivo including increased angiogenic capacity, altered cell morphology, increased invasiveness, and enhanced resistance to cytotoxic drugs (44, 79). To specifically evaluate the role of HA in breast cancer bone metastasis we have developed a novel 3-D tumor model based on mineral-containing scaffolds. This system allowed us to examine various stages of secondary tumor growth within bone microenvironments (i.e., initial colonization and subsequent tumor progression, osteolytic capability) under well-defined and pathologically relevant conditions in vitro. Our findings indicate for the first time that HA plays a critical role in controlling the osteolytic phenotype of breast cancer bone metastasis and that tissue-engineered, mineral-containing tumor models may be an invaluable in vitro platform to reveal the underlying physicochemical and biological relationships.

2.3 Results

2.3.1 Physicochemical Characterization of Scaffolds

Scaffold characterization was performed initially to determine the properties of the matrices and verify the presence of HA. EDS analysis indicated that HA was available for cellular interactions at the porous surface of the mineral-containing scaffolds, while non-mineral-containing control scaffolds did not contain detectable amounts of calcium or phosphate (Fig. 2.1A). Additionally, image reconstruction of microCT scans confirmed that HA was uniformly distributed throughout the mineral-containing scaffolds, whereas no X-ray absorption was detected for non-mineral-containing control scaffolds (Fig. 2.1B). Not surprisingly, DMA

analysis revealed that mineral-containing scaffolds exhibited compressive moduli that were 2-fold higher than for non-mineral-containing control scaffolds (data not shown). These differences were related to the presence of HA as opposed to alterations in the microarchitecture, as mineral-containing and non-mineral-containing control scaffolds exhibited similar wall thicknesses (mineral-containing scaffolds: 58 ± 27 μm, non-mineral-containing scaffolds: 50 ± 30 μm) and pore diameters (mineral-containing scaffolds: 432 ± 106 μm, non-mineral-containing scaffolds: 451 ± 123 μm) (Fig. 2.1C, D).

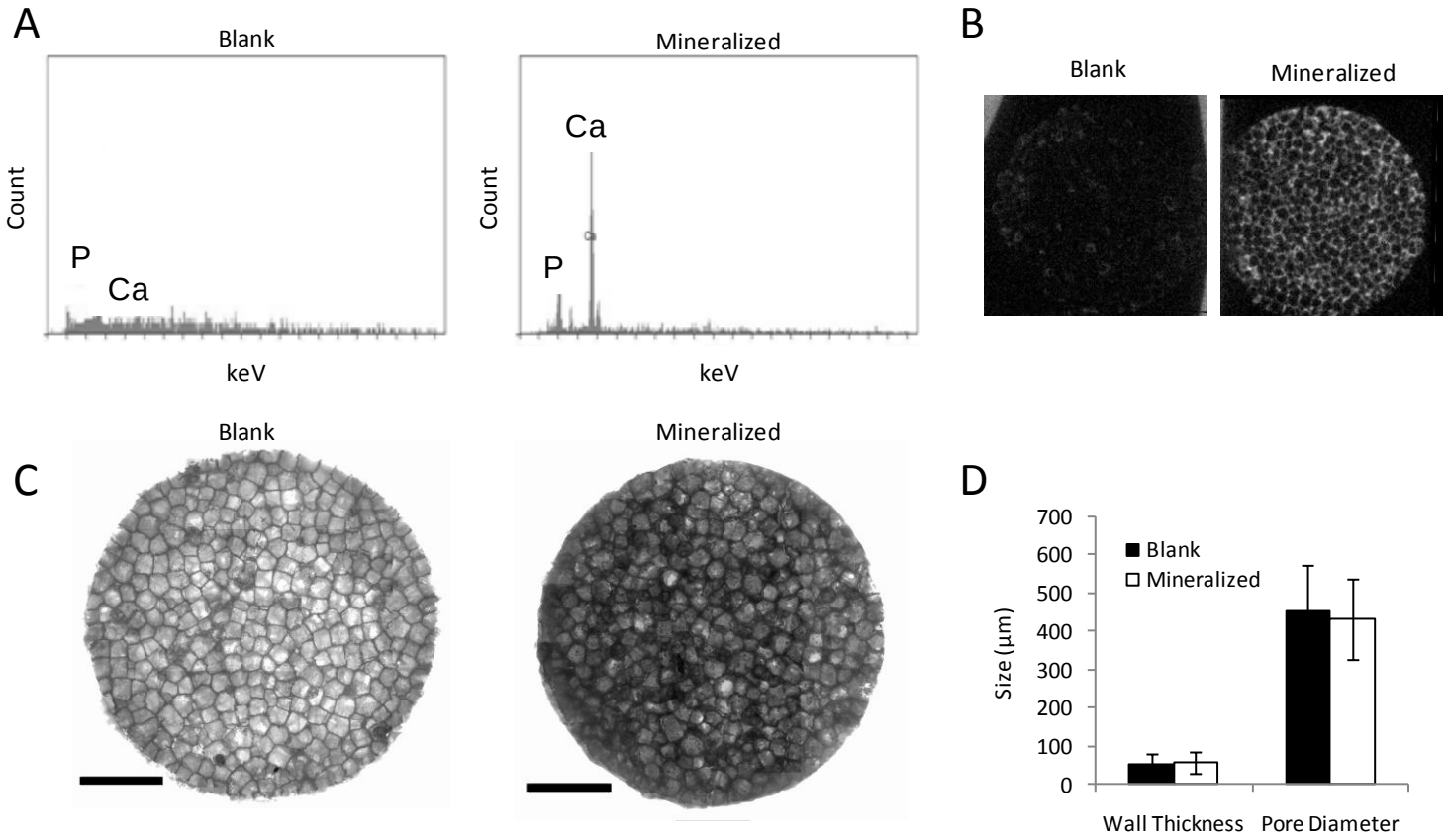

Figure 2.1: Physicochemical characterization of scaffold system
(A) HA in biomineral-containing scaffolds is available for cellular interactions as EDS analysis indicates Ca and P at the porous surface of the scaffolds, while no mineral was detected for blank control scaffolds. (B) MicroCT scans indicate that HA is uniformly distributed throughout biomineral-containing scaffold, but was not present blank control scaffolds. (C) Incorporation of HA did not alter the scaffold microarchitecture relative to blank control scaffolds. Scale bars represent 2 mm. (D) Image analysis of micrographs indicates that pore size and polymer wall thickness are similar for both biomineral-containing and blank scaffolds.

2.3.2 Mineral-containing scaffolds promote MDA-MB231 adhesion and proliferation

The ability of HA to affect breast cancer cell colonization and tumor growth within the bone microenvironment was next assessed by studying MDA-MB231 adhesion and proliferation within mineral-containing and non-mineral-containing control scaffolds. Relative to non-mineral-containing scaffolds MDA-MB231 cells displayed greater penetration into the center of the mineral-containing scaffolds and increased adhesion onto HA-containing surfaces, as indicated by von Kossa staining of transverse histological sections of scaffolds (Fig. 2.2A). Quantification of seeding efficiency confirmed increased adhesion of tumor cells into mineral-containing scaffolds (Fig. 2.2B). These differences were likely related to increased adsorption of adhesion proteins because Western Blot analysis showed that fibronectin was more readily adsorbed onto mineral-containing scaffolds as compared to non-mineral-containing scaffolds (Fig. 2.2C). Furthermore, blockade of fibronectin-binding integrins by pre-incubation with soluble RGD peptides decreased initial adhesion into mineral-containing scaffolds by 36%. Interestingly, the proliferative capacity of MDA-MB231 cells was also increased in the presence of HA, as a Hoechst DNA assay showed augmented cell numbers in mineral-containing scaffolds relative to control scaffolds (Fig. 2.3A). Similarly, MCF-7 cells exhibited a 20% increase in proliferation in mineral-containing scaffolds (data not shown) verifying the relevance of our findings with a second cell type. In agreement with these results, von Kossa and live/dead staining of the different MDA-MB231 tumor models indicated enhanced tumor tissue formation in the presence of HA after 5 days in culture (Fig. 2.3B, C).

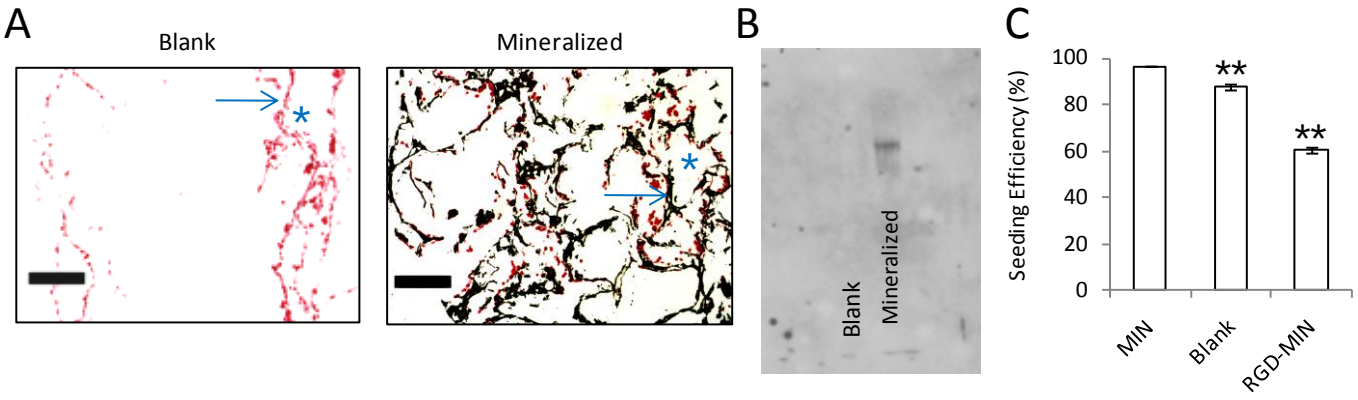

Figure 2.2 Effect of HA on breast cancer cell adhesion
(A) MDA-MB231 breast cancer cells adhere more efficiently to biomineral-containing scaffolds than blank scaffolds (**$p<0.01$). (B) Analysis of von Kossa stained histological cross-sections indicates that MDA-MB231 cells (stained red) penetrate to the center of biomineral-containing scaffolds (HA stained black) more effectively. Arrows and asterisks indicate representative scaffold walls and pores, respectively. Scale bars represent 2000 μm. (C) Fibronectin adsorption within the polymer scaffold is increased in biomineral-containing scaffolds (lane 2) relative to blank scaffolds (lane 1) as indicated by Western Blot analysis of scaffold lysates.

2.3.3 Minerals promote tumor-mediated osteoclast differentiation and activity

To assess a potential role of HA in the osteolytic phenotype of bone metastases, conditioned media were collected from the different tumor models, normalized to cell number, and used to test their effect on osteoclastogenesis of RAW 264.7 cells. Quantification of TRAP+ cells indicated that breast cancer cells cultured within 3-D non-mineral-containing scaffolds increased osteoclastogenesis as compared to control media that was not exposed to tumor cells and media collected from 2-D cultures (data not shown), but a much more dramatic effect was detected for mineral-containing tumor models (Fig. 2.4A, B). More specifically, media collected from mineral-containing tumor models increased osteoclast differentiation by 65% with respect to media collected from non-mineral-containing scaffold cultures and this effect was comparable to media supplemented with pro-osteoclastic RANKL (Fig. 2.4A, B). To ensure that tumor-derived soluble factors in the mineral-containing culture media, and not soluble products of the scaffold itself (e.g., Ca^{2+}, PO_4^{3-}), were directing osteoclast differentiation, we cultured RAW 264.7 in cell-free scaffold-incubated media and found no differential effects on osteoclastogenesis relative to control media (data not shown). Accordingly, atomic absorption analysis did not yield detectable amounts of Ca^{2+} and PO_4^{3-} in media collected from non-mineral-containing or mineral-containing scaffold cultures. Furthermore, the detected differences in osteoclastogenesis were not due to altered cell proliferation as an AlamarBlue assay showed similar cell numbers for all tested conditions (data not shown). Evaluation of osteoclast resorptive activity via analysis of Ca^{2+} release from Corning Bone Cell Assay Surfaces (81), confirmed our results by revealing significantly higher free Ca^{2+} concentrations in response to media collected from mineral-containing tumor models exceeding even the osteolytic potential mediated by 50 ng/mL RANKL (Fig. 2.4C).

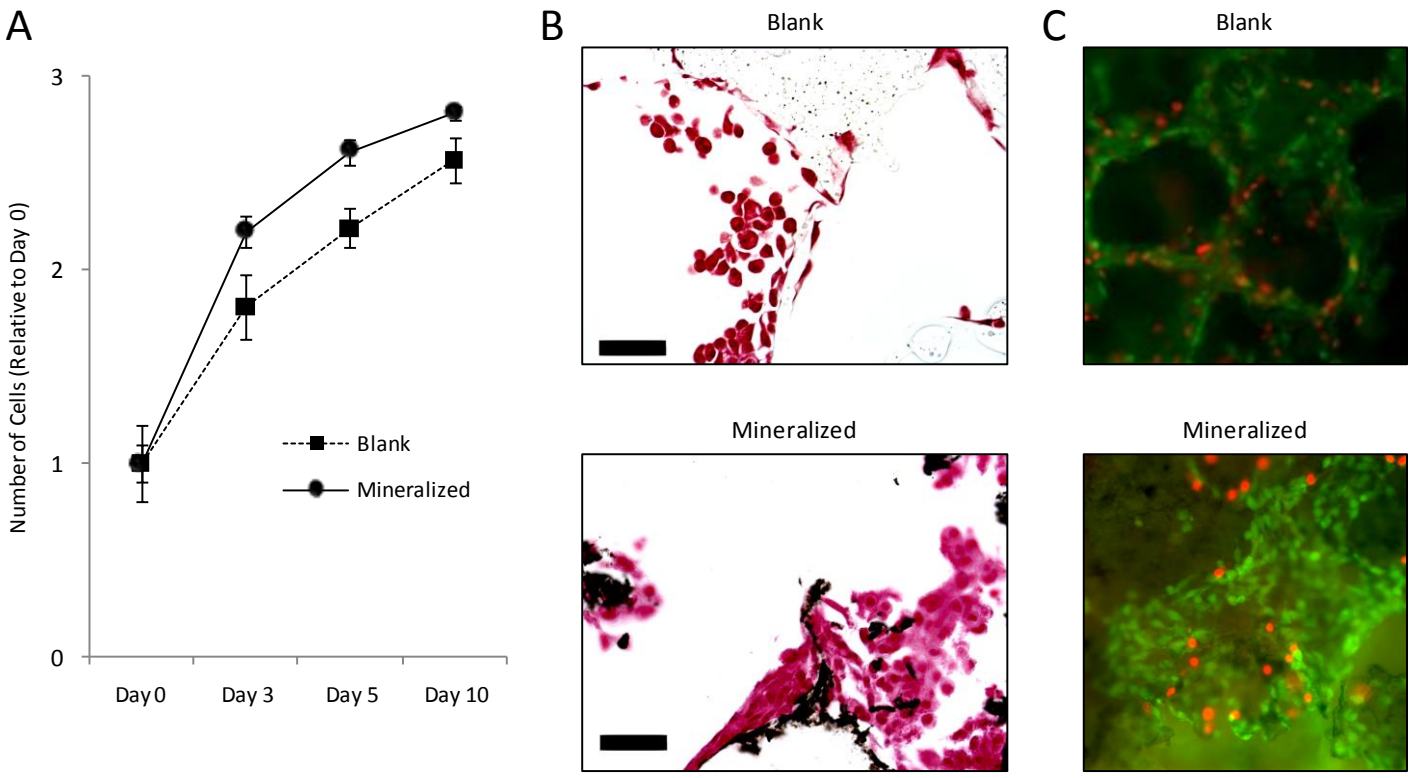

Figure 2.3: Effect of HA on 3-D tumor tissue formation
(A) Quantification of DNA indicates enhanced proliferation of MDA-MB231 cells within biomineral-containing scaffolds as compared to blank scaffolds. (B) Analysis of von Kossa stained histological cross-sections reveaed that 5 days after seeding, coherent tissue begins to form in biomineral-containing scaffolds but not blank scaffolds (MDA-MB-231 cells stained red, HA stained black). Scale bars represent 50 μm. (C) Live and dead staining with calcein (green) and propidium iodide (red), respectively, shows increased cell number and tissue formation into pores of biomineral-containing scaffolds relative to control scaffolds, while the relative ratio of live to dead cells remains unchanged.

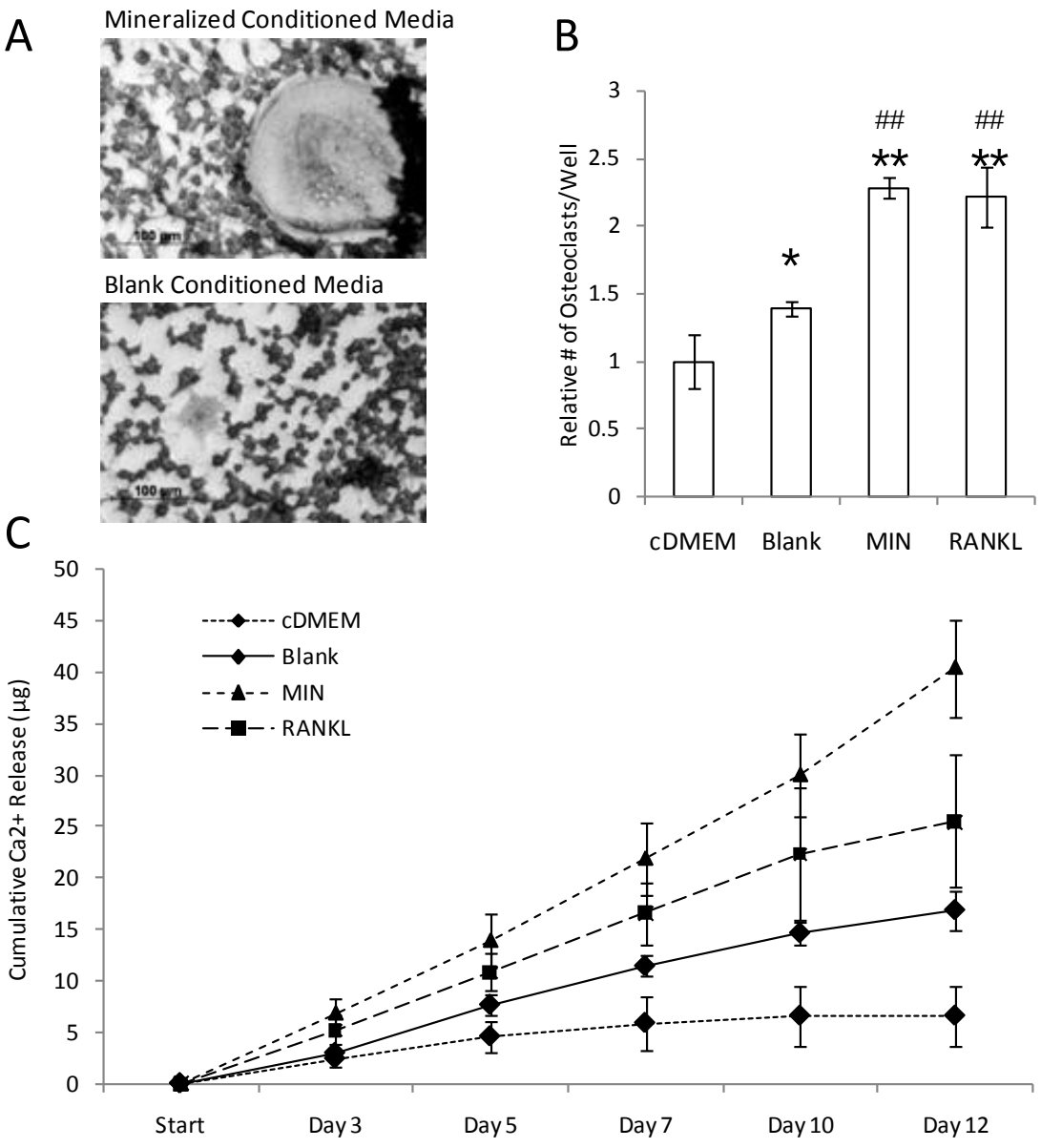

Figure 2.4: Osteoclastogenesis in response to conditioned media
(A) Conditioned media collected from biomineral-containing tumor models (Biomineral-containing Conditioned Media) increased RAW 264.7 osteoclastogenesis relative to conditioned media collected from non-biomineral-containing tumor models (Blank Conditioned Media) as revealed by TRAP staining of large multinucleated cells. (B) Quantification of TRAP+ cells indicated that culture media collected from biomineral-containing scaffold cultures promoted RAW 264.7 osteoclastogenesis relative to control media (cDMEM) and media collected from blank scaffold cultures (82) in a manner that was similar to osteoclastic RANKL. Asterisks [*$p<0.05$, **$p<0.01$] and pound signs [#$p<0.05$, ##$p<0.01$] indicate statistical significance with respect to 'cDMEM' and 'Blank', respectively. (C) Conditioned media collected from biomineral-containing models enhances the resorptive activity of RAW 264.7 relative to all other tested conditions as indicated by 2-D culture on calcium phosphate disks and subsequent analysis of calcium release by a colorimetric assay.

2.3.4 Minerals enhance tumor-mediated osteoclastogenesis by up-regulation of IL-8

The ability of HA to modulate the molecular interplay involved in tumor-mediated bone osteolysis was next tested by examining VEGF, PTHrP, and IL-8 as specific examples of tumorigenic and pro-osteoclastic factors. While VEGF secretion by MDA-MB231 cells was not affected by the scaffold type (Fig. 2.5A) and PTHrP was secreted at undetectable levels (<0.3 pM) from either mineral-containing or non-mineral-containing tumor models (data not shown), IL-8 secretion was increased by 38% in mineral-containing scaffold cultures relative to tumor cells grown within non-mineral-containing scaffolds. Similarly, MCF-7 cells secreted 40% more IL-8 when cultured within mineral-containing scaffolds as compared to non-mineral-containing scaffolds. These differences were attributed to the inherent bioactivity of HA rather than the different mechanical stiffness of the matrices (non-mineral-containing scaffolds: 0.5 MPa, mineral-containing scaffolds: 1.1 MPa), as scaffolds with lower (50% HA) and higher HA content (200% HA) and thus lower (0.7 MPa) and higher elastic modulus (2.1 MPa) exhibited similar effects on breast cancer cell proliferation and IL-8 secretion (data not shown). IL-8 up-regulation mediated pro-osteoclastic effects, as inhibition of this signaling by an IL-8 neutralizing antibody yielded similar numbers of TRAP+, differentiated RAW 264.7 osteoclasts as media collected from non-mineral-containing scaffolds (Fig. 2.5B).

Directed migration may be important to the fusion of RAW 264.7 cells to multinucleated, differentiated osteoclasts and we hypothesized that IL-8 may play a role in this process. Analysis of RAW 264.7 cell motility in response to the different culture media indicated that breast cancer cells maintained in mineral-containing tumor models induced RAW 264.7 migration more significantly relative to media collected from non-mineral-containing scaffold cultures or media supplemented with 50 ng/mL RANKL. Blockade of IL-8 signaling dramatically reduced motility

to levels comparable with cDMEM control media (Fig. 2.5C). Finally, both pit resorption and calcium release assays revealed that IL-8 inhibition more dramatically reduced the resorptive activity of RAW 264.7 cells cultured within media from mineral-containing tumor models relative to media collected from non-mineral-containing tumor models (Fig. 2.5D-F).

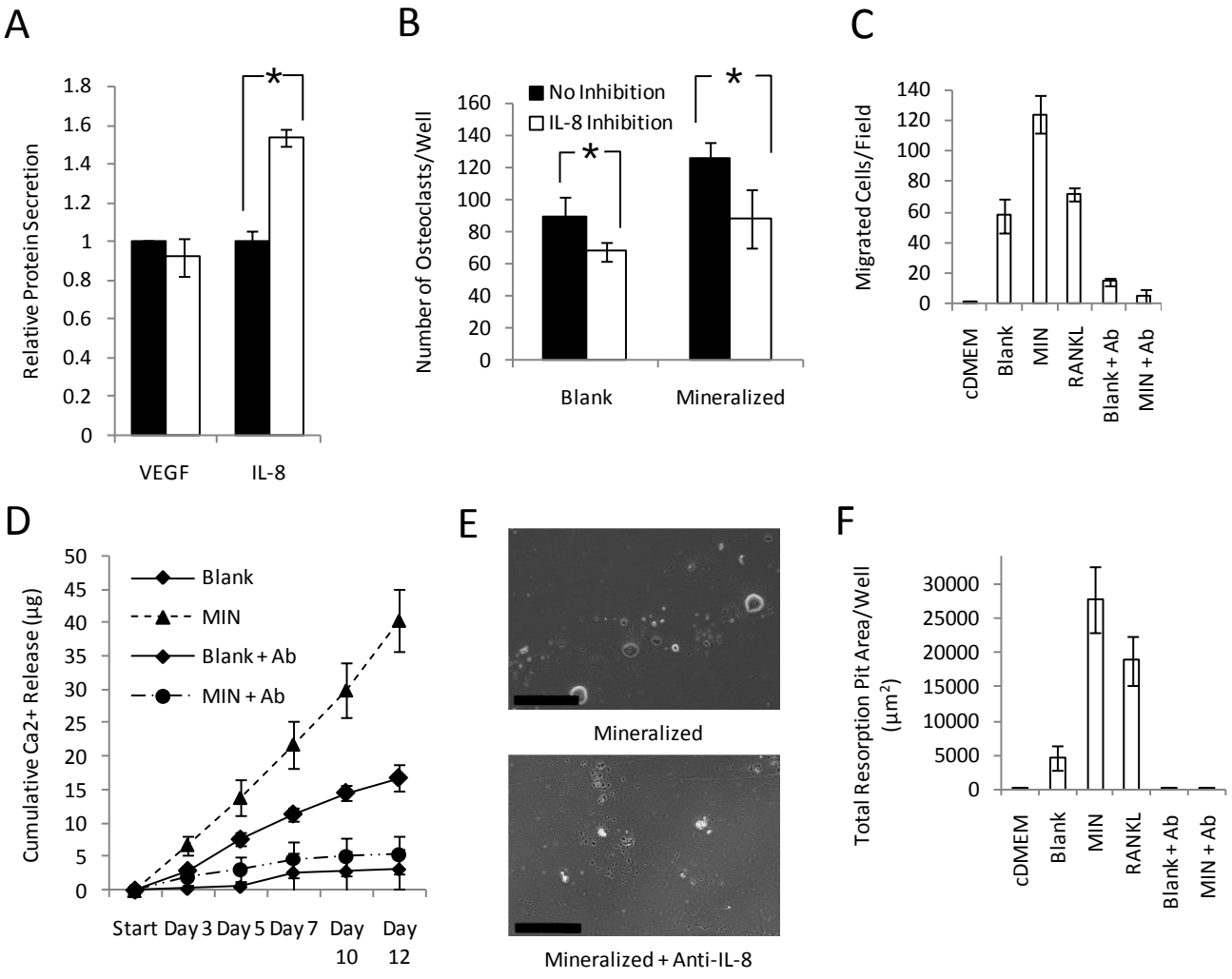

Figure 2.5: Osteoclastogenesis in response to HA-dependent IL-8 signaling
(A) Tumor cells cultured within biomineral-containing scaffolds (black bars) up-regulated secretion of IL-8 relative to culture within blank control scaffolds (white bars), while no effect was detected for VEGF secretion (*$p<0.05$). (B) Blockade of IL-8 signaling by addition of a neutralizing antibody inhibited the pro-osteoclastic effect of conditioned media collected from biomineral-containing tumors to levels comparable to non-biomineral-containing cultures (*$p<0.05$). (C) Transwell assays with conditioned media indicate that tumor cells cultured within biomineral-containing cultures markedly increase the motility of RAW 264.7 relative to all other conditions. Inhibition with a function blocking antibody suggested that this effect was IL-8 dependent. (D) Colorimetric analysis of Ca-release indicates that IL-8 neutralization in media collected from biomineral-containing tumor models (BM+Ab) results in a much more pronounced decrease in osteoclast activity as compared to media collected from blank scaffold cultures (Blank+Ab). (E) Micrographs of osteoclast-mediated pit formation on bone mineral surface in the presence of conditioned media from biomineral-containing tumor models with and without anti-IL-8 antibody. Scale bars represent 200 µm. (F) Quantification of pit formation in response to the different media in the presence and absence of functional IL-8 signaling.

2.4 Discussion

By integrating biomaterials and tissue engineering strategies, we have developed a novel, mineral-containing 3-D tumor model and have employed this culture system to systematically investigate the pro-metastatic role of HA under pathologically relevant conditions *in vitro*. The results of our study indicate for the first time that HA controls critical aspects of breast cancer bone metastasis by directing mammary tumor cells towards a phenotype that promotes secondary tumor growth and bone destruction via up-regulation of IL-8.

Our data suggest that cellular interactions with HA are involved in the colonization and proliferation of breast cancer cells within the bone microenvironment and that RGD-containing fibronectin plays a role in this process. This possible relationship is supported by previous studies, which showed that stromal cell adhesion to HA is mediated by RGD-containing proteins (83, 84) and that a truncated version of fibronectin can block breast cancer growth and metastasis in vivo (85). Accordingly, HA promoted tumor tissue formation within the biomimetic tumor models in our studies and this effect was likely due to the integrated effects of increased adhesion and proliferation. Typically, secondary tumor formation within the bone microenvironment is considered a function of bone resorption because the degrading bone mineral matrix releases bioactive ions and growth factors critical to the proliferation of both normal and transformed cells (4, 86-88). Our data now suggests that not only soluble, but also insoluble cues inherent to the inorganic component of the bone mineral matrix regulate the metastatic growth of breast cancer cells within bone.

Tumor-derived soluble factors shift the balance between bone formation and bone degradation towards osteolysis (1, 4, 18, 51, 66, 86, 87), and our results indicate that HA is strongly implicated in this process. More specifically, pre-osteoclast motility, osteoclast

differentiation, and osteoclast activity were all increased in response to conditioned media collected from mineral-containing tumor models relative to non-mineral-containing tumor models. To identify a potential molecular mediator that may be involved in these effects, we investigated the secretion of a number of growth factors and cytokines that are pivotal to bone metastasis. While VEGF and PTHrP, critical regulators of tumor angiogenesis (44, 89) and osteoclast resorption (1, 86, 87), respectively, were not affected by the presence of HA, IL-8 was up-regulated under these conditions. IL-8 promotes tumorigenesis through inflammatory and pro-angiogenic effects, but increasing evidence additionally implicates IL-8 as a pro-osteoclastic factor (51, 66, 90). Our data supports this concept and additionally suggests that HA increases the pro-osteolytic secretion of IL-8. In our studies, there was no significant difference in the number of differentiated osteoclasts in culture media collected from the mineral-containing tumor models relative to media supplemented with RANKL. However, conditioned media collected from HA-containing scaffold cultures induced higher resorptive activities of osteoclasts, and these effects may be due to the activation of IL-8 related signaling pathways that may play a role in ruffled-border formation and subsequent bone degradation (91, 92). While in the present study, we have identified that the osteoclastogenic signaling of IL-8 is regulated by HA, it should be further noted that cancer cell expression of other bone proteins may also be affected by the presence of bone mineral. For example, osteopontin and osteocalcin are expressed by breast cancer cells, are involved in bone cell signaling, and have a strong affinity for HA (32, 84, 93-95).

A variety of mechanisms may be involved by which HA mediates the pro-metastatic effects noted in our studies. Differences in protein adsorption may support the initial colonization of tumor cells extravasated from blood vessels into the bone microenvironment. Changes in

protein adsorption may, in turn, alter the engagement of integrins, which is implicated in IL-8 dependent tumor growth (44). Differences in cell signaling may thereby not only be related to quantitative differences in protein adsorption as detected in our studies, but also to conformational changes associated with HA-protein interactions (96). Additionally, HA confers the bone ECM with enhanced mechanical stiffness, and differences in tissue stiffness play a role in regulating tumor cell phenotype (97). However, in our studies the inherent bioactivity of HA, and not enhanced substrate stiffness, was responsible for our data. It has to be noted that these results do not exclude the possibility that mechanical stiffness influences bone metastasis over a different range of elastic moduli. Finally, the presence of HA may induce enhanced extracellular Ca^{2+} concentrations, a cue known to affect cancer cell behavior (98). However, HA is not highly soluble in the absence of strongly acidic conditions, which were not detected in our studies, and atomic absorption confirmed that Ca^{2+} release from mineral-containing scaffolds was negligible. Accordingly, no enhanced Ca^{2+} concentrations were detected in the respective culture media.

Tissue engineering strategies can be invaluable in meeting the increasing demand for more physiologically-relevant models of bone metastasis in the future. In this study, we have utilized polymeric scaffolds that incorporated HA in the absence of bone cells and were able to specifically test the role of HA in breast cancer bone metastasis without confounding effects mediated by other cell-derived factors. By increasing the complexity of this culture model through, for example, incorporation of stromal cells inherent to the bone microenvironment (e.g., osteoblasts) (99, 100) or biologically inspired release of growth factors (101) the developed tumor model may become much more broadly applicable and may revolutionize in vitro studies of metastatic tumor cell interactions with bone. Finally, it should be noted that although in the current study we have investigated metastases with predominantly osteolytic characteristics, it

remains possible to use the mineral-containing scaffold system to model metastases with osteoblastic potential (e.g., prostate cancer) as well (1, 64, 72, 86).

In conclusion, HA induces secondary tumor growth and IL-8 secretion by breast cancer cells, providing a molecular mechanism by which the mineral matrix of the bone microenvironment regulates the pathological bone remodeling associated with breast cancer bone metastasis. Directly targeting HA as an integral component of the bone mineral matrix may not represent a viable option for therapy. However, tissue-engineered tumor models will enable studies that will lead to an improved understanding of the molecular mechanisms by which HA mediates its pro-metastatic effects. This information will be critical to the identification of novel and specific therapeutic targets that will permit the improved therapy of patients with advanced breast cancer.

2.5 Materials and Methods

2.5.1 Cell Culture

Human MDA-MB231 (44, 65, 86, 102) and MCF-7 (67, 79, 86) breast cancer cells (ATCC), and murine monocytic RAW 264.7 (103-105)cells (ATCC) were routinely maintained in complete DMEM (cDMEM) (i.e., DMEM (Invitrogen) supplemented with 10% fetal bovine serum [FBS, from Tissue Culture Biologicals] and 1% penicillin/streptomycin [PS, from Invitrogen]), under standard cell culture conditions (37°C, 5% CO_2).

2.5.2 Scaffold Fabrication

Porous mineral-containing scaffolds, composed of poly(lactide-co-glycolide) (PLG) and hydroxyapatite (HA), were fabricated by a modified gas forming/particulate leaching method (60). Briefly, scaffolds were prepared with PLG particles (Lakeshore Biomaterials; average diameter = 250 μm), PLG microspheres (formed through a double emulsion process, average

diameter = 5 – 50 μm), HA particles (Sigma, average diameter of 200 nm confirmed with transmission electron microscopy), and sodium chloride particles (sieved to a diameter of 250-400 μm, J.T. Baker). A total of 8 mg of polymer, 8 mg of HA nanoparticles, and 152 mg of NaCl was used and resulted in final scaffold dimensions of 8.5 mm diameter by 1 mm thickness after cold-pressing with a Carver Press (Fred S. Carver). Following high-pressure immersion in carbon dioxide gas and polymer foaming in a non-stirred pressure vessel (Parr Instruments), the scaffolds were leached in de-ionized water for 24 hours to remove NaCl porogen particles. Non-mineral-containing PLG scaffolds, which were HA-free, were also fabricated, as were mineral-containing scaffolds with varying amounts of HA (1:2, 1:4, 2:1 mass ratio with PLG). Prior to cell culture, scaffolds were sterilized by submersion in 70% ethanol for 30 minutes followed by 5 washes in sterile PBS.

2.5.3 Scaffold Characterization

Scanning electron microscopy (SEM) (Leica 440) and light microscopy (Observer.Z1, Zeiss) were used to characterize the microarchitecture and porosity of scaffolds. Energy dispersive spectroscopy (EDS) (Leica 440) was employed to provide elemental analysis of scaffolds, including determination of surface presentation of HA in mineral-containing scaffolds. For SEM and EDS, scaffolds were sputter-coated with gold-palladium to reduce surface charge buildup (Denton Desk II). Scaffolds were tested with MicroCT (GE Healthcare, eXplore CT120) for further microarchitectural analysis and to ensure uniform distribution of HA in mineral-containing scaffolds. Dynamic mechanical analysis (TA Instruments Q800) was used to determine the compressive moduli of the scaffolds.

2.5.4 Western Blot Analysis

Unseeded scaffolds were incubated in cDMEM for 30 minutes, allowing serum proteins to adsorb. Subsequently, the adsorbed proteins were released from the scaffolds by mechanically disintegrating the polymer matrices in a solution of RIPA buffer (Sigma), protease inhibitor cocktail (Sigma), and PMSF (Sigma). Following centrifugation, the resulting scaffold lysates were resolved by SDS-PAGE and were blotted onto a PVDF membrane (BioRad). The membrane was incubated overnight with a rabbit anti-human fibronectin (Sigma) antibody. The membrane was then washed and incubated with a species-specific HRP-conjugated secondary antibody (Novus Biologicals), followed by ECL detection (Amersham Biosciences).

2.5.5 Development and Characterization of 3-D Mineral-containing Tumor Models

1.5 million MDA-MB231 or MCF-7 cells suspended in 30 μL cDMEM were seeded into each scaffold and maintained under dynamic culture conditions on an orbital shaker at 37°C and 5% CO_2 for up to 10 days. Live/Dead assay was performed with calcein/propidium iodide (Invitrogen) staining and visualization on an Epi-fluorescence microscope (Observer.Z1, Zeiss). Cell adhesion was determined by quantifying the number of non-adhered cells 30 min after scaffold seeding using a cell counter (Beckman-Coulter). Blockade of RGD-binding integrins was performed by incubating the cells with 20 μg/mL of soluble RGD (Sigma) for 30 min prior to seeding. To measure cell proliferation, tumor cell-seeded constructs were washed in PBS and lysed in Caron's buffer by sonication. Following centrifugation the DNA content in the supernatant was quantified through fluorescent Hoechst Assay (Invitrogen). For histological analysis tumor constructs were fixed in 10% formaldehyde and embedded in paraffin for sectioning and staining (H&E, von Kossa) according to established protocols.

2.5.6 Analysis of Conditioned Media

Prior to each time point, breast cancer cell seeded-scaffolds were transferred to fresh culture plates, and media was changed to DMEM/1% FBS. Conditioned media were harvested after 24 hours for analysis. VEGF and IL-8 ELISAs (R&D) were performed on these samples according to manufacturer's instructions, while PTHrP secretion was measured using a two-site immunoradiometric assay (Beckman Coulter). Protein secretion was normalized to DNA content as determined by fluorimetric Hoechst Assay. Scaffold-conditioned control media (i.e. media incubated with unseeded scaffolds) was also analyzed for calcium and phosphate ion concentration by atomic absorption.

2.5.7 Osteoclastogenic Response

2.5.7.1 TRAP Stain

RAW 264.7 monocytes were seeded in tissue culture plates and cultured in tumor-conditioned media collected from mineral-containing and non-mineral-containing 3-D tumor models for 5 days with or without 10 μg/mL of IL-8 neutralizing antibody (R&D). cDMEM and scaffold-conditioned control media (i.e. media incubated with unseeded scaffolds) were used as a negative controls, while cDMEM supplemented with RANKL (Sigma) served as a positive control (106). RANKL was added at a concentration of 50 ng/mL, which has previously been shown to induce osteoclastogenesis (66). To quantify osteoclastogenesis, a tartrate-resistant acid phosphatase (TRAP) staining kit (Sigma) was used according to manufacturer's instructions in conjunction with image analysis of TRAP positive, multinucleated cells using AxioVision software (Zeiss). Similar cell numbers between the different experimental conditions were verified with an AlamarBlue assay (AbD Serotec Ltd) as indicated by the manufacturer.

2.5.7.2 Migration Assay

RAW 264.7 monocytes were seeded on top of collagen-coated polycarbonate tissue culture inserts (8 μm pore diameter, Nunc), which were placed into well plates with tumor-conditioned media or control media as specified above. After 8h of incubation, a cotton swab was used to remove cells from the top of the inserts, while cells that had migrated through the polycarbonate membrane towards the conditioned media, were stained with DAPI. Stained inserts were then imaged, and the number of migrated cells was analyzed by AxioVision (Zeiss) image analysis.

2.5.7.3 Osteoclast Activity Assays

RAW 264.7 monocytes were seeded onto Corning Bone Cell Assay Surfaces (81)(kindly provided by Corning Life Sciences) and cultured in the culture media specified above. Osteoclast activity was determined by quantifying calcium release from the Bone Cell Assay Surfaces into culture media due to osteoclast-mediated resorption. Specifically, calcium release was measured by colorimetric detection of complexation of free calcium ions to o-cresolphthalein complexone (Sigma). Additionally, osteoclast activity was determined by light microscopic quantification of resorption pit area on the Bone Cell Assay Surface plates.

2.5.8 Statistical Analysis

One-way ANOVA and Student's t-test were used to determine statistical significance, and $p < 0.05$ is indicated by (*) while $p < 0.01$ is indicated by (**) in all figures. For all experiments, sample size is greater than or equal to 3 for each condition. Data are presented as average; error bars indicate standard deviation.

2.6 Acknowledgments

We thank Dr. Jonathan Butcher and Mark Riccio from Cornell University for their help with microCT analysis, Dr. John Wysolmerski and Pamela Dann from Yale University for their assistance in analysis of PTHrP secretions, Dr. Adele Boskey and Hayat Taleb for atomic absorption analysis of calcium and phosphate, and Corning Life Sciences for kindly providing Bone Cell Assay Surfaces for osteoclast activity assays. This work was supported by an NSF graduate research fellowship (SPP) and funding by the Musculoskeletal Repair and Regeneration Core Center at the Hospital for Special Surgery in New York (Grant AR046121).

CHAPTER 3: HA DRIVES BONE METASTASIS BY INCREASING IL-8 SECRETION TO ACTIVATE SDF-1/CXCR4 METASTATIC AXIS

3.1 Contributors

Frank He performed 3-D culture of MDA-MB231 and the MCF-10A line cells in scaffolds for this study. He also harvested these samples and measured gene expression and IL-8 secretion. Angela Du measured DNA from similar samples. MCF-10A and associated lines were used in collaboration with Dr. Scott Coonrad's lab. Conditioned media studies with hMSCs were performed by Chris Patuwo, who also quantified SDF-1 secretion for these experiments Angela Du also performed all cryosections for this chapter, both scaffold samples and human tissue samples. She also assisted in CXCR4 immunostaining and Western Blotting on scaffold samples. Sunish Mohanan provided pathological diagnosis for human sections stained for IL-8. Drs. Cliff Hudis and Patrick Morris provided human samples from Memorial Sloan Kettering Cancer Center and their accompanying pathological and radiological diagnoses. I performed all other experiments and conceived of experimental design with Dr. Claudia Fischbach.

3.2 Introduction

It is currently estimated that up to 50% of breast cancers are associated with microcalcifications (23). While the presence of microcalcifications was first observed nearly 100 years ago, the number of breast cancers that are diagnosed through screening mammograms that reveal mineral crystals in the breast continues to increase today (107). Mammography is thought to increase the odds of early detection, and this is important due the stark drop off in survival rates (from >90% to <25%) for tumors that are not diagnosed prior to the onset of initial metastasis (9).

Despite their value as diagnostic markers, the relation between microcalcifications and disease progression remains unclear. Firstly, even when microcalcifications are found, they are most frequently not found to be associated with malignant disease (24). Though the reasons for this are not entirely clear, it is worth noting that ectopic calcifications are a common feature of other minor diseases and aging in general. It is also now known that differences in the chemical composition of microcalcifications are correlated with differences in invasiveness. Specifically, only breast calcifications that are composed of bona fide hydroxyapatite (HA) tend to be associated with invasive metastases (24, 27). Secondly, the interaction between HA at microcalcifications and breast cancer cells remains unclear. Currently, microcalcifications are treated strictly as passive indicators of cancer. However, *in vitro* data has shown that HA is bioactive and has pronounced effects on breast cancer cell behavior (24, 63, 108).While correlation with patient data is limited thus far, these findings in conjunction with clinical observations of calcification composition strongly suggest that HA microcalcifications may actively influence and even direct tumor progression and potentially metastasis.

An overwhelming majority of late stage breast cancers metastasize to bone (1, 52). Bone metastases are associated with a number of debilitating symptoms including pain, susceptibility to fracture, and hypercalcaemia (64). The particular avidity to colonize in bone for metastatic breast cancer is well-known, but the specific mediators of this process remain not entirely clear. The long-established seed and soil theory proposes that sites of metastases are fundamentally similar to the primary tumor tissue in some way (1). In this context, it is possible that the appearance of microcalcifications, and specifically the bone-like mineral HA, prime breast cancer cells to metastasize specifically to bone. This thought is supported by studies showing that ductal carcinomas in situ (DCIS) that become invasive tend to display mammographic

microcalcifications (109). In understanding the molecular players that might be involved, past work has highlighted the existence of a "bone metastasis signature". Elevated expression of this set of 5 genes (*matrix metalloproteinase-1* [MMP1], *osteopontin* [OPN], *chemokine CXC receptor-4* [CXCR4], *connective tissue growth factor* [CTGF], and *interleukin-11* [IL11]) (18, 110) is highly correlated with metastasis to bone. Studies have shown that within tumors, there is heterogeneous expression of the bone metastasis gene signature, but the mechanistic origin of the signature is unknown. We hypothesize that microenvironmental features such as calcifications might play a role in inducing enhanced expression of the bone metastasis signature.

Beyond expression of these 5 genes, cytokine signaling networks are expected to play a role in metastagenicity (111, 112). Specifically, tumor-derived interleukin-8 (IL-8) may be involved in driving metastasis to bone. Elevated plasma levels of IL-8 have been correlated with increased prevalence of bone metastasis clinically (113, 114). Further, specific inhibition of IL-8 has blocked tumor growth in xenograft models (115). There is also evidence to suggest that IL-8 may be specifically upregulated in the presence of mineral (63, 108), a mechanism that could be related to physiological interactions between microcalcifications and developing mammary tumor cells. Soluble factors in the bone microenvironment may also be critical. Stromal-derived factor-1 (SDF-1) is known to be enriched in marrow compartment of bone, and it has also been shown to function as a chemoattractant for cancer cells through the surface receptor CXCR4 (116, 117). The establishment of a pre-metastatic niche has been thought to be an initial prerequisite to support metastatic colonization (49), and upregulation of SDF-1 in the bone could feasibly be a part of this process. Emerging data suggests that IL-8 may actually induce increased SDF-1 secretion from stromal cells found in the bone or sensitize the SDF-1/CXCR4 axis by promoting CXCR4 surface expression (57, 118). Taken together, these data strongly suggest that

the interplay between microcalcifications, tumor-derived IL-8, and SDF-1 in bone marrow mediates breast cancer metastasis to bone.

Three-dimensional (3-D) tissue culture has been used to create *in vitro* tumor models that recapitulate microenvironmental conditions much more accurately than conventional two-dimensional cultures (119, 120). Within fabricated 3-D scaffolds, cancer cells organize themselves into tumor-like structures and have been shown to exhibit behavior reflective of *in vivo* conditions (79, 121). 3-D scaffolds have also proven to be useful in presenting mineral, such as HA, to cells, as they allow direct cell-mineral interaction (60, 63, 108). Previous scaffold systems have provided fundamental insight on how cells might target bone and respond to the bone microenvironment (100, 122). However, mineral in scaffolds is actually extremely well-suited to the study of cell-microcalification interactions. We therefore used an engineered mineral-containing scaffold that had previously been confirmed to allow cell-mineral interactions (63) to investigate how cancer cell behavior may be regulated by HA and how this may affect migration towards bone. Our findings suggest that microcalcifications may direct tumor cell colonization of bone by providing a microenvironmental trigger that alters gene expression and regulates metastasis via the SDF-1/CXCR4 axis.

3.3 Materials and Methods

3.3.1 Scaffold Fabrication

Scaffolds were created as previously described (60, 123). For mineral-containing (MIN) scaffolds (124), poly(lactide-co-glycolide (PLG) particles (Lakeshore Biomaterials, ground and sieved, average diameter 250 μm) and PLG microspheres (formed through double emulsion process, 5-50 μm diameter) were dry-mixed with nanocrystalline hydroxyapatite (Sigma) and porogenic NaCl (J.T. Baker, sieved, average diameter 250-400 μm). The mixture was then

pressed using a dye press (Fred S. Carver). The resulting matrices (8.5 mm diameter, 1 mm thickness) were pressurized in carbon dioxide (800 psi) in a non-stirred vessel (Parr Instruments 4677). Following de-pressurization to allow polymer foaming, scaffold were soaked for 24 hours in DI water to leach out the salt. Non-mineral-containing (125) scaffolds (NM) were fabricated similarly, excluding the hydroxyapatite in the starting mixture. For characterization of mineralization, scaffolds were soaked in Alizarin Red (20%) and then washed 4 times in PBS. To observe general cell morphology upon seeding, scaffolds were fixed in 10% formalin, embedded in paraffin blocks, cut in cross section, and stained with hematoxylin and eosin (H&E) or von Kossa for visualization of tissue formation and cell association with mineral. Mineral-containing scaffolds were decalcified prior to sectioning.

3.3.2 Cell Culture

MDA-MB231 human mammary tumor cells (ATCC), bone-metastatic (2287), and lung-metastatic (4175) MDA-MB231 subpopulations (kindly provided by Dr. Joan Massague), MCF-10A cells and derivative lines (62) (used in collaboration with Dr. Scott Coonrod), and human mesenchymal stem cells (hMSCs, Lonza) were maintained under standard culture conditions (37°C, 5% CO_2). Complete DMEM (10% FBS [Tissue Culture Biologics], 1% PS [Gibco]) was used to culture MDA-MB231, Lonza MSCBM with SingleQuots was used for hMSCs, and DMEM/F12 (5% Horse serum [Invitrogen], 1 % PS, 100 ng/mL Cholera toxin [Sigma], 20 ng/mL EGF [Millipore], 0.5 µg/mL Hydrocortisone [Sigma], 10 µg/mL Insulin [Sigma]) was used for the culture of MCF10A-derived series of cells.

For 3-D culture, MIN and NM scaffolds were sterilized in 70% ethanol for 30 minutes. The NM scaffolds were used as controls in all studies to specifically examine effects mediated by presence of HA. After sterilization, scaffolds were subsequently washed 5X in sterile PBS,

and then soaked in culture medium for 30 minutes at 37°C to allow adhesive protein adsorption. Following incubation in medium, scaffolds were transferred to fresh culture plates, and 1.5 X 10^6 MDA-MB231 cells were statically seeded on top. 3-D cultures were maintained under standard culture conditions on an orbital shaker for up to 10 days. Adhesion was measured by harvesting scaffolds 30 minutes after seeding, while other time points were used for analysis of protein secretions (3 days), gene expression (10 days), and pre-culture for intracardiac injections (10 days).

3.3.3 Analysis of Bone Metastatic Gene Signature

For analysis of gene expression, scaffolds were harvested after 10 days in culture. RNA was collected by degrading tumor cell-seeded scaffolds in TRIzol® (Invitrogen) and then extracting total RNA according to manufacturer protocol. Total RNA (1 μg) was reverse transcribed to cDNA (High Capacity cDNA Reverse Transcription Kit with random hexamers [(Applied Biosystems)]), and subjected to real-time RT-PCR (25 ng template, run in triplicate) using SYBR green detection (Quanta) on an Applied Biosystems 7500 System. All primer sequences were synthesized by IDT Technologies , and β-actin was used as an endogenous loading control gene. The following sequences were used: human IL-8 (fwd: 5'-agaaaccaccggaaggaaccatct-3', rev: 5'-agagctgcagaaatcaggaaggct-3'), human OPN (fwd: 5'-agttctgaggaaaagcagc-3', rev: 5'-cccctaccggaacatacg-3'), human MMP1 (fwd: 5'-aatgcaggaattctttggg, rev: atggtccacatctgctcttg-3'), human IL11 (fwd: 5'-agatatcctgacattggccaggca-3', rev: 5'-acttcagtgatccactcgcttcgt-3'), human CXCR4 (fwd: 5'-agggaactgaacattccagagcgt-3', rev: 5'-aaacgttccacgggaatggagag-3'), human IL13Rα2 (fwd: 5'-acggaatttggagtgagtgg-3', rev: 5'-tggtagccagaaacgtagca-3'), human MMP2 (fwd: 5'-gcggcggtcacagctactt, rev: 5'-cacgctcttcagactttggttct-3'), and human β-actin (fwd: 5'-

aatgtggccgaggactttgattgc-3', rev: 5'-aggatggcaagggacttcctgtaa-3') For quantitative analysis, the previously developed $\Delta\Delta C_t$ method was employed (126).

3.3.4 Collection of Conditioned Media

3-D cultures were used to generated conditioned media. After 2 days in culture, scaffolds were transferred to fresh culture plates to eliminate the influence of cells that had initially adhered to the culture plate during seeding. Concurrently, culture medium was refreshed with serum-depleted medium (1% serum). After 24 hours, media was harvested. First, it was centrifuged at 4000 rpm for 10 minutes, and the supernatant was collected to eliminate any cellular debris. Subsequently, it was concentrated to 10X using a centrifugal concentrator with 5 kDa molecular weight cutoff (Millipore). To directly compare the effects of soluble factors between NM and MIN scaffold cultures, conditioned media was normalized to cell number by diluting in fresh serum-depleted media. 10X conditioned medium was stored at -20 prior to use in culture. The medium was then re-diluted with fresh basal medium to a final concentration of 2X for use as culture medium.

3.3.5 Luciferase Labeling

Cells were labeled with luciferase using the Cignal Lenti Reporter system (Qiagen). MDA-MB231 cells and subpopulations were plated in minimal medium and allowed to adhere overnight. Lentivirus was added to cells according to manufacturer's instructions to stably induce luciferase expression. After 16 hours, lentivirus was removed, and cells were refreshed with basal media. Cells were then fed puromycin (puromycin.com) for selection of positively transduced cells. Puromycin was given every 3 days for one week at 0.5 µg/mL in basal media. Following selection, cells were maintained again under standard conditions.

3.3.6 SDF-1 and IL-8 ELISA

To quantify secretion of IL-8 by breast cancer cells in 3-D, seeded-scaffolds were transferred to fresh culture plates, and media was changed to DMEM/1% FBS 24 hours prior to collection of media. Upon collection, IL-8 ELISA (R&D) was performed on these samples according to manufacturer's instructions. When media was harvested, scaffolds were lysed in Caron's Buffer and sonicated to liberate DNA. Total DNA content was measured from these samples by Quantifluor assay according to manufacturer instructions (Invitrogen). For hMSC secretion of SDF-1, a 2-D culture of hMSCs was pre-treated with conditioned media from tumor-cell seeded scaffolds for 24 hours. Next, media was refreshed to hMSC basal media. 24 hours after this, hMSC media was collected for SDF-1 analysis. SDF-1 ELISA was used (R&D systems) according to manufacturer instructions, and secretion was normalized to cell number as assessed by hemacytometer.

3.3.7 Transwell Migration Assay

Migration assays were performed using a transwell (8.0 μm pores, BD Falcon fluoroblock) in a 24-well culture plate. Prior to assay, transwells were coated with collagen I (Gibco) on one side by soaking. In all assays, the bottom chamber either contained 5 X 10^3 plated hMSCs or 0.5 ng/mL SDF-1 (R&D Systems). The top chamber was seeded with 5 X 10^3 cells, and migration took place over 8 hours, after which time transwells were fixed in formalin and stained with DAPI. DAPI stained images were analyzed manually to determine cells per field with 20X objective. For each well, at least 5 fields were analyzed. Fields were selected away from the edges of the wells to avoid autofluorescent interference. For each condition, at least 3 wells were quantified, and all migration graphs represent an overall pooled average of counts from all wells. For inhibition studies, cells in the top chamber were pre-incubated with 25 μg/mL of anti-CXCR4 (R&D Systems) to inhibit the migratory receptor prior to seeding.

Alternatively, 150 µg/mL of anti-SDF-1 or 10 µg/mL of anti-IL-8 (R&D Systems) was added to the bottom chamber to inhibit molecules in solution.

3.3.8 CXCR4 Western Blot

Lysates from 3-D scaffold cultures were collected in 300 µL RIPA buffer (Sigma) with protease/phosphatase inhibitors (Sigma) and PMSF (Calibochem) per sample. Scaffolds were mechanically chopped in buffer followed by sonication. The samples were then pelleted via microcentrifuge and the supernatant collected for Western Blot analysis. Protein concentrations were determined by bicinchoninic acid proteins assay (Thermo Scientific), and equal amounts were loaded into the gel. Proteins were separated by SDS/PAGE and transferred to a PVDF membrane (bio-rad). The membrane was incubated overnight at 4°C with primary antibodies against GAPDH (0.1 µg/mL, Sigma) and CXCR4 (2 µg/mL, Abcam), followed by 1 hr incubation with HRP-conjugated anti-rabbit secondary antibody (Novus Bio) and HRP-conjugated anti-mouse secondary antibody (Millipore) at room temperature. Chemiluminescence detection was performed to visualize the protein using an ECL kit (Thermo Scientific). ImageJ software was used in gel analysis mode to quantify differences in observed bands.

3.3.9 Animal Studies

All work was performed in accordance with standards set by the Cornell University Institution Animal Care and Use Committee. BALB/C-nu nude mice (Taconic Farms) were used for all studies.

For intracardiac injection, luciferase-labeled cells were prepared by pre-culture in scaffolds for 10 days. Prior to injection, cells were trypsinized for removal from scaffolds, and suspended in PBS at a concentration of 10^6/mL. 100 µl of the suspension was injected into the left-ventricle of 4-week old mice. After injection, mice were imaged by bioluminescence under

isoflurane weekly for up to 12 weeks. Upon euthanasia, blood, tumors, lungs, and bones were harvested for *ex vivo* analysis. Tumors were divided for collection of lysates in T-PER buffer (pierce) and formalin-fixation/paraffin-embedding. Bones and lungs were collected in formalin for paraffin embedding. Blood was collected via cardiac puncture and immediately added to ice cold EDTA at 1 mL blood per 50 µL EDTA in a microcentrifuge tube. The tube was inverted and kept on ice prior to centrifugation, after which the plasma supernatant was collected and stored for analysis.

For all studies, paraffin sections were stained with H&E and analyzed for characterization of malignant features using the ScanScope System and software (Aperio). H&E sections of bone were analyzed for trabecular thickness and bone volume fraction by measuring dimensions of trabeculae with the ScanScope software. Lysates were analyzed for IL-8 and plasma for SDF-1 by ELISA (R&D Sytems DuoSet) according to manufacturer's instructions.

3.3.10 Bioluminescent Imaging (BLI)

Mice were injected intraperitoneally with Luciferin (Gold Biotechnology) (150 mg/kg) 5 minutes prior to imaging. On-board isoflurane (2%) was used during imaging in the system (Xenogen IVIS-200). Settings and analysis were controlled via the accompanying software (Living Image). All luminescence scales are reported in photons/second/square cm/steradian ($p/sec/cm^2/sr$).

3.3.11 Cryosectioning and Immunostaining

Scaffold cultures were washed with cold PBS and then fixed in 4% paraformaldehyde. After fixation, scaffolds were soaked in 20% sucrose at 4°C overnight to prevent crystal formation during freezing and subsequently mounted in OCT (Bio-Tek). Tissue samples were provided as frozen blocks on transfer from Memorial-Sloan Kettering. Frozen blocks were

cryosectioned to 12 µm thickness and mounted on pre-cleaned glass slides. Prior to staining, sections were baked for 20 minutes at 65°C and re-hydrated in Tris-buffer. For IL-8 immunohistochemsitry (IHC), sections were then blocked with 3% hydrogen peroxide to prevent signal interference from endogenous activity. Antigen retrieval was performed with Proteinase K (Dako), and TNB solution (Perkin-Elmer) was used for blocking. Sections were incubated with primary antibody against IL-8 (5 µg/mL, R&D Systems) overnight at 4°C, followed by a 30 min incubation at room temperature with a biotinylated secondary antibody against mouse (Vector Labs). To increase signal, the TSA amplification kit (Perkin-Elmer) was used according to manufacturer's direction. Signal detection was performed with DAB chromogen (Thermo Scientific), and sections were counter-stained with hematoxylin. Slides were then dehydrated via ethanol gradient and mounted with Entellan (Merck). Slides were scanned using the ScanScope System (Aperio) for imaging purposes. For CXCR4 immunofluorescence, antigen retrieval was performed in citrate buffer before sections were incubated with a primary antibody against CXCR4 (25 µg/mL, R&D Systems), followed by an AlexaFluor 647-conjugated anti-mouse secondary antibody (Invitrogen). For luciferase immunofluorescence, antigen retrieval was done through digestion with proteinase K for 10 minutes, and then sections were incubated with primary antibody against luciferase (1 µg/mL, Sigma), followed by an AlexaFluor 488-conjugated antimouse secondary antidbody (Invitrogen). All immunofluorescence samples were counterstained with DAPI (Invitrogen) and mounted in ProLong Gold Antifade Reagent (Invitrogen). Fluorescence imaging was performed with a Confocal Microscope (Zeiss 710) or epi-fluorescence microscope (Zeiss Observer.Z1).

3.3.12 Human Sample Analysis

16 patient samples overall were obtained for analysis. Scanned IHC images with IL-8 stain were transferred to a pathologist for specific evaluation and diagnosis. Slides were scored for gross intensity of IL-8 staining, and individual acini and ductal structures were identified for each slide and scored according to ductal integrity/proliferative capacity as well as intensity of IL-8 stain. Sections were comprehensively analyzed to identify all ductal structures, and all ductal structures in each section were included in analysis. If at least 3 ducts were not able to be indentified in a section, the section was not used in analysis All metrics were scored on a 0-3 scale, with 0 representing negligible intensity or proliferation and 3 representing maximal staining or excessive proliferation and total deterioration of acinar architecture. This analysis was performed blind, without knowledge of radiology or pathology reports from consulting clinicians. After full evaluation was completed, IHC evaluation was compared with radiology and pathology notes and CXCR4 immunofluorescence results for final analysis.

3.3.13 Statistical Analysis

For figures, experiments were run independently in triplicate to verify trends. Graphs and images represent these trends. For all *in vitro* studies, experiments were run with sample number of 3 or 4. For *in vivo* work, groups of mice initially consisted of five mice, but groups of 3 or 4 were also included in analysis in the case of unexpected animal death. Statistical analysis was performed in GraphPad Prism 5. Student's t test or ANOVA with Tukey post-hoc analysis was used to establish statistical significance ($p<0.05$), and in all graphs, (*) indicates $p < 0.05$. All data are represented as average ± standard deviation.

3.4 Results

3.4.1 Cell-mineral interactions in scaffolds

Scaffolds were tested to ensure that they allowed direct interaction of HA with breast cancer cells. To test surface presence of mineral within scaffold pores, scaffolds were soaked in calcium-binding Alizarin Red. When compared to non-mineral-containing control scaffolds, the mineral-containing scaffolds showed strong absorption of the red stain, suggesting surface availability of HA (Fig.3.1A). Upon static seeding of scaffolds (shown schematically in Fig. 3.1B), cross-sectional H& E staining showed that cells are able to adhere throughout the scaffold (Fig. 3.1C), and von Kossa staining showed that cells attach along mineral-containing surface (Fig. 3.1D). The adhesion of cells to HA is in agreement with our past findings, indicating that cells have >90% seeding efficiency in mineral-containing scaffolds, significantly enhanced relative to non-mineral-containing controls (63).

3.4.2 Growth and IL-8 secretion by ductal carcinoma in situ (DCIS) cells in mineral-containing scaffolds

Our previous work has indicated that HA stimulates IL-8 secretion and growth in MDA-MB231 cells (63). To understand if these changes in phenotype were a cell line specific phenomenon or if this trend holds for other transitioning or malignant cells, these effects were studied with MCF10A-DCIS cells. Similar behavior was observed for DCIS cells in mineral-containing scaffolds. A DNA assay indicated that growth and adhesion are enhanced for these cells HA-containing constructs, with 50% more growth overall due to either cell division or induction of polyploidy, which could contribute to genetic instability (Fig. 3.2A). Additionally, ELISA analysis showed that DCIS cells also increased IL-8 secretion 3-fold in mineral-containing scaffolds relative to non-mineral-containing controls (Fig. 3.2B). Interestingly, a similar increase in IL-8 secretion was observed for MCF10CA1A invasive carcinoma cells, but not for MCF10A normal mammary epithelial cells (Fig. 3.2B).

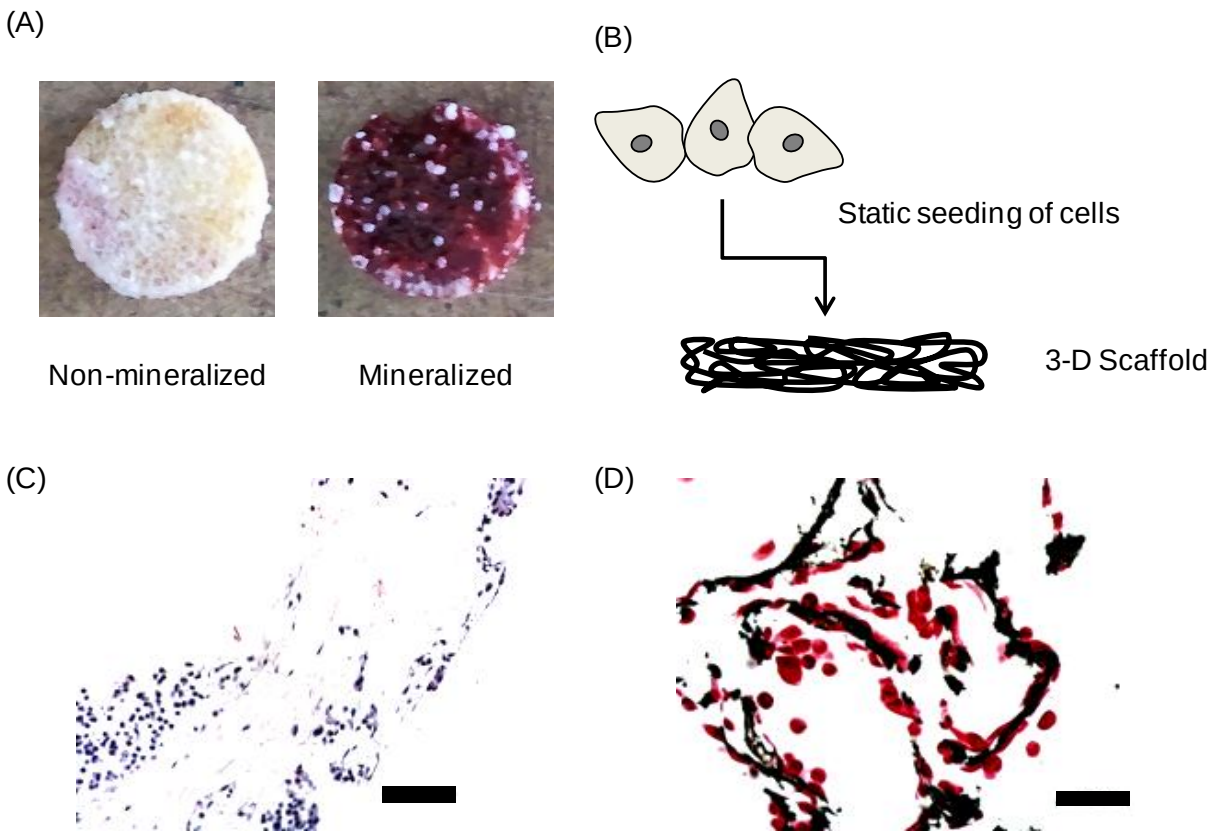

Figure 3.1: Gas foaming/particulate leaching for scaffold creation
(A) Alizarin red calcium-binding stain shows that mineral-containing scaffolds present HA at surface for cellular availability. (B) Schematic showing that simple static seeding is used for scaffold prior to dynamic cell culture. (C) H&E stain indicating heterogeneity of cells in scaffold upon seeding. Scale bar represents 100 µm. (D) Von Kossa stain (mineral in black, cell nuclei in red) indicating that cells attach around mineral in scaffolds. Scale bar represents 50 µm.

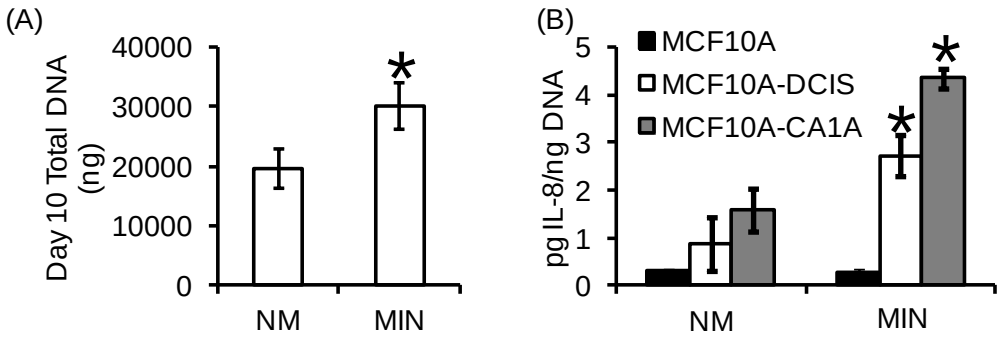

Figure 3.2: Cellular response of MCF10A line of cells in scaffolds
(A) DNA assay indicated that MCF10A-DCIS cell grow more in MIN scaffolds. (B) Tumorigenic MCF-10A cells (CAIA and DCIS) increase IL-8 secretion in MIN scaffolds according to ELISA.

3.4.3 Bone metastasis signature in mineral-containing scaffolds

To determine if expression of the bone metastasis gene signature might be related to the presence of HA, the transcription of these gene was investigated for cells cultured within scaffolds. It was found that the majority of the genes in the bone metastasis signature were upregulated in the presence of mineral for parental MDA-MB231 cells (Fig. 3.3A). These included OPN, CXCR4, and MMP1. Gene expression analysis also confirmed that IL8 mRNA levels increase in response to the presence of HA (Fig. 3.3A). Furthermore, when a lung-specific subpopulation of MDA-MB231 cells (4175LM) was cultured in mineral-containing scaffolds, expression of IL8, CXCR4, and OPN all increased (Fig. 3.3B). It was found that over time in mineral-containing culture, 4175LM expression of these genes approached levels found in an established bone-specific subpopulation of MDA-MB231 cells (2287BM). Conversely, 4175LM cells downregulated expression of CXCL1, IL13Rα2, and MMP2 (Fig. 3.3C), which are genes that have been identified as part of a lung metastasis gene signature (124).

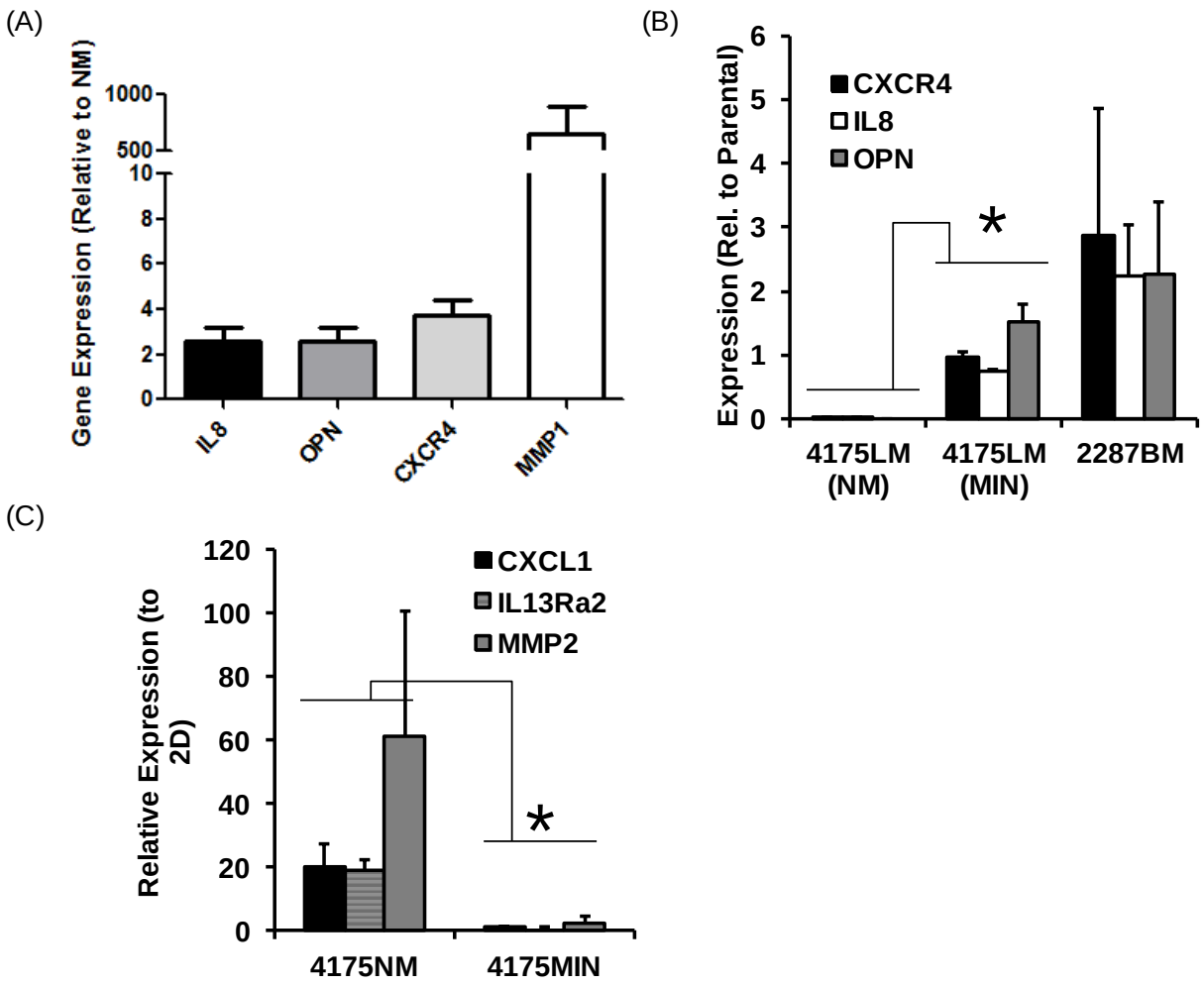

Figure 3.3: Expression of tissue-tropic metastasis signatures in scaffolds
(A) mRNA analysis shows that bone metastasis gene signature is partially enriched on mineral-containing scaffolds for general parental population of MDA-MB231 cells. (B) Mineral also "reprograms" cells, as it induces increased expression of these genes for cells that previously were directed to lung (4175 LM) and (C) decreases expression part of the lung metastasis gene signature.

3.4.4 Effect of tumor-derived IL-8 on mesenchymal stem cells and tumor cell migration

The functional effects of HA-regulated secretion of IL-8 were studied next. To understand the potential role IL-8 plays in paracrine or endocrine signaling, its effect on MSCs, the prevalent stromal cell type in bone, was explored. Culturing MSCs with tumor-conditioned media (TCM), it was initially found that tumor-derived soluble factors stimulated MSC secretion of SDF-1 (Fig. 3.4A). Furthermore, this response was enhanced for TCM from mineral-

containing cultures (124) relative to non-mineral-containing cultures (125). Looking specifically at the role of IL-8 among the milieu of factors in TCM, SDF-1 secretion increase in response to purified IL-8 was similar to that provoked by TCM (Fig. 3.4B). Monoclonal antibody inhibition of IL-8, indicated that IL-8 in TCM did indeed underlie increased MSC secretion of SDF-1. Finally, by inhibiting MSC surface receptors to IL-8 (CXCR1 and CXCR2), it was determined that IL-8 based induction of SDF-1 happens via the CXCR1 receptor (Fig. 3.4B).

SDF-1 is known to attract breast cancer cells via CXCR4, and the effects of TCM-induced, MSC-derived SDF-1 on MDA-MB231 migration were next investigated using a transwell migration assay. The experimental setup is shown schematically in Fig. 3.5A. The transwell membrane allows soluble factor exchange and directed migration of MDA-MB231 cells. When MSCs were first treated with IL-8, they strongly attracted MDA-MB231 cells relative to control conditions. However, when antibodies against SDF-1 or its cognate receptor CXCR4 were introduced into the setup, this effect was strongly attenuated (Fig. 3.5B). Since overall results indicated that HA-containing cultures did not just stimulate increased SDF-1 secretion by MSCs, but also upregulation of CXCR4 for breast cancer cells (Fig. 3.3), the contribution of higher receptor concentration to migration was also explored. Immunofluorescence and Western blot analysis confirmed that both DCIS (data not shown) and MDA-MB231 cells in HA-containing scaffolds have more of the CXCR4 receptor (Fig. 3.6A). When cells were pre-conditioned in mineral-containing scaffolds prior to seeding in the transwell, they exhibited enhanced migration as well, and this effect was abolished by treatment with a monoclonal antibody against CXCR4 (Fig. 3.6B).

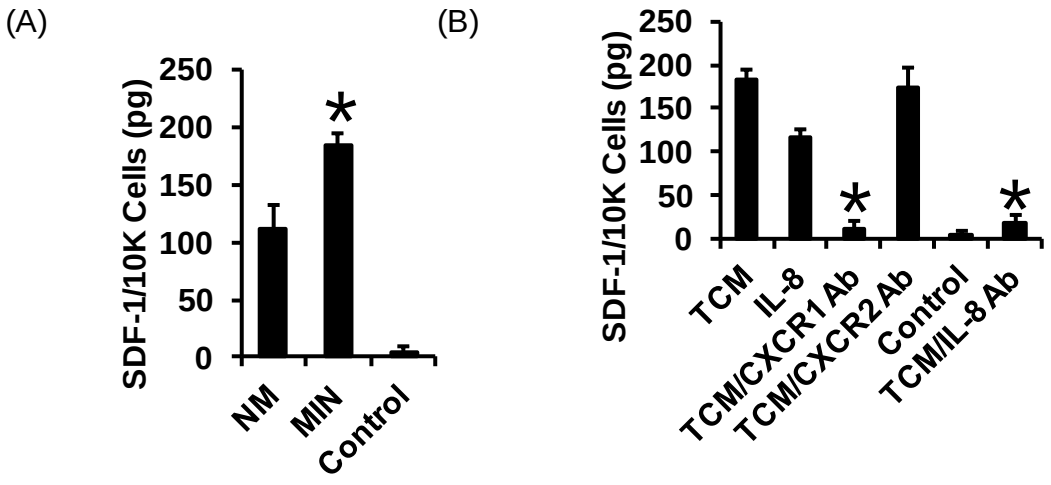

Figure 3.4: SDF-1 Secretion by MDA-MB231 cells in response to IL-8
(A) Tumor conditioned media (TCM) stimulates SDF-1 secretion by mesenchymal stem cells (hMSCs), and media from mineral-containing scaffold cultures evokes larger response. (B) Inhibition studies with monoclonal antibodies suggest that IL-8 in TCM is responsible for induction of SDF-1 secretion via CXCR1

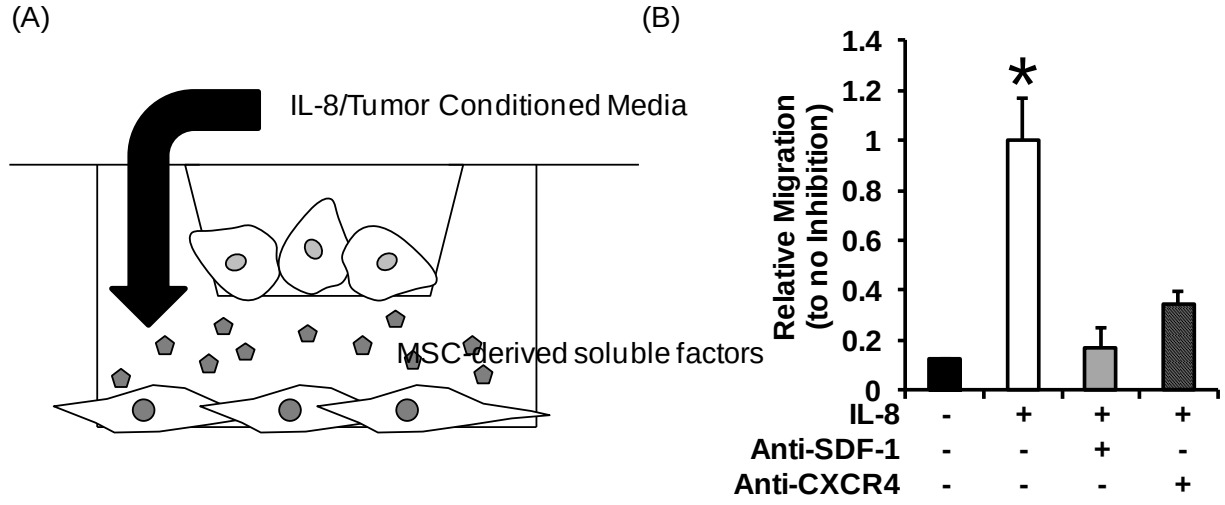

Figure 3.5: Migratory response due to IL-8 stimulation of SDF-1/CXCR4 axis
(A) Schematic of Transwell migration assay set up. (B) hMSCs treated with IL-8 produced strong migratory response from MDA-MB231 cells in a Transwell migration assay, and inhibiting SDF-1 in media or its cognate receptor CXCR4 on tumor cell surface with antibodies attenuated this migratory response.

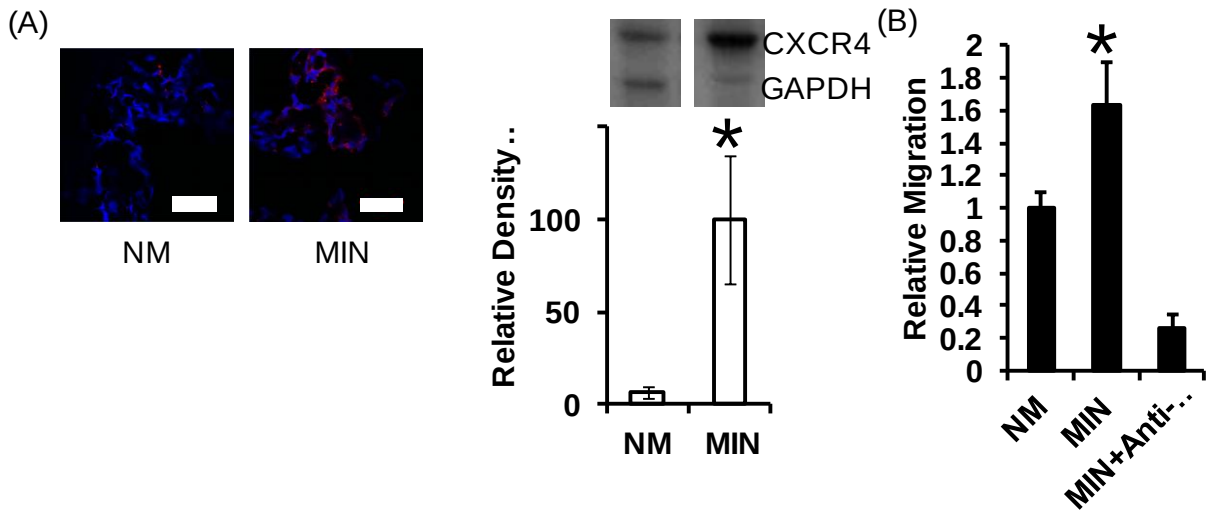

Figure 3.6: Modulation of CXCR4 levels by HA and effect on tumor cell migration
(A) Immunofluorescence and Western Blot confirmed increased levels of CXCR4 protein in and on the surface of cells cultured in mineral-containing scaffolds. Scale bars represent 50 μm. (B) Cells that were pre-cultured in mineral-containing scaffolds displayed enhanced migratory capability relative to those cultured in non-mineral-containing scaffolds, and this effect was inhibited by anti-CXCR4.

3.4.5 Changes in metastatic tropism in vivo due to exposure to HA

Because significant gene expression changes were observed for MDA-MB231 cells *in vitro*, the functional consequences for *in vivo* behavior were next examined. 4175LM cells that had been pre-cultured in HA-containing scaffolds (4175MIN) were found to predominantly colonize bone, while 4175LM cells from control scaffolds (4175NM) maintained their original pattern of lung seeding, based on luminescent tracking of tumor cells (Fig. 3.7A-B). Histological analysis showed pleomorphism and osteolytic effects in bones of mice injected with 4175MIN, including trabecluar thinning and loss of trabeculae relative to control conditions (Fig. 3.7C). Further confirmation of cells from mineral-containing scaffolds was attained through anti-luciferase staining for tumor cells (Fig. 3.8D). Histology and immunofluorescence also showed severe lung lesions only for mice injected with 4175NM (Fig. 3.9).

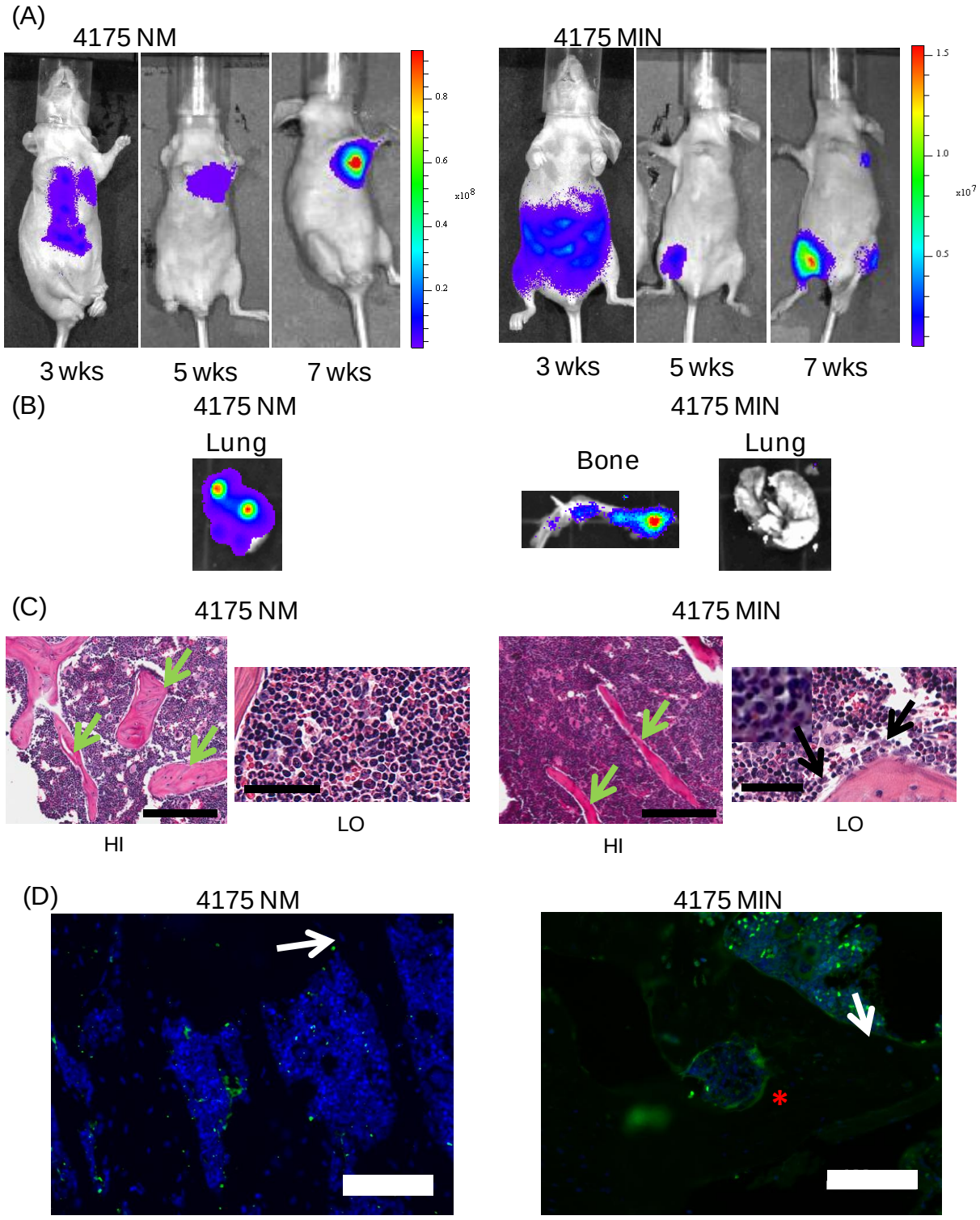

Figure 3.7: *in vivo* colonization of intracardailly injected MDA-MB231 4175LM cells pre-conditioned in scaffolds

(A) 4175 cells pre-conditioned in non-mineral-containing scaffolds (4175NM) colonize lungs, while those pre-conditioned in mineral-containing scaffolds (4175MIN) colonize bone as demonstrated by *in vivo*

bioluminescent tracking. Heat bars indicate radiance in photons/sec/cm^2/sr. (B) *ex vivo* BLI shows positive signal indicative of tumor cell colonization in lungs of 4175NM and femur bone of 4175MIN-injected mice (C) H&E sections of femur indicate potential thinning of trabeculae and neoplastic transformation. Green arrows indicate trabeculae and black arrows show pleomorphism that suggested transformation. Scale bars in "HI" magnification represent 100 µm and scale bars in "Lo" magnification represent 200 µm. Inset in panel four shows 20X magnification of pleomorphic cells. (D) Luciferase immunofluorescence on sections of bone indicate the presence of injected tumor cells. Positive stain is in green, while cell nuclei are counterstained with DAPI in blue. White arrows indicate cortical bone surfaces, while red star shows presence of positively stained cells invaded into bone. Scale bars represent 100 µm.

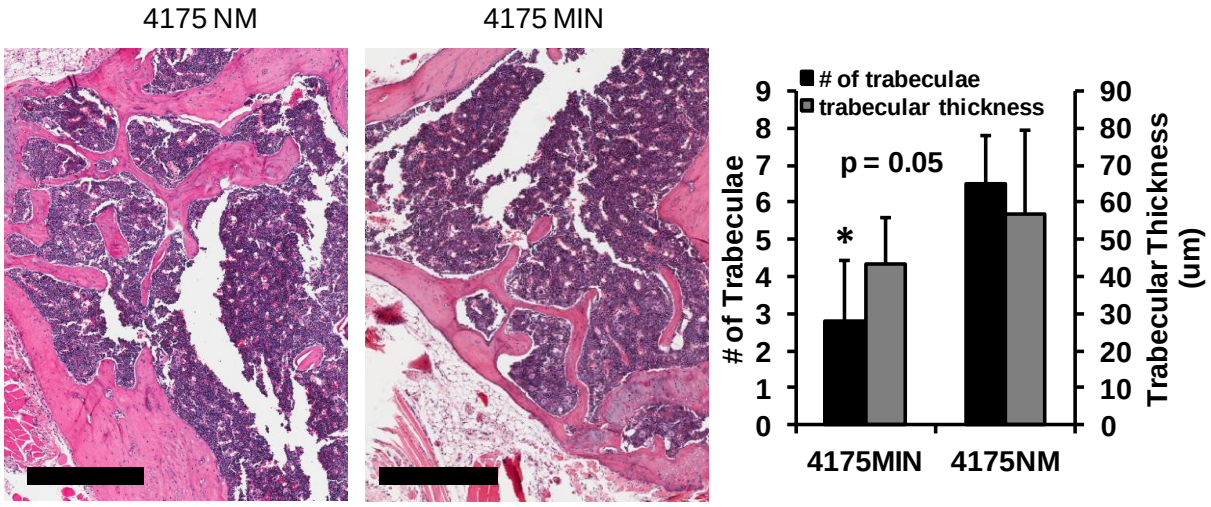

Figure 3.8: Quantification of osteolysis in intracardially injected mice
Osteolysis was quantified by general decrease in number and thickness of trabeculae in mice as observed in H&E images. Images for quantification were sampled from proximal femur of mice. Representative images used for quantification are shown. Scale bars represent 500µm, and green boxes indicate trabeuclae that were sampled in analysis

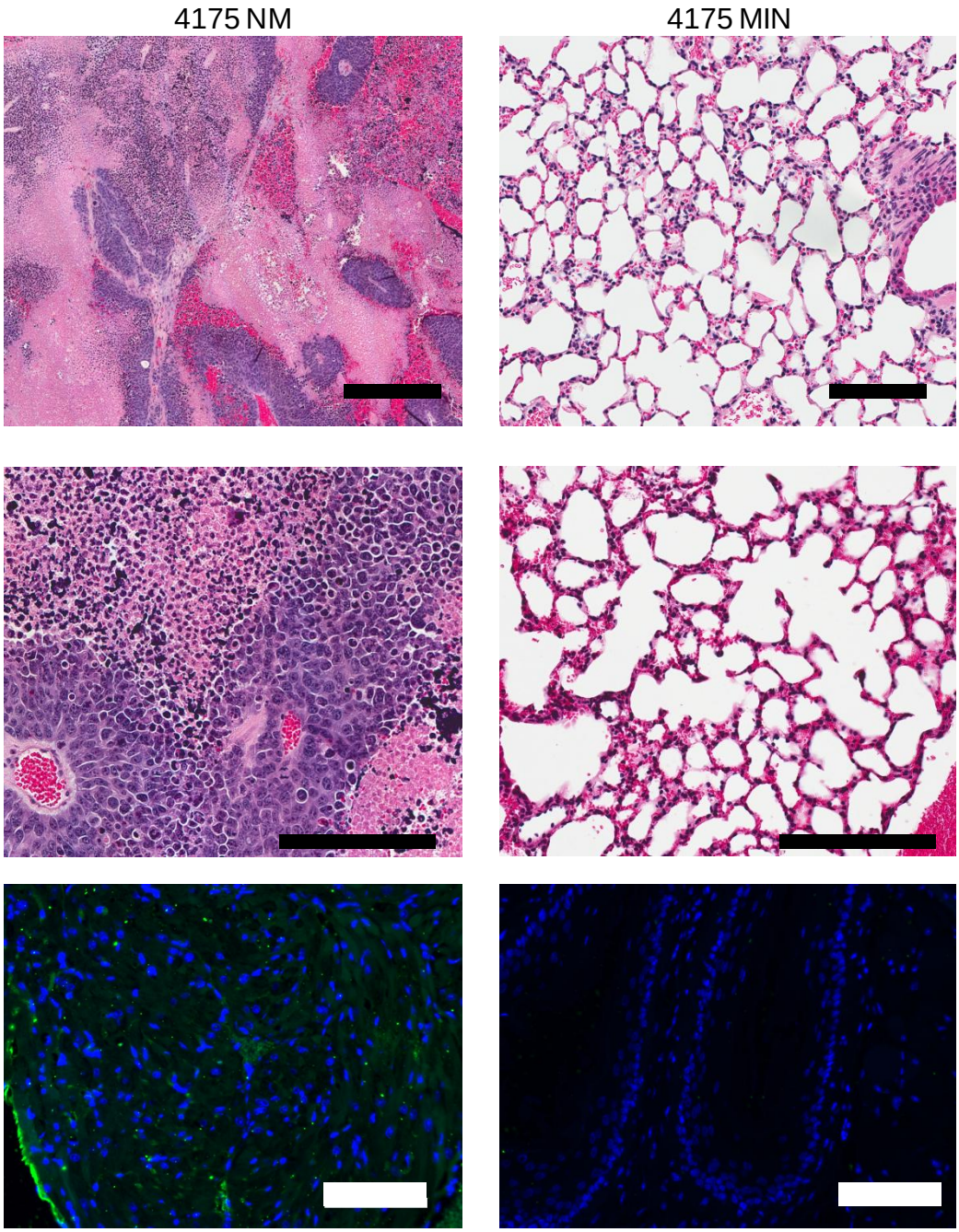

Figure 3.9: Colonization of lung by intracardially injected MDA-MB231 cells pre-conditioned in scaffolds

Low (top) and higher magnification (middle) images of H&E-stained lung sections of mice show aggressive colonization of lungs only for mice injected with cells pre-conditioned in non-mineral-containing scaffolds. Black scale bars indicated 200µm. Luciferase immunofluorescence (bottom) shows positive staining in green, indicative of tumor cell colonization, also only for 4175NM. White Scale bars represent 100 µm.

3.4.6 Preliminary correlations between ductal proliferation, presence of IL-8, and microcalcifications

As *in vitro* data indicate a potentially crucial role for IL-8 in conjunction with microcalcifications, human tumor samples were analyzed histologically for both. Samples demonstrated variable staining patterns, with IL-8 present in ducts, stroma, or both (Fig. 3.10A). Within samples, it was observed that there was at least preliminary correlation between a pathological score of ductal proliferation and IL-8 levels within the corresponding duct (Fig. 3.10B). Total tissue IL-8 levels were found to generally correlate with a pathology diagnosis of microcalcifications, as well as a radiology diagnosis of microcalcifications, but these findings were limited by a small sample size and few disease-free tissues included in the study. Finally, tissue samples were also fluorescently stained for CXCR4. Distribution of CXCR4 varied, also being identified as stromal or ductal. Overall, there were far more sections that did not stain at all for CXCR4 as compared to IL-8 (7/16 vs. 2/16). Notably, sections that stained positive for CXCR4 were also sections observed to have the highest ductal IL-8 levels and were more likely to be from patients that had detectable microcalcifications according to mammography (Table 3.1). Furthermore, sections with higher gross staining of IL-8 throughout tissue were largely associated with mammographic calcifications and positive CXCR4 immunofluorescence.

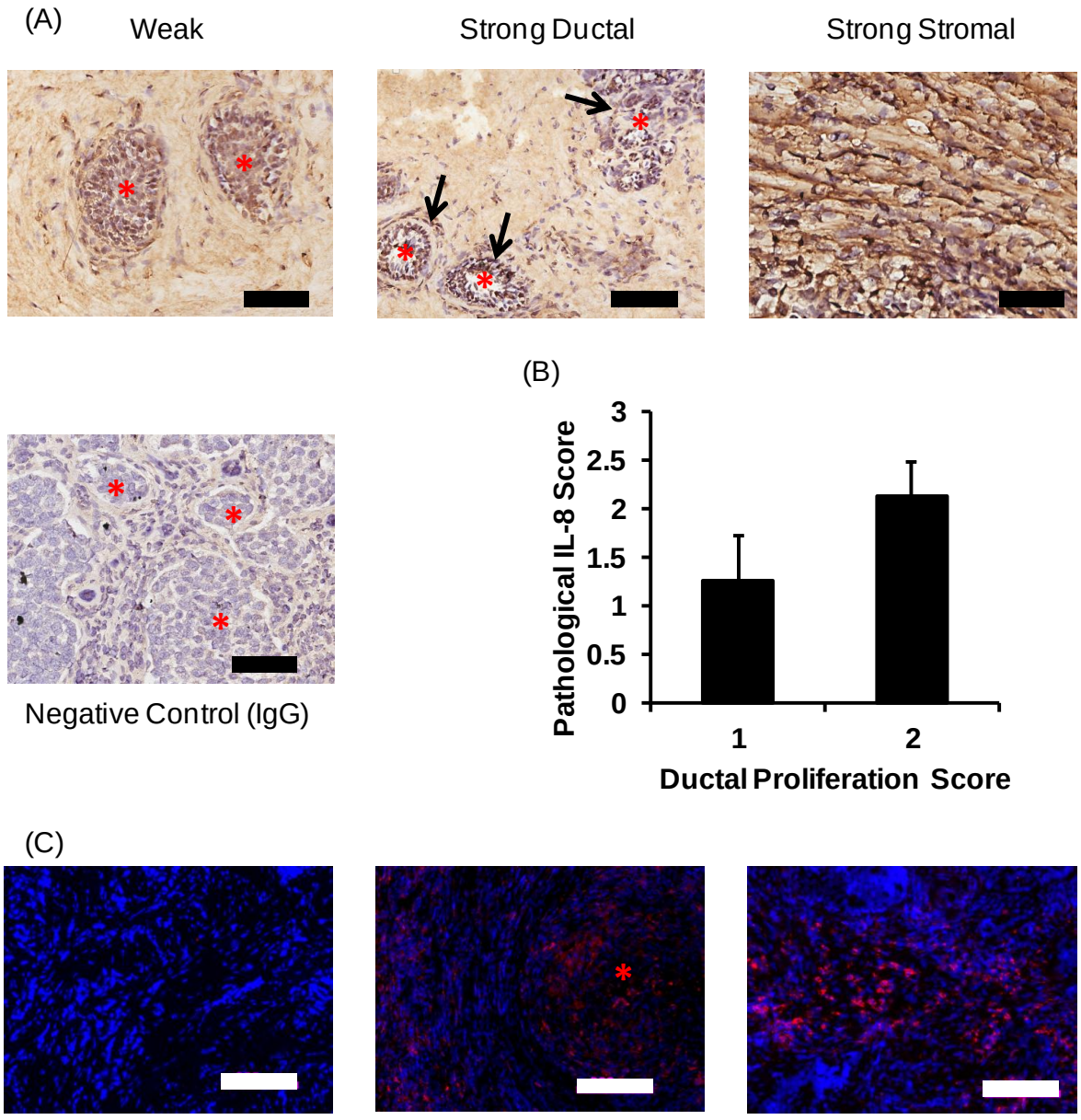

Figure 3.10: Immunostaining and pathology analysis of human mammary tissue sections
(A) IL-8 IHC with hematoxylin counterstain. Red stars show observed ducts, and black arrows indicate areas of strong positive IL-8 stain. Scale bars represent 100 µm. (B) Ductal proliferation score correlated with pathologist diagnosis of IL-8 staining intensity per duct over all patient samples (no statistical significance) (C) CXCR4 immunofluorescencewith DAPI counterstain. Red star shows observed duct. Scale bars represent 200 µm.

	Total	Calcifications in Mammogram	Ductal IL-8 Score >3
CXCR4+	9	6/9	3/9
CXCR4-	7	3/7	0/7
	Total	Calcification in Mammogram	CXCR4+
Total IL-8 Score >2	11	8/11	7/11

Table 3.1 Correlational evaluation of parameters analyzed for human mammary tissue sections
CXCR4 status was correlated with mammographic detection of calcification and high IL-8 staining; Moderate to high IL-8 staining was correlated with mammographic detection of calcification and CXCR4+ status

3.5 Discussion

As microcalcifications are one of the most salient markers and pertinent microenvironmental features in breast cancer (24, 27, 127), the understanding of mammary tumor biology would greatly benefit from mineral-containing culture systems that allow probing of cell-HA interactions. The use of tissue engineering principles to develop physiologically relevant material systems as culture models has provided new insight into cancer biology (79, 122, 128), but few systems that recapitulate the interplay of mineral, cells, and soluble factors have been thoroughly explored. The role of HA as a bioactive and cell-instructive material has been highlighted (32, 129, 130), and our past work has generated basic knowledge on how gas-foamed/particulate leached scaffolds can present mineral to cells and how cell behavior is regulated by HA (63, 108). Here, scaffold studies have been integrated with a molecular approach to provide a robust model describing how cytokine-based signaling drives metastasis under the influence of mineral. The data suggest that HA in the form of microcalcifications can

bias breast cancer metastases to bone by activating the SDF-1/CXCR4 chemoattractant axis via increased secretion of IL-8.

Screening mammograms are currently one of the most widespread tools for diagnosing breast cancer (23, 27). Presently, there is only limited evidence to suggest that microcalcifications detected in this manner can play an active role in promoting metastasis (131). However, the presence of HA and elevated level of proteins normally found in bone (31, 36) is in line with the theory that sites of metastases share tissue properties with primary tumor location (119, 132). Additionally, previous work indicates that HA can specifically induce enhanced secretion of various growth factors and cytokines in breast cancer cells (24, 63, 108). Our data here further implicate elevated secretion levels of these cytokines, specifically IL-8, in driving bone metastasis. A potentially crucial role in breast cancer metastasis for IL-8 is supported by other studies, which have shown that IL-8 is highly expressed by metastatic subpopulations of breast cancer cells (61, 113, 115, 133, 134) and that high IL-8 levels are observed clinically in bone metastasis patients (114, 135, 136). Additional studies have also shown that IL-8 can play a role in secondary processes that are required for metastasis, including angiogenesis (44, 137) and hypoxia response (79). Importantly, work with this scaffold system has shown that HA-regulated IL-8 secretion occurs for a number of breast cancer cell lines with varying molecular phenotypes, including MDA-MB231, MCF10A-DCIS, MCF10CA1A, and MCF-7 (63). Conversely, non-transformed cell lines do not seem to respond to HA in the same way (Fig. 3.2C). From this, we can infer that microcalcifications may be pro-metastatic, but they do not seem to induce cancerous transformation on their own.

Based on our findings, IL-8 may be involved in determining the skeletal tropism exhibited by breast cancer metastases. We have shown that IL-8 can stimulate stromal

production of SDF-1, and other studies have demonstrated that the SDF-1/CXCR4 axis is specifically activated for bone, but not lung, metastasis (55, 116, 117, 138). In fact, SDF-1 gradients are known to be important in mobilizing homing of many cell types to bone marrow (49, 57, 139). Blockade of CXCR4 has been shown to prevent metastasis in past studies, and several CXCR4 inhibitors are in clinical trials currently (140, 141) We hypothesize that tumor-derived IL-8 signals to stromal cells in the marrow compartment in an endocrine manner, initiating the formation of an SDF-1-rich pre-metastatic niche. Additionally, we have observed that HA stimulates enhanced surface receptor concentrations of CXCR4, thereby sensitizing breast cancer cells to the dramatically elevated levels of SDF-1. An endocrine mechanism is supported by past work on the establishment of pre-metastatic niches that suggests that the bone microenvironment is altered prior to cancer cell colonization (49, 56, 139). Moreover, clinical data shows that patients with bone metastasis have higher plasma concentrations of IL-8 (114, 135), indicating that IL-8 is circulating and available to stromal cells in the marrow. While it is well-known that IL-8 is a key cytokine regulator of tumor cell behavior and malignant progression, our data show that it could be an important player in directing breast cancer metastasis to bone specifically. Along with the observation that IL-8 is potentially regulated by HA in the form of microcalcifications at the primary tumor, there is strong evidence to suggest a mechanistic model wherein microcalcifications promote metastasis to bone through a combination of IL-8 signaling and CXCR4 enrichment.

Cancer genomics has shed much light on fundamental mechanisms underlying disease inception and progression. However, it is clear that microenvironmental cues may be crucial to understanding patterns of expression that are associated with malignancy. In the case of bone metastasis, the identification of the bone metastasis gene signature shows great promise for use

in cancer diagnostics and therapeutic intervention (11, 18). In this study, it was shown that microenvironmental HA may induce expression of the bone metastasis signature, and the functional consequences of upregulation of these genes in the context of metastatic disease was explored. Firstly, it was found that OPN, CXCR4, and MMP1 were consistently upregulated in response to HA for general populations of breast cancer cells (Fig. 3.3A). All of these genes produce proteins that are vital to the combination of enzymatic cleavage of ECM, motility, and chemotaxis that are required for metastasis to bone (117, 140, 142, 143). It is possible that in breast tumors, microcalcifications that form play a role in activating these genes, thereby being essential to drive bone metastasis. Interestingly, microcalcifications did not just upregulate these genes for heterogeneous populations of breast cancer cells, but they elicited similar response from 4175LM cells that had previously been established as 100% lung metastatic (Fig. 3.3B). This finding suggests that microenvironmental control may be paramount in defining tissue tropism of metastasis. Though initially assumed that genetic variation was a natural component of the heterogeneity of a tumor, it is possible that heterogeneous exposure to HA underlies initially differing affinities for specific tissues upon metastasis. In this case, once breast cancer cells that were initially conditioned *in vivo* in lung are cultured with HA, they revert or are "re-programmed" to a bone-colonizing phenotype. This possibility is supported by *in vivo* data that shows bone colonization by 4175MIN cells. From a radiologic standpoint, microcalcification patterns that are classified as "aggressive" tend to have the highest surface areas and therefore the most exposure to cells (144), potentially explaining why these microcalcification patterns are associated with a more frequent occurrence of bone metastasis.

Insights provided thus far from image analysis of patient samples is limited but somewhat illuminating. Qualitative assessment indicated that ductal proliferation showed reasonable

correlation with IL-8 levels in individual acinar structures. In some slides, largely visible microcalcifications were apparent, and in these cases dramatic IL-8 staining was observed. This preliminary data lacked sufficient sample size for establishment of statistical significance by traditional methods (Exact Fisher's Test). Furthermore, unfortunately, specifically located microcalcifications could not be correlated with specific IL-8 staining, as tissues were heterogeneous structural identifications were made through H&E stains of separate pieces of tissue from the same patient. In the majority of cases, we found significant IL-8 staining in the stromal compartment of the tumor, indicating that support cells may also be producing substantial amounts of IL-8. This is not entirely unexpected, as previous work has shown that disease-associated cells in adipose tissue secrete significant levels of IL-8 (128, 145). Nonetheless, this finding illustrates the vastly increased complexity of physiological tumors that are interacting with a wide range of normal and co-opted cells. Data on CXCR4 was also promising, showing that CXCR4 expression within ducts was correlated with ductal microcalcifications found in mammograms. This result agrees with our *in vitro* data, and helps to provide validation for the scaffold system as an appropriate tumor microenvironment mimic.

HA appears to facilitate signaling that promotes metastasis of breast cancer specifically to bone. By stimulating IL-8 secretion, which in turn induces enrichment of soluble SDF-1 in bone, and sensitizing breast cancer cells to SDF-1 by increasing expression of CXCR4, HA-containing microcalcifications are a pro-metastatic microenvironmental cue. All of the molecules discussed here have been highlighted as strong candidates for targeted anticancer therapies, however mechanistic insight into how they are regulated may allow for better implementation of these strategies for more efficacious treatment. Based on our overall findings here, future studies could

focus on understanding the genesis of microcalcifications, as inhibiting their formation could lay the foundation for the creation of novel therapeutic options.

CHAPTER 4: HYDROXYAPATITE NANOPARTICLE-CONTAINING SCAFFOLDS FOR THE STUDY OF BREAST CANCER BONE METASTASIS

PUBLISHED IN BIOMATERIALS (108)

4.1 Contributors

Synthetic HA was made by Dr. Debra Lin, and she also performed all material characterization (FTIR spectroscopy, XRD, TEM, SEM). I performed all biological assays and other experiments. The overall study design was a collaborative effort between Dr. Debra Lin, Dr. Lara Estroff, Dr. Claudia Fischbach, and myself.

4.2 Introduction

The bone microenvironment is defined by a composite matrix that consists primarily of organic collagen and inorganic mineral. Bone mineral is closely related structurally to geologic hydroxyapatite (HA) ($Ca_{10}(PO_4)_6(OH)_2$); however, bone apatites are less crystalline, more soluble, and vary in their molecular composition as carbonate ions often substitute for the hydroxide and phosphate ions ($Ca_{10-2x/3}(PO_4)_{6-x}(CO_3)_x(OH)_{2-x/3}$) (146). Furthermore, the size and crystallinity of bone apatite crystals change during development, growth, and as a result of bone pathologies (26, 147). While HA is largely known for its role in conferring structural and mechanical properties to bone, it also functions as a bioactive material that directly regulates the behavior of both normal and transformed cells (22, 63). For example, HA has been shown to enhance normal bone formation (60) and to alter growth and expression profiles of bone metastatic tumors (63, 148). Nevertheless, it remains unclear whether or not apatite crystal properties directly modulate the pathogenesis of bone diseases, in general, and bone metastasis,

in particular. This lack of understanding is partly due to a paucity of culture systems that recreate 3-D tumor microenvironmental conditions to study changes in tumor cell behavior as a function of varying HA nanoscale properties. Therefore, we sought to utilize synthetically prepared HA nanoparticles to determine the impact of particle size and crystallinity on mammary cancer cell activity.

The vast majority of advanced stage breast cancers metastasize to the skeleton, forming secondary tumors and interfering with bone remodeling to create predominantly osteolytic lesions (1). These lesions can lead to severe bone pain, pathological fracture, hypercalcaemia, and an overall poor clinical prognosis (64). Osteolysis due to bone metastasis is linked to tumor-derived soluble factors, such as interleukin-8 (IL-8) and parathyroid hormone related peptide (PTHrP), that de-couple the homeostatic balance between bone formation and bone resorption(1, 66). In particular, IL-8, a molecular mediator of osteolysis (63, 66) and tumor progression (79, 115), is dramatically upregulated in breast cancer tissue relative to normal breast tissue in patients (61), and in breast cancer cells that preferentially metastasize to bone rather than lungs (18).

Though the exact mechanisms by which breast cancer cells preferentially target bone and induce pathological remodeling remain unclear, mounting evidence implicates the bone microenvironment and specifically HA in this pathogenesis. For example, mammary tumor cells increase expression of osteoclastogenic factors upon colonizing bone *in vivo* (18). Additionally, IL-8 secretion by breast cancer cells is enhanced through cell-HA interactions, and stimulates osteoclast-mediated osteolysis (63, 66). These studies illustrate the important role that bone mineral might play in influencing osteolytic metastasis. Since the size and crystallinity of biogenic apatite nanocrystals change as a function of age and disease (26, 147), further study is

required to evaluate the role of these nanoscale properties of HA itself on metastatic bone disease.

Tissue engineered (TE) systems, originally created for regenerative medicine, can be used as tools to recreate tumor microenvironmental conditions *in vitro*. Tumor cells seeded in scaffold-based TE systems assemble into tumor-like tissues (79) and exhibit phenotypes that more closely mimic *in vivo* behavior as compared to conventional two-dimensional (2-D) cultures (148). Furthermore, biologically active materials or molecules, such as mineral particles or proteins, can be incorporated into TE scaffolds and presented to cells in a spatially controlled manner (137). Bone-like TE systems, including silk-based scaffold systems (100), decellularized osteoblast matrices (148), and polymer-HA composites (60, 63, 149) have been created to mimic certain features of bone, and several of these systems have been used to study tumor cell behavior (63, 148). Since bone metastasis can modify the crystallinity and particle size of the mineral component of bone (26), a controllable platform is needed to independently interrogate cellular responses to a wide range of HA particle sizes and crystallinities in a pathologically-relevant culture microenvironment.

4.3 Materials and Method

4.3.1 Particle Preparation

HA nanoparticles were synthesized through a two-step process in which a typical precipitation reaction of a calcium salt with a phosphate salt was followed by hydrothermal aging of the precipitate to obtain particles with a narrow size distribution (Fig. 4.1). All chemicals for these reactions were obtained from Sigma Aldrich and used as received. A solution of $(NH_4)_2HPO_4$ (90 mL, 10 mM) was added drop-wise into a solution of $Ca(NO_3)_2$ (150 mL, 10 mM) under rapid stirring at 4 °C in an ice-water bath for a final calcium to phosphate ratio of

1.67 (A1-A3 particles). The pH of the starting solutions was adjusted to 9-9.5 with 0.1 M NH_4OH. Alternatively, in lieu of hydrothermal aging, dry annealing was performed on precipitated particles for 3 or 5 days at 200°C (A1-3 and A1-5, respectively). In a second reaction, particles were synthesized from a different set of precursors. A solution of Na_2HPO_4 (90 mL, 10 mM) was added drop-wise into a solution of $CaCl_2$ (150 mL, 10 mM) under rapid stirring at 4 °C until the calcium to phosphate ratio was 1.67 (B1 particles). The pH of the starting solutions was adjusted to 9-9.5 with 0.1 M NaOH. In both cases, the reactions were allowed to proceed for 1 hr, and then stirred at 20 °C for an additional 12 hrs. The resulting opaque suspensions were concentrated 3-fold by centrifugation (Thermo Scientific Sorvall Legend RT+ Centrifuge, 3600 g, 5 min) of 45 mL aliquots. After centrifugation, two-thirds of the clear supernatant was decanted. The remaining suspension (15 mL) was sonicated for 30 mins (Bransonic 1510R-MT), placed into a pressure vessel (Parr Instrument Company 276AC-7304), and aged at 180 °C for the indicated time periods (Table 1) in an oven (model no. OV12A, GS Blue M Electric). After aging, the particles were removed from the pressure vessel, washed with NH_4OH (0.1 M) and deionized water (DI-H_2O) to remove soluble salts, rinsed with acetone, and then dried at 20 °C (A2, A3, and B1 particles). Poorly crystalline particles were collected following the precipitation reaction of $Ca(NO_3)_2$ and $(NH_4)_2HPO_4$. The precipitate was washed with NH_4OH and DI-H_2O, rinsed with acetone, and dried at 20 °C (A1 particles). Commercial HA nanopowder obtained from Sigma Aldrich (provider specified particle size <200 nm) was used for comparison.

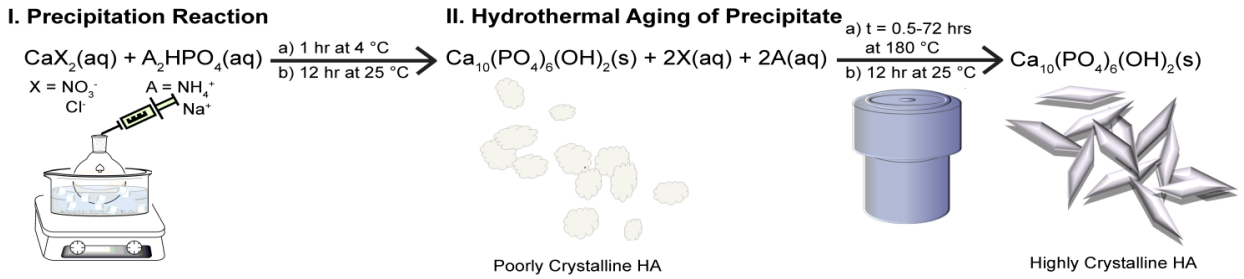

Figure 4.1: HA nanoparticle synthesis
Schematic showing the two-step precipitation reaction to obtain poorly crystalline HA followed by hydrothermal aging of the precipitate to obtain crystalline HA nanoparticles

Sample ID	Precipitation Precursors	Aging time [hrs]	Length [nm][a] (TEM)	Bulk Length [nm][b] (pXRD)	Splitting Factor (FTIR)[c]
SIG	Commercial Sigma	N/A	20-600	125	2.07
A1	$Ca(NO_3)_2$, $(NH_4)_2HPO_4$	0	---	24	2.56
A2	$Ca(NO_3)_2$, $(NH_4)_2HPO_4$	0.5	20-40	32	3.61
A3	$Ca(NO_3)_2$, $(NH_4)_2HPO_4$	72	60-130	103	3.99
B1	$CaCl_2$, Na_2HPO_4	1.5	50-120	99	6.60

[a]The range of particle lengths observed from TEM micrographs along the {002} axis.
[b]Bulk size of the particles were obtained via Scherrer's analysis of the {002} peak from pXRD.
[c]Splitting factor was obtained from normalizing the sum of the absorbance at 562 cm^{-1} and 602 cm^{-1} from PO_4 bond bending (v_4) to the minima between the two peaks to compare relative crystallinities from FTIR.

Table 4.1 Summary of particle characterization
Details of precursor material, hydrothermal aging time, size of particles determined via TEM and XRD, and splitting factor determined via FTIR

4.3.2 Particle Characterization

Particles were characterized by Transmission Electron Microscopy for shape and morphology, and X-ray Diffraction (XRD) and Fourier Transform Infrared (FTIR) Spectroscopy for crystallinity and phase information. For TEM, particles were suspended in acetone and dropped onto a carbon-coated grid (Electron Microscopy Sciences). Samples were examined by brightfield TEM (FEI Tecnai T-12 Spirit, 120 kV), and particle sizes were determined by image analysis of the TEM images through ImageJ (NIH). Dried particles were examined via powder

XRD (PAD-X theta-theta X-ray Diffractometer, Scintag Inc., CuKα 1.54 Å, accelerating voltage 45 kV, current 40 mA, continuous scan, 2.0 deg/min). Particle sizes were determined from the peak broadening of the {002}peak of HA (25.88°) by application of the Scherrer equation using a Al_2O_3 standard (Software: JADE 9, Materials Data, Inc.). For FTIR (2020 Galaxy Series FT-IR, Mattson Instruments), KBr pellets were prepared from dried particles and spectra acquired (res 4.0 cm^{-1}, 253 scans). Particle crystallinities were determined from the splitting factor obtained via normalizing the sum of the absorbance at 562 cm^{-1} and 600 cm^{-1} to the minimum between the doublet following Weiner and Bar-Yosef (150).

4.3.3 Scaffold Fabrication

Porous mineral-containing scaffolds were fabricated by a gas-foaming/particulate leaching technique as previously described (60, 63). Briefly, 4 mg of poly(lactide-co-glycolide) (PLG) particles (Lakeshore Biomaterials, ground and sieved, average diameter 250 μm), 4 mg of PLG microspheres (formed through a double emulsion process, average diameter 5-50 μm), 8 mg of HA nanoparticles (A1-A3, B1, SIG), and 152 mg of NaCl (J.T. Baker, sieved to a diameter of 250-400 μm) were mixed and subsequently cold pressed in a Carver Press (Fred S. Carver). The resulting matrices (8.5 mm diameter, 1 mm in thickness) were exposed to high-pressure carbon dioxide gas (800 psi) inside a non-stirred pressure vessel (Parr Instruments 4677). Following rapid release of pressure that allowed polymer foaming, scaffolds were soaked in de-ionized water for 24 hrs to leach out porogenic NaCl particles. Non-mineral-containing (NM) scaffolds that did not contain HA were also fabricated as controls. Prior to cell culture, scaffolds were sterilized in 70% ethanol for 30 min and washed five times in sterile PBS.

4.3.4 Microscopic Characterization of Scaffolds

Scaffolds were characterized through TEM, scanning electron microscopy (SEM) and brightfield light microscopy to assess particle distribution throughout the polymer matrix. For TEM (FEI Tecnai T-12 Spirit, 120 kV), scaffolds were embedded in a UV-active Quetal resin (EM Sciences, Fort Washington, PA) and sectioned with a microtome (MT2-B Ultra-Microtome, Sorvall Porter-Blum) prior to analysis. For SEM, scaffolds were fractured to expose inner pore surfaces and mounted on aluminum SEM stubs (Electron Microscopy Sciences) with carbon tape in a manner that allowed subsequent imaging of the exposed surfaces. Particle distribution on PLG surfaces were examined on exposed pore surfaces within the scaffold that were unaffected by the sample preparation (i.e., not on the fractured surface) and imaged uncoated using a Field-Emission SEM (Zeiss LEO 1550, 1 kV). Brightfield microscopy of scaffolds was performed on an Axio Observer.Z1 (Zeiss).

4.3.5 Analysis of Protein Adsorption on Scaffolds

To quantify the degree of protein adsorption as a function of HA nanoparticle characteristics, scaffolds were incubated in complete DMEM (cDMEM ; i.e., DMEM [Invitrogen] supplemented with 10% fetal bovine serum [Tissue Culture Biologicals] and 1% penicillin/streptomycin [Invitrogen]). Following 30 min of incubation, scaffolds were washed twice in PBS (Invitrogen) and then sonicated (Branson Sonifier 150) in RIPA buffer (Sigma). After centrifugation, total protein in the supernatant was quantified using a Bicinchonic Acid (BCA) Kit (Thermo) and colorimetric analysis on a plate reader (Tecan M1000) according to manufacturer's instructions. Additionally, scaffolds were incubated in DMEM supplemented with 20 µg/mL of fibronectin (Sigma) and adsorbed fibronectin was analyzed by immunofluorescence. Briefly, scaffolds were fixed with 10% formalin, rinsed twice in PBS, and

then incubated with a polyclonal rabbit anti–fibronectin antibody (Sigma). After a second wash with PBS containing bovine serum albumin, scaffolds were incubated with an Alexa Fluor 488 secondary antibody (Molecular Probes). Whole-mount scaffolds were imaged using an epi-fluorescence microscope (Zeiss Axio Observer.Z1).

4.3.6 Cell Culture

Human MDA-MB231 breast cancer cells (ATCC) were maintained under standard culture conditions (37°C, 5% CO_2) in cDMEM. For 3-D cell culture, scaffolds were statically seeded with 1.5 million MDA-MB231 cells and subsequently maintained under dynamic culture conditions on an orbital shaker for up to 10 days as previously described (63).

4.3.7 Analysis of Ion Content in Media from Scaffolds

To determine changes in calcium and phosphate content in media during culture, acellular NM- and A1-scaffolds were incubated in cDMEM under standard culture conditions (37°C, 5% CO_2). The media was harvested after 2 days, digested in 5% nitric acid, and analyzed with inductively coupled plasma spectroscopy (ICP; ICAP 61E Trace Analyzer, Thermo). Additionally, ICP analysis was performed with media harvested from tumor cell-seeded NM- and A1-scaffolds after 2 days of 3-D culture.

4.3.8 Characterization of Tumor Cell Behavior

To measure tumor cell growth, tumor constructs were harvested 30 min after seeding (day 0) and again after 72 hrs. Constructs were washed five times in PBS and mechanically disintegrated, before being sonicated (Branson Sonifier 150) in lysis buffer (25 mM Tris-HCl, 0.4 M NaCl, 0.5% SDS). Subsequently, lysates were centrifuged, and the supernatant was assayed for DNA content using PicoGreen® assay (Invitrogen) and a fluorescence plate reader

(Tecan M1000) according to manufacturer's instructions. Protein secretions in media from constructs were also analyzed 72 hrs after seeding. Briefly, breast cancer cell-seeded scaffolds were transferred to fresh well plates 24 hrs prior to harvesting media for analysis, and culture medium was changed to DMEM containing 1% FBS. IL-8 of harvested media was measured via ELISA (R&D) according to manufacturer's instructions and normalized to DNA content to account for differences in cell number. For analysis of IL-8 expression, RNA was collected by dissolving tumor cell-seeded scaffolds in TRIzol® (Invitrogen) and then extracting total RNA according to manufacturer protocol. Total RNA (1 μg) was then reverse transcribed to cDNA (High Capacity cDNA Reverse Transcription Kit with random hexamers [(Applied Biosystems)]), and subjected to real-time RT-PCR (25 ng template, run in triplicate) using SYBR green detection (Quanta) on an Applied Biosystems 7500 System. Primer sequences for human IL-8 (fwd: 5'-agaaaccaccggaaggaaccatct-3', rev: 5'-agagctgcagaaatcaggaaggct-3') and β-actin (fwd: 5'-aatgtggccgaggactttgattgc-3', rev: 5'-aggatggcaagggacttcctgtaa-3') were synthesized by IDT Technologies. β-actin was used as an endogenous loading control gene, and relative quantification was performed using the $\Delta\Delta C_t$ method as previously described (126).

4.3.9 Statistical Analysis

One-way ANOVA and Student's t-test were used to determine statistical significance between conditions. Tukey's post test was used for pairwise comparisons. Significance between groups and NM, A2, and B1 scaffolds (see Table 1) are denoted by (*), (#), and (o) respectively. In all cases, $P<0.01$ is indicated by a single symbol and $P<0.005$ is denoted by double symbols. For all experiments, sample conditions were run in triplicate or greater. Data are presented as averages, and error bars represent standard deviations.

4.4 Results

4.4.1 Particle Synthesis and Characterization

Synthetic HA (sHA) with varying nanoscale characteristics can be formed via solution-based precipitation reactions, hydrothermal synthesis, electrodeposition, or sintering (146, 151). The sHA nanoparticles used for the fabrication of mineral-containing scaffolds were obtained from either a two-step synthesis involving a precipitation reaction followed by hydrothermal aging or a commercial source for comparison (Fig. 4.1, Table 4.1). To synthesize poorly crystalline particles (A1), solutions of calcium and phosphate salts were mixed together rapidly at low temperature. Remaining particles (A2, A3, and B1) were prepared by hydrothermally aging a suspension of the particles from the precipitation reaction. The size and crystallinity of the particles increased with aging time (A2, A3), and could also be varied by changing the precursor salts (B1).

Particle shape and size distributions of both the sHA and commercial HA were determined by TEM (Fig. 4.2). The sHA particles that were formed from the initial precipitation reaction (A1) were small and poorly crystalline; however, hydrothermally aging these same particles resulted in the formation of uniform, larger, faceted, and elongated particles with a narrow size distribution (A2 and A3). Similar to previous observations (146), the length of the rod-like particles increased with aging time from 20-40 nm after 0.5 hrs of aging (A2) to 60-170 nm after 72 hrs of aging (A3). Using a different set of precursor salts and shorter aging time (1.5 hrs), rod-like particles (B1), with lengths similar to A3 (50-150 nm), were also obtained. In contrast to the sHA particles, the SIG particles were spherical and exhibited a wide range of sizes (20-600 nm in diameter).

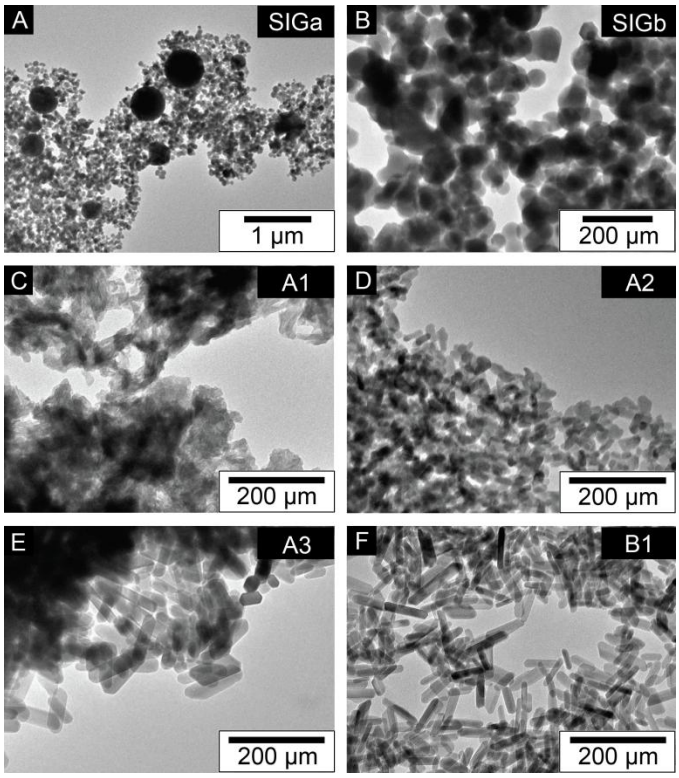

Figure 4.2: TEM images of HA particles used to prepare mineral-containing PLG-scaffolds
(A) and (B) Commercial Sigma Aldrich particles, (shown at low [SIGa], and high [SIGb] magnification), (C-F) HA particles synthesized from $Ca(NO_3)_2$ and $(NH_4)_2HPO_4$ precursors with hydrothermal aging times of 0 hrs (A1), 0.5 hrs (A2), and 72 hrs (A3), and particles synthesized from $CaCl_2$ and Na_2HPO_4 precursors aged for 1.5 hrs (B1).

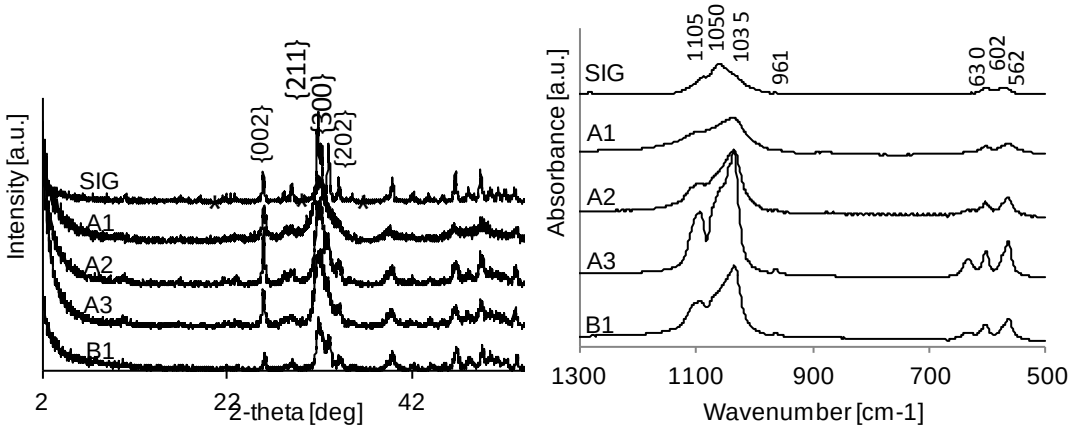

Figure 4.3: XRD and FTIR for sHA
(Left) pXRD patterns of particles SIG, A1-A3, and B1. All samples are confirmed to be HA. Major peaks have been labeled with HA crystal indices. (ICDD PDF no. 09-0432) (152) FTIR spectra of particles SIG, A1-A3, and B1. Positions of characteristic HA peaks are indicated.

All of the synthetic particles were pure HA according to powder X-ray diffraction (pXRD) (Fig. 4.3, left). The diffraction pattern of the SIG particles, however, contained unidentified peaks in addition to those indexed to HA (ICDD PDF no. 09-0432). The pXRD also provides information regarding the particle size and crystallinity. Scherrer analysis of the {002} peak width (25.88°) revealed that the average length of the particles to be 24 nm (A1), 32 nm (A2), 103 nm (A3), 100 nm (B1), and 125 (Table 4.1). The increase in the number of clearly resolvable peaks at higher angles for A3 and B1 particles suggest an increase in crystallinity compared to A1 and A2 particles.

FTIR results confirmed the increase in crystallinity for the larger particles obtained from longer hydrothermal aging times and varying precursor salts (A3, B1). The absorbance at 630 cm^{-1} is attributed to structural hydroxides in HA and is known to increase with enhanced crystallinity (Fig. 4.3, right) (153). This absorbance was undetectable for the poorly crystalline HA (A1), and increased in intensity for nanoparticles A2, A3, and B1. The increase in crystallinity was further confirmed from calculation of the splitting factor (Table 4.1). The splitting factor, which quantifies the degree of splitting of the PO_4 bond bending (ν_4) peaks (562 cm^{-1} and 600 cm^{-1}), is known to increase with increasing crystallinity (150). Interestingly, although A3 and B1 are similar in length, B1 had nearly twice as large a splitting factor, indicating differences in crystallinity between the two similarly sized particles made from different precursor salts (Table 4.1).

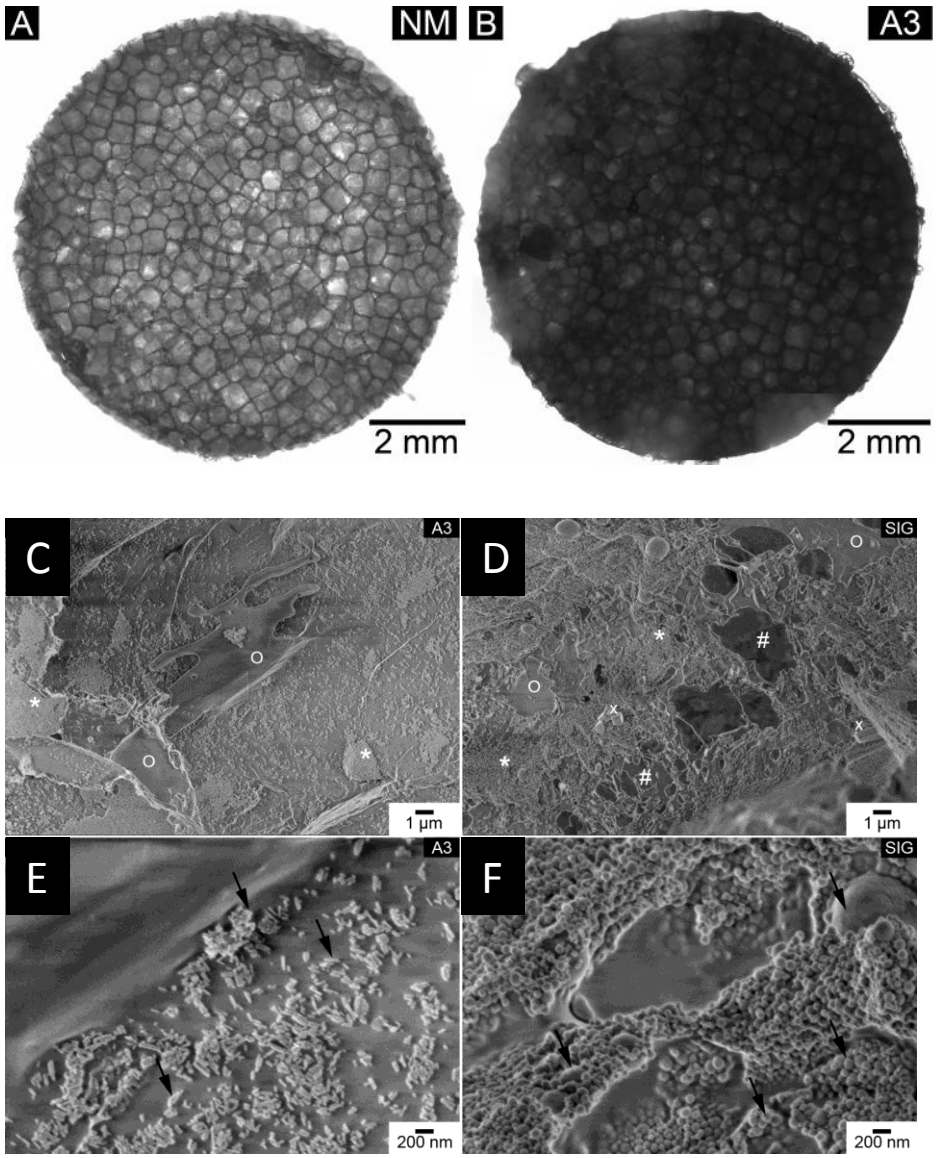

Figure 4.4: Visualization of pore structure and HA distribution in scaffolds
Brightfield micrographs show no change in architectural properties with addition of hydrothermally aged particles (A, B). SEM micrographs of A3-scaffold (C, E) and SIG-scaffold (D,F) show the distribution of A3 and SIG particles on pore surfaces exposed after fracture of a scaffold. Regions of high particle density (*), low particle density (O), and pores in the scaffold (#) were observed for both scaffolds (C,D). Residual salt crystals are indicated (x). Arrows point to individual A3 particles (E) and SIG particles (F).

4.4.2 Scaffold Characterization

The micro- and nano-architecture of the scaffolds was analyzed via brightfield light microscopy, SEM and TEM. Mineral-free (NM-scaffolds), SIG-scaffolds, and A3-scaffolds were

compared to assess the integration of different particles into the bulk-PLG. Incorporation of the SIG and A3 nanoparticles did not change the microarchitectural characteristics (i.e., pore size and wall thickness) of the scaffolds compared to the NM-scaffold as shown by brightfield light microscopy (Fig. 4.4A-B). The distribution of both A3 and SIG particles on pore surfaces within the scaffolds was revealed by SEM micrographs. Despite the differences in particle morphology, similar surface coverage was observed for both the rod-like A3 particles and spherical SIG particles. Both scaffold types contained regions of high and low particle density, as well as areas without surface-associated HA (Fig. 4.4C-F). High magnification SEM images of the A3 and SIG scaffolds (Fig. 4.4E-F) further illustrated that the surface topography is dictated by the morphology of the incorporated particles and reflects the rod-like and spherical morphology of A3 and SIG particles. TEM micrographs of sectioned A3-scaffolds revealed that HA particles were localized at or near the pore surfaces, with a small number of particles completely embedded within the bulk-PLG (Fig. 4.5). This distribution of particles suggests that a majority of the particles are accessible for interaction with seeded cancer cells.

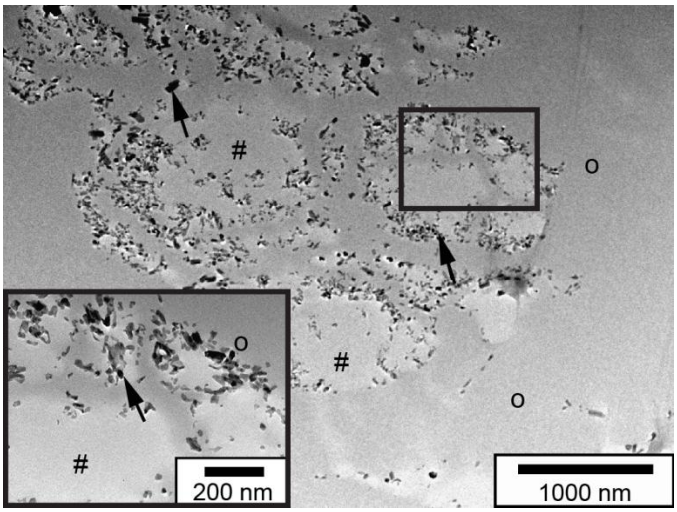

Figure 4.5: TEM micrograph of sHA scaffold
The distirbution of the particles (indicated by arrows) in the bulk (indicated by 'O') and the pores (indicated by '#') of the polymeric matrix is shown. Inset: Higher magnification image of the area indicated by a box.

4.4.3 Serum Protein Adsorption

To assess whether the HA nanoscale characteristics modulate cellular interactions with scaffolds, we next determined the capacity for protein adsorption of the different mineral-containing scaffolds. When incubated in serum-containing media (DMEM + 10% FBS), mineral-containing scaffolds adsorbed significantly more protein than control NM-scaffolds, and furthermore, the scaffolds with the smallest and least crystalline HA nanoparticles (A1) adsorbed the most serum proteins, as determined by a colorimetric assay (Fig. 4.6A). Specifically, scaffolds with poorly crystalline particles (A1) adsorbed two-fold more serum protein as scaffolds with 103 nm long particles (A3). Furthermore, A3-scaffolds adsorbed significantly more protein than the more crystalline B1 scaffolds, yet these two particles did not vary in size. Incubating scaffolds in pure solutions of fibronectin, an adhesive serum protein that readily adsorbs onto most biomaterial surfaces (154), yielded similar trends as indicated by fibronectin immunofluorescence (Fig. 4.6B). To control for changes in surface area as a function of particle size and/or shape, fibronectin adsorption experiments were repeated with scaffolds containing HA nanoparticles in amounts normalized to surface area. Under these conditions, scaffolds containing smaller, poorly crystalline nanoparticles (i.e. 20 nm long) adsorbed significantly more fibronectin relative to those with longer, more crystalline particles (i.e. 80 nm and 100 nm long) (Fig. 4.6C). These results suggest that HA particle characteristics, in addition to purely surface area, regulate the adsorption of serum proteins that may in turn modulate cell behavior.

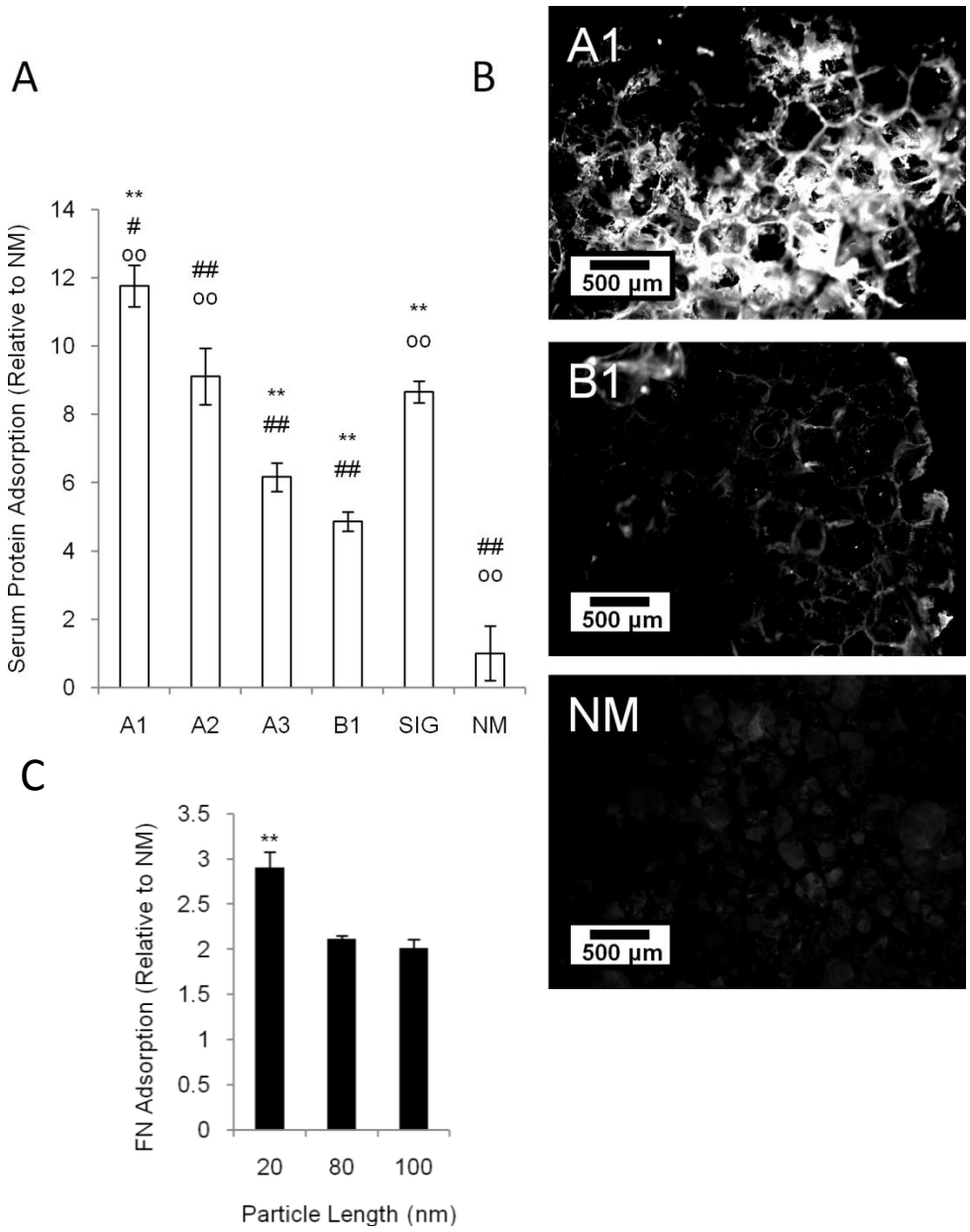

Figure 4.6 Protein adsorption for sHA scaffolds (A) Serum protein adsorption on non-mineral-containing (NM) and mineral-containing (A1-A3, B1, SIG) scaffolds as quantified via colorimetric BCA analysis of scaffold lysates prepared after incubation with serum-containing cell culture media. (B) Immunofluorescence analysis of fibronectin (FN) adsorption onto non-mineral-containing (NM) and mineral-containing scaffolds containing small, poorly crystalline (A1) and highly crystalline HA particles (B1). Significance between groups and NM, A2, and B1 scaffolds are denoted by (*), (#), and (o) respectively. (C) FN adsorption as quantified by BCA analysis indicated that smaller crystals in scaffolds stills adsorbed more protein, even when mass of crystals used was less to normalize surface area within scaffold. In all cases, $P<0.01$ is indicated by a single symbol and $P<0.005$ is denoted by double symbols.

4.4.4 Scaffold and Particle Integrity in Culture Conditions

To determine if HA nanoparticle solubility contributes to calcium and phosphate content in media, which during cell culture could lead to differences in cell behavior, the elemental composition of media harvested from scaffolds was analyzed via ICP (Fig. 4.7). A1-scaffolds were used for this experiment since poorly crystalline HA has increased solubility compared to more crystalline HA (146) and would be most susceptible to potential dissolution. Analysis was performed on both cell-seeded and cell-free scaffolds, revealing that the calcium concentrations remained unchanged for all conditions and matched concentrations found in cDMEM. Similarly, non-seeded scaffolds exhibited unfettered phosphorous levels equal to concentrations found in cDMEM. In contrast, phosphorus concentrations increased for both the NM and A1-scaffolds that were seeded with cells. This increase was attributed to the presence of the cancer cells rather than the dissolution of HA particles. Overall, our findings show that any observed effects of mineral-containing scaffolds on cell behavior are related to cell-material interactions with HA nanoparticles and not the presence of increased levels of soluble calcium and phosphorous.

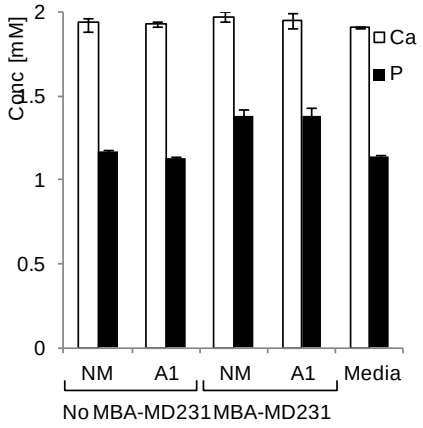

Figure 4.7: Solubility of sHA in scaffolds Calcium (155) and phosphorus (black) content of media harvested from non-mineral-containing (NM) and mineral-containing (A1) scaffolds after 2 days of culture in the presence and absence of MDA-MB231 breast cancer cells as determined by ICP. Culture media incubated for the same period of time, but not exposed to scaffolds or cells was used as a control (Media).

4.4.5 Effect of HA Crystallinity and Particle Size on MDA-MB231 Adhesion and Growth

To determine the relevance of mineral characteristics to breast cancer cell colonization and growth within bone, we seeded MDA-MB231 breast cancer cells into mineral-containing PLG scaffolds and evaluated their adhesion and proliferation as a function of HA nanoparticle characteristics. In comparison to NM scaffolds, all of the mineral-containing scaffolds enabled significantly more cell adhesion as detected by DNA quantification following initial cell seeding (Fig. 4.8A). Similar to the increased protein adsorption (Fig. 4.6), cell adhesion was greatest within scaffolds containing small, poorly-crystalline nanoparticles (A1) as compared to larger and more crystalline HA scaffolds (A2, A3, and B1) suggesting a possible link between HA-regulated protein adsorption and cell adhesion. Likewise, significantly more cells adhered to A3 scaffolds than B1 scaffolds, suggesting that increased HA crystallinity inhibits breast cancer cell adhesion by suppressing protein adsorption. Importantly, tumor cell proliferation was also affected by the presence of different HA nanoparticles and followed similar trends as observed for cell adhesion (Fig. 4.8B).

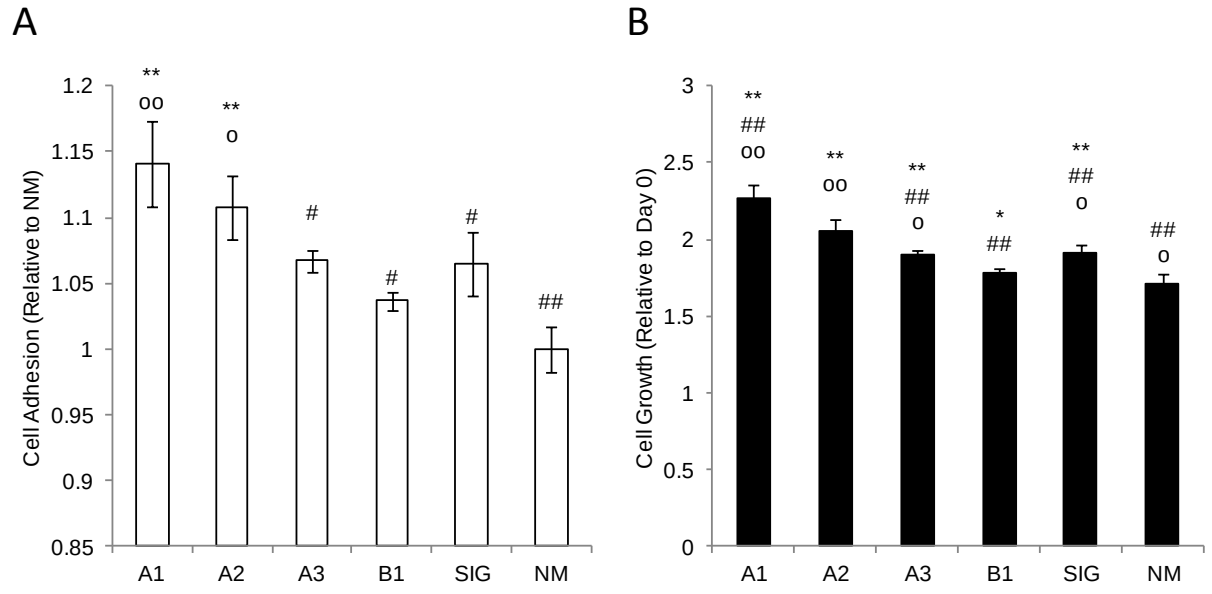

Figure 4.8: Effect of sHA particle characteristics of growth and adhesion of MDA-MB231 cells (A) MDA-MB231 cell adhesion onto non-mineral-containing (NM) and mineral-containing scaffolds (A1-A3, B1, SIG) as quantified via PicoGreen DNA assay of cell lysates 3 hours after seeding. (B) MDA-MB231 growth 3 days after seeding of non-mineral-containing (NM) and mineral-containing scaffolds (A1-A3, B1, SIG) as analyzed by PicoGreen DNA assay. Values are depicted relative to day 0 to account for variations in initial cell adhesion between the individual groups. Significance between groups and NM, A2, and B1 scaffolds are denoted by (*), (#), and (o) respectively. In all cases, $P<0.01$ is indicated by a single symbol and $P<0.005$ is denoted by double symbols.

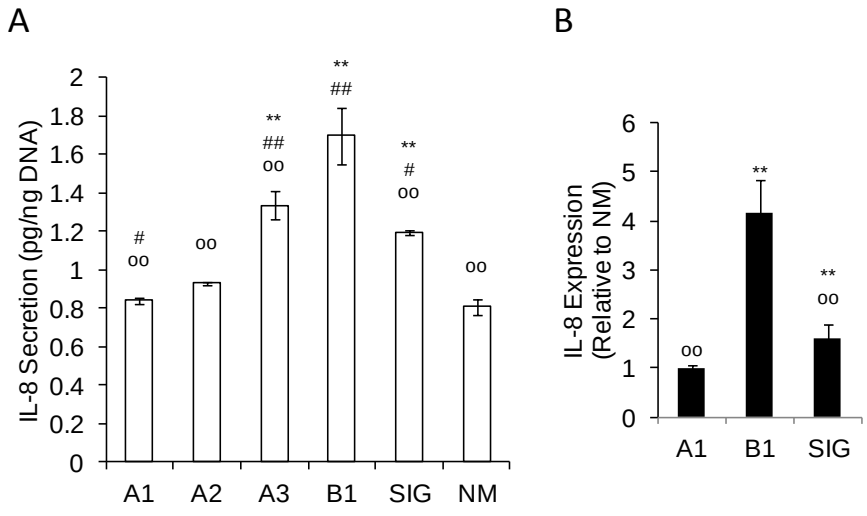

Figure 4.9 Effect of sHA particle characteristics on IL-8 production by MDA-MB231 cells (A) IL-8 secretion by MDA-MB231 breast cancer cells as analyzed through ELISA of conditioned media collected

from non-mineral-containing (NM) and mineral-containing scaffold cultures (A1-A3, B1, SIG). Values were normalized to cell numbers as determined via PicoGreen DNA assay to account for changes in cell proliferation. (B) IL-8 mRNA expression by MDA-MB231 breast cancer cells as analyzed through quantitative real-time RT-PCR of lysates collected from non-mineral-containing (NM) and representative mineral-containing scaffold cultures (A1, B1, SIG). Values are shown as normalized to expression levels in NM scaffold cultures. Significance between groups and NM, A2, and B1 scaffolds are denoted by (*), (#), and (o) respectively. In all cases, $P<0.01$ is indicated by a single symbol and $P<0.005$ is denoted by double symbols.

4.4.6 IL-8 Secretion by MDA-MB231 Cells as a Function of HA Crystallinity and Particle Size

To evaluate the effect of HA nanoparticle characteristics on the osteolytic capability of breast cancer cells, we analyzed IL-8 secretion by MDA-MB231 cells in the different scaffolds. Interestingly, in contrast to cell adhesion and proliferation, IL-8 secretion was inversely regulated by HA crystallinity and size. Specifically, cellular secretion of IL-8 was greatest in scaffolds that incorporated highly crystalline HA (B1) (Fig. 4.9A), while scaffolds that contained similarly sized, but less crystalline HA (A3) secreted significantly less IL-8. Furthermore, tumor cells cultured in scaffolds with the smaller and less crystalline particles (A1, A2) secreted less IL-8 relative to the highly crystalline particles (B1). These changes in secretion were mimicked at the expression level, as real-time RT-PCR demonstrated upregulation of IL-8 in cells seeded in scaffolds containing larger HA crystals as compared to less crystalline HA conditions or NM controls (Fig. 4.9B). To confirm that these outcomes resulted from nanoparticle characteristics and not a change in surface area due to particle size and/or shape, experiments were repeated with scaffolds containing HA nanoparticles in amounts normalized to surface area. In these experiments, the scaffolds containing larger, more crystalline HA still increased IL-8 secretion (Fig. 4.10A). Culture with dry annealed particles, which presumably differ only in crystallinity but not size, indicated similar trends in IL-8 levels, though sample size was insufficient to establish statistical significance in this measure due to variability in DNA quantification (Fig.

4.10B). Taken together, these data suggest a role of HA nanoparticle characteristics, beyond size, in regulating the osteolytic potential of MDA-MB231 breast cancer cells.

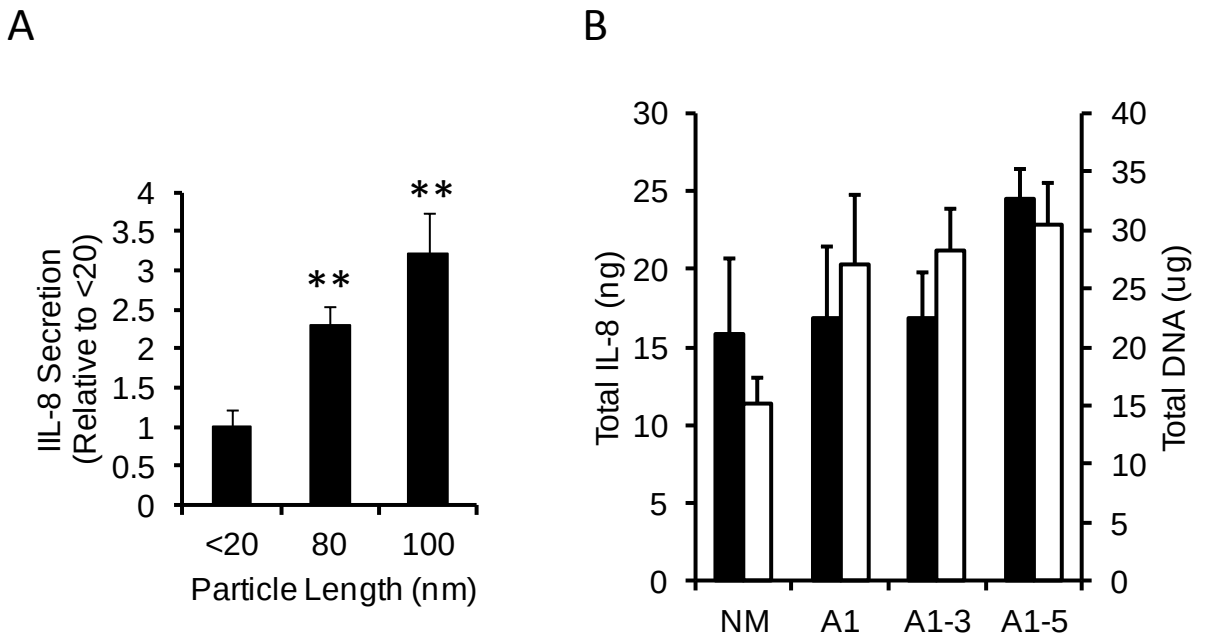

Figure 4.10: IL-8 secretion in response to varying geometry and crystallinity of sHA particles in scaffolds (A) IL-8 secretion by MDA-MB231 breast cancer cells as analyzed through ELISA of media collected from mineral-containing scaffold cultures with mass of HA per scaffold normalized by surface area available within scaffold. Values were normalized to cell numbers as determined via PicoGreen DNA assay to account for changes in cell proliferation. (B) Total IL-8 and DNA in scaffolds containing dry-annealed HA crystals. In all cases, $P<0.01$ is indicated by a single symbol and $P<0.005$ is denoted by double symbols.

4.5 Discussion

Since bone metastasis often leads to the formation of osteolytic lesions [8] that are characterized by less crystalline and smaller apatite particles relative to healthy bone [2], studies of breast cancer bone metastasis would benefit from HA-containing scaffold systems in which particle size and crystallinity can be independently varied. While 3-D culture approaches have enhanced the physiological relevance of *in vitro* studies (79, 120), models to investigate cell-mineral interactions in response to specific HA nanoparticle characteristics currently do not

exist. Commercially available HA particles, which are routinely employed for the fabrication of mineral-containing scaffolds (60, 63), are heterogeneous in size, shape, and chemical composition as shown by us (Fig. 4.2A, B) and others (156). Gas-foamed/particulate-leached polymer composite scaffolds have previously been used to effectively present mineral to cultured cells (60, 63), and we have applied this platform to present hydrothermally grown HA particles with tunable nanoscale characteristics to cells in a 3-D culture context. Specifically, we have used these scaffolds to study the effects of HA particle size and crystallinity on breast cancer cell behavior and have demonstrated that altering the crystal properties of HA may control the osteolytic and metastatic phenotype of breast cancer cells.

Several methods have previously been used to synthesize HA nanoparticles with narrow size distributions (151, 157). Many of these methods depend on the presence of surfactants or fractionation to control the size distribution, and the resulting particles have organic impurities and are produced in low yields (158, 159). Here, we describe an optimized technique for the synthesis of HA nanoparticles, which does not require additives or elaborate separation techniques to obtain narrow size distributions. The two-step process involves a wet chemical precipitation followed by hydrothermal aging and yields hydroxyapatite nanoparticles of tunable sizes, crystallinity, and, possibly, composition. Compared to conventional hydrothermal HA particle synthesis methods whereby particles are made directly in hydrothermal reactions (146, 151), the division of the process into two steps ensures size uniformity by separating the nucleation and growth processes of the HA particles. The precipitation step nucleates HA seed crystals, while the hydrothermal aging step controls the growth of the seed crystals into larger particles (160). To generate HA nanoparticles of systematically varying crystallinity and size, we varied the hydrothermal aging times (A1, A2, A3) and utilized different precursor salts (B1),

while maintaining temperature and pH. Extensive characterization via TEM, SEM, FTIR, and pXRD defined the specific nanoscale properties of the resulting particles (Table 4.1). In particular, the importance of the choice of precursor salts is evident in comparing A3 particles and B1 particles, which exhibited similar length, but varied in crystallinity. The resulting particles ranged from having biologically relevant lengths and crystallinities (A1) (26, 147) to longer dimensions and higher crystallinities (A2, A3, B1), enabling us to systematically evaluate the effects of nanoparticle size on tumor cell behavior. Incorporation of these well-defined particles into PLG scaffolds resulted in the presentation of the particles at the porous surface of the scaffolds, enabling interactions with seeded cells (Fig. 4.5). Such scaffold systems will be critical for the identification of parameters for the design of non-tumorigenic mineral-containing and mineral-containing matrices for bone regeneration.

It has been shown that HA and other calcium phosphate surfaces efficiently adsorb adhesive and serum proteins (e.g. fibronectin) that are crucial in mediating cell attachment and tissue formation (63, 84, 161, 162). Other studies with different material systems have demonstrated that nanoparticle size modulates protein adsorption (163), and our results further indicate that altering the nanoscale properties of HA affects overall protein adsorption behavior (Fig. 4.6). Specifically, our studies reveal that the overall magnitude of protein adsorption decreases monotonically with increasing HA crystal size. Additionally, decreasing the crystallinity of HA nanoparticles (assessed by the IR splitting factor) independent of overall size also increases the protein adsorption capacity of the scaffolds, as indicated by differences in serum protein adsorption between scaffolds fabricated from particle sets A3 and B1 (Fig. 4.6A). Overall available scaffold surface area may vary based on particle size and shape, and these changes may contribute to the observed differences in protein adsorption. Nevertheless, our

results measured with scaffolds in which the amount of HA was normalized to surface area indicate that nanoparticle characteristics also modulate total adsorption capacity (Fig. 4.6C). These changes in protein adsorption may have important implications for general bone function as well as metastatic bone disease, as altered protein adsorption broadly modulates cell adhesion, proliferation, and survival of osteoclasts (164), osteoblasts (22, 161, 162), and breast cancer cells (63). It is likely that adsorbed RGD-containing proteins, such as fibronectin, may be involved in these effects, as these biomolecules regulate cell attachment (165), focal adhesion formation (166), and proliferative signaling pathways (167).

Cell behavior is affected by mineral characteristics. For example, osteoblasts respond differently to HA as compared to tricalcium phosphate (TCP) (168), and amorphous calcium phosphate and highly crystalline HA exhibit varying levels of osteoconductivity (76). Similarly, HA and TCP elicit varying levels of differentiation in pre-osteoclasts (169) and resorptive activity in mature osteoclasts (170). Additionally, the results of our study indicate that nanoscale mineral properties are crucial regulators of tumor cell behavior. In particular, scaffolds that contained smaller and less crystalline particles and adsorbed more adhesive proteins out of serum also supported more initial breast cancer cell adhesion and proliferation (Fig. 4.7A, B). While enhanced secondary tumor formation in the bone is generally attributed to resorptive release of growth factors and other soluble cues (1), our data support the idea that direct interactions with the mineral matrix could give rise to increased tumor formation and cancer cell growth in the bone microenvironment. Pathologically, our data suggest that exogenously introduced HA may regulate cellular adhesion and growth through adhesive protein adsorption, and thereby serve as a high affinity-substrate for metastasizing breast cancer cells. *In vivo*, TE bone has been observed to serve as a metastasis target (100), and recent evidence indicates that cancer cell-bone matrix

interactions activate invasive and proliferative potential (148), further supporting the contention that HA may be involved in the breast cancer cell avidity for bone.

IL-8 secretion is linked closely to osteoclast-mediated osteolysis in metastatic breast cancer (66) and is known to be enhanced through cell-HA interactions (63). Our current study suggests that the nanoscale properties of HA strongly affect overall IL-8 expression, with larger and more crystalline HA stimulating significant IL-8 upregulation in breast cancer cells (Fig. 4.8). This finding is somewhat surprising since IL-8 expression may be expected to correlate with protein adsorption, as integrin engagement affects IL-8 transcription in certain cancers (44). However, upon adsorption onto surfaces, in particular crystals, protein conformation, and possibly the presentation of cellular binding sites, may change (84, 171). Therefore, it is possible that though more protein is adsorbed to the smaller, less crystalline particles, these proteins no longer have their native conformation and do not trigger IL-8 expression. It is also possible that the cell-mineral interactions affect IL-8 production by breast cancer cells through other mechanisms. For example, nanoparticles could become loosened from the scaffold during cell growth and induce an inflammatory reaction, as environmental particles are known to activate proinflammatory signaling (172). Although not clear from the current study, our mineral-containing system could be further employed to investigate these possibilities.

While the insights provided by our system have pathological significance, future studies can take into account the broader complexity of breast cancer and the bone microenvironment. For example, in this study we have solely tested the cellular response of a highly metastatic breast cancer cell line, but it is possible that non-metastatic breast cancer cells may also be responsive to HA. In fact, HA may promote growth and invasiveness in non-metastatic breast cancer cell lines, and this response may be clinically significant, as microcalcifications in the

breast are associated with malignancies and could potentially play a role in driving tumor progression (173). Furthermore, this platform could be used to investigate interactions between breast cancer cells and osteoblasts and osteoclasts to fully recapture the cellular aspect of bone. Both of these cell types induce the osteolytic capability of breast cancer cells (63, 66, 174), and both may be affected by nanoscale HA characteristics (175, 176). Mineral-containing tumor models incorporating hydrothermally-aged HA nanoparticles provide the capability to address these aspects of the bone microenvironment and thereby have the potential to improve our understanding of the molecular mechanisms underlying bone metastasis that may ultimately enable the discovery of novel therapeutic targets for patient care. Moreover, the use of sHA in culture models could broadly provide insight into basic bone biology and the potential risks of new classes of mineral-containing and mineral-containing matrices for bone regenerative technologies.

4.6 Conclusions

We have created a mineral-containing platform that recreates certain aspects of the 3-D bone microenvironment by incorporating well-defined sHA nanoparticles into a TE biomaterial scaffold. We have used this platform to investigate the effect of nanoscale HA characteristics on breast cancer cell behavior, and our study indicates that the nanoscale properties of HA play a key role in regulating breast cancer cell behavior. In conjunction with previous evidence that osteolytic lesions are sites of low-crystallinity and smaller mineral particles (26), this work suggests that altering the nanoscale properties of microenvironmental bone mineral could play a role in the formation of a metastatic niche in bone supporting enhanced tumor cell colonization and growth. Specifically, we have demonstrated that smaller, less crystalline HA particles increase cellular adhesion and growth, while larger and more crystalline HA enhances breast

cancer cell expression of the osteolytic factor IL-8. Overall, our findings provide new evidence that the vicious cycle of bone metastasis is not only mediated by growth factors in the bone microenvironment, but also by the actual materials characteristics of the mineral matrix.

4.7 Acknowledgments

CF and LAE acknowledge support from the Cornell Nanobiotechnology Center (NBTC), a Science and Technology Center (STC) of the National Science Foundation under Agreement No. ECS-9876771 and the Cornell Center for Materials Research (CCMR) with funding from the Materials Research Science and Engineering Center program of the National Science Foundation (cooperative agreement DMR 0520404). SPP and DWL acknowledge support from National Science Foundation Graduate Research Fellowships. In addition, CF acknowledges partial support from the National Institutes of Health through the Musculoskeletal Repair and Regeneration Core Center at the Hosptial for Special Surgery in New York (Grant AR046121). Particular acknowledgement is made of the use of the microscopy and x-ray facilities of the CCMR. We thank Dr. Michael Rutzke (USDA Robert W. Holley Center, Cornell University) for his help with ICP, Mr. John Grazul and Dr. Yuanming Zhang (both CCMR) for assistance with sample preparation and electron microscopy, and Prof. Paul Soloway and Dr. David Infanger (both Cornell University) for support with RT-PCR measurements.

CHAPTER 5: MINERAL-CONTAINING FILMS TO STUDY INTEGRIN-MEDIATED CELL-HA INTERACTIONS

5.1 Contributors

I performed all of the experiments in this chapter independently. However, I was assisted greatly by technical insights from Dr. Debra Lin and Dr. Lara Estroff. Dr. Claudia Fischbach and I designed this study.

5.2 Introduction

Osteopontin (OPN) has been identified as both a marker and mediator of metastatic breast cancer. Patient data indicates that ectopic expression of highly-phosporylated OPN in breast tissue is a common feature in mammary malignancies (142), and levels of soluble OPN in plasma are generally observed to be elevated in cases of bone metastasis (177, 178). Work with cancer cell lines has also revealed that OPN is an integral part of the recently developed bone metastasis gene signature (18, 110, 179). Functionally, OPN is thought to be a major player in cell attachment (127), cell motility and migratory capacity (180), and matrix metalloproteinase (MMP)-mediated extravasation (181). Given the importance of all of these cellular characteristics in controlling tumor progression and metastasis, further study of the specific effect of OPN on mammary tumor cells in justified.

Notably, OPN was first identified as a protein within bone (182). Further studies have indicated its natural presence in other tissues, but OPN remains one of the most abundant noncaollagenous proteins in bone (183). The accumulation of OPN in bone may be due to its intimate interaction with hydroxyapatite (HA), the inorganic mineral component of bone (30, 184). The proclivity for OPN to interact with and bind to HA is controlled by its poly-aspartic acid domain: this long chain of negatively-charged aspartate residues mediates electrostatic

attraction to the mineral substrate (47, 185, 186). In addition to its poly-aspartic acid domain, OPN contains cell attachment sequences, including the well known RGD motif (48, 187). In bone, OPN is known to mediate adhesion of both osteoblasts and osteoclasts, helping to facilitate a wide variety of cellular activities required normal skeletal function. For example, OPN is involved in homing and adhesion of osteoblast progenitor cells during de novo mineralization (188). OPN has also been discovered to be critical in allowing osteoclast attachment and the initiation of bone turnover (189, 190). The ability of OPN to bind mineral and subsequently dictate cellular behavior may play an important role in breast cancer metastasis, given that mammary tumors are frequently associated with ectopic microcalcifications composed of HA that are detected by mammography (24, 27, 130).

Despite mounting evidence suggesting that HA directly contributes to the genesis of malignancies (27), and previous studies that have implicated HA as a potentially pro-metastatic biomaterial (23, 24, 63), no definitive mechanisms by which these phenomena could potentially occur have been suggested. In particular, HA has been shown to induce secretion of pro-tumorigneic cytokines, including interleukin-8 (IL-8). Here, we investigate the ability of OPN to mediate the pro-metastatic effects of HA. The results could be physiologically relevant considering the ability of OPN to mediate cell-mineral interactions and the consistent overexpression of OPN in breast cancer. Due to its RGD-domain, OPN can interact with cancer cells through integrin receptors (191). Integrins are the most widely-studied mediators of cell-ECM interactions. They are a large family of heterodimeric surface receptors that as a whole bind a wide range of ECM proteins to anchor cells through the formation of focal adhesions. Focal adhesions are not purely structural complexes, as they are fully capable of activating intracellular signaling machinery (46). In particular, integrin engagement is often accompanied

by activation of focal adhesion kinase (FAK), which in turn stimulates a host of proliferative and transcriptive cellular responses (192). Understanding how HA affects integrin engagement will help to reveal how mineral acts as a microenvironmental regulator of cell behavior through ECM binding. Past work has demonstrated that integrin engagement can be affected by various features in the tumor microenvironment including three-dimensionality (44) and protein folding (21), and it is quite possible that mineral acts in a similar manner.

Because mammary tumors have a predilection to metastasize to bone and are often found in conjunction with microcalcifications in the breast, the relationship between breast cancer cells and HA should be explored. Drawing from Paget's seed and soil theory, it is possible that HA microcalcifications represent a microenvironmental feature that primes cancer cells to colonize the bone. Though HA interactions with proteins found in ECM have been widely observed, few connections to how these effect integrin engagement and cell behavior, especially in the context of cancer, have been found. Further studies into the underlying molecular mechanism are required to truly exploit this as a point of therapeutic intervention. To help address this challenge, we developed a mineral-containing film model that allowed the study of integrin function in the presence of HA. This model has been designed to reflect certain features of malignant microcalcifications like mineral-clustering that may be critical to recreating effects of tissue structure on cell-ECM interactions. Our findings indicate that integrin engagement may indeed be a mediator of HA-regulated tumor progression and illustrate the need for mineral-containing platforms in studies of metastatic breast cancer.

5.3 Materials and Methods

5.3.1 Film fabrication and characterization

Films were fabricated based on a modified protocol previously used for spin casting poly-(lactide-co-glycolide) (PLG) (193). A theoretical film thickness of 30 nm was used to define parameters based on an equation developed by Daly et al. (194). First, glass slides (Fisher) were cut to 25 mm X 25 mm using a diamond scribe. They were then washed sequentially in acetone, isopropyl alcohol, and DI water in an ultrasonic bath to clear dust and any organic residue. PLG solutions were prepared by dissolving PLG pellets (Lakeshore Biometerials) in chloroform (Sigma). PLG concentration was varied between 1% and 2% by weight. For mineral-containing films, HA particles (Sigma) were dispersed into the PLG solutions at varying weight concentrations. To ensure optimal dispersion, the solutions were subjected to sonication just prior to film deposition.

Film deposition was performed under clean room conditions using a spin casting set up. The spin speed was set to 2000 rpm, and casting took place over 60 seconds. 1 mL of PLG solution (either mineral-containing or not) was used for each glass square (Fig. 5.1). Just after spin casting, the films were placed in an oven at 60°C for 2 hours. This allowed excess chloroform to completely evaporate. After casting of films, they were stored for no more than 1 week in sterile DI-water prior to use in cell culture. Both mineral-containing films and non-mineral-containing films were generated.

Films were characterized by AFM and protein adsorption measurements. AFM was performed in tapping mode on 100 μm^2 sampled areas to determine overall mineral distribution and surface roughness. For determining overall levels of protein adsorption, films were first incubated with 50 ng/mL of recombinant human OPN (R&D systems) for 1 hour to enable adsorption. This OPN variant is expected to be highly-phosphorylated according to the

manufacturer. After one hour, the OPN-containing solution was collected and unadsorbed protein was measured through ELISA (R&D) according to manufacturer's instructions.

5.3.2 Scaffold fabrication

Three-dimensional (3-D) non-mineral-containing and mineral-containing scaffolds were created according to a past protocol (60). Scaffolds were also composed of PLG and HA nanoparticles (Sigma), and were synthesized through a gas-foaming/particulate-leaching procedure in which

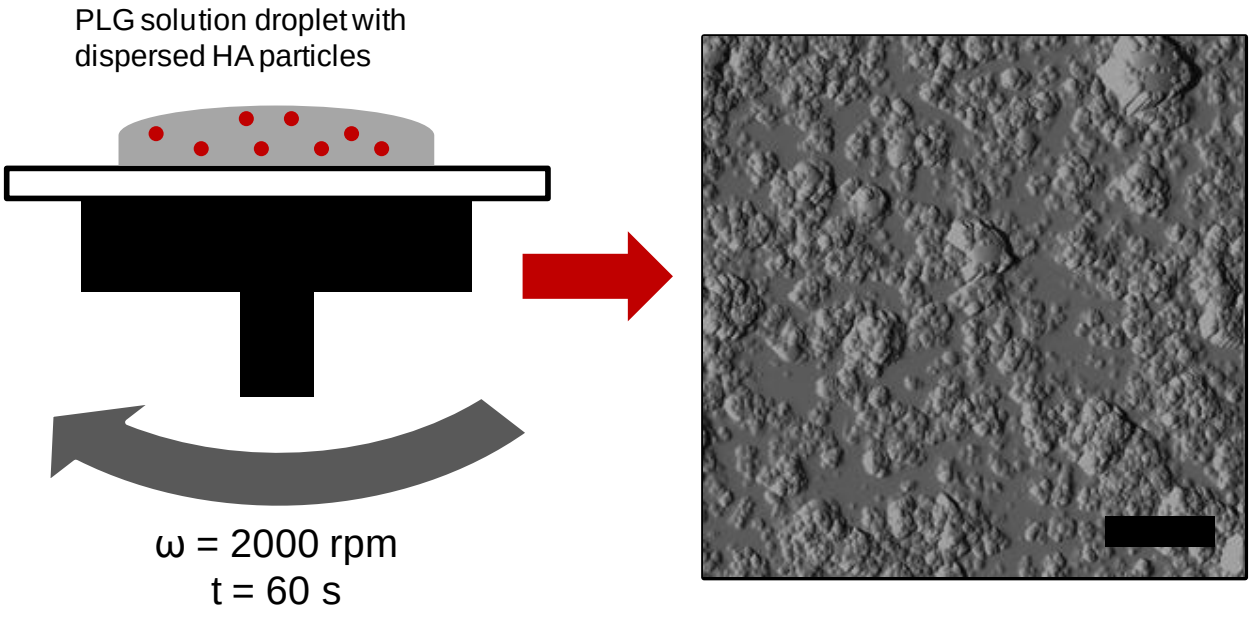

Figure 5.1: Spin casting mineral-containing films
Schematic of spin casting technique as used for generation of mineral-containing films. Parameters were developed based on empirical equations defined in (153). Representative micrograph from AFM shown on the right. Scale bar represents 2 μm.

NaCl was used as a porogen. Scaffolds were used to determine if trends observed for 2-D mineral-containing films remained true in a 3-D context.

5.3.3 Cell Culture

All experiments were performed using MDA-MB231 cells (ATCC). Cells were maintained under standard culture conditions (37°C, 5% CO_2) in complete DMEM (10% FBS [Tissue Culture Biologics], 1% PS [Gibco]). Films were sterilized in 70% ethanol for 30 minutes and then washed with sterile PBS prior to seeding. Seeded films were also cultured in standard conditions within a 6-well tissue culture plate for up to 5 days. 3-D cultures were performed in the same way as previously described (108). Cell growth was quantified in two ways. First, cells would be trypsined and detached from their substrate and counted using a Coulter Counter (Beckman Coulter). Alternatively, cells were lysed in Caron's Buffer, DNA was labeled with a fluorophore (PicoGreen, Invitrogen), and total DNA content was measured using a spectrophotometric plate assay.

5.3.4 IL-8 quantification and inhibitory studies

24 hours prior to assay time points, culture media was changed to DMEM/1% FBS for serum starvation. Upon collection, media was centrifuged to remove cell debris prior to assaying. To quantify IL-8, ELISA (R&D) was run on collected media according to manufacturer's instructions. To inhibit integrin $\alpha_v\beta_3$, a monoclonal antibody against this receptor was used (LM609, Millipore). Similarly, an antibody to block the β_1-containing integrins was also used (MAB17781, R&D systems). Cells were pre-incubated with these antibodies for 30 minutes prior to seeding. For inhibition of FAK phosphorylation, the small molecule PF573228 (Tocris) (1 μM) was included in media, while the small molecule B581 (Sigma) (100 nM) was used to block Ras function. Both PF573228 and B581 were tested at various concentrations to determine dose response and potential cytotoxicity. While B581 was soluble in aqueous media, because PF573228 was only soluble in DMSO, DMSO-only was also tested. All three inhibitors were

administered on the day of seeding and were also given during media refreshment 24 hours prior to sample collection. After media was collected, it was also characterized for total IL-8 through ELISA as described above.

5.3.5 Statistical Analysis

All samples were run in triplicate. A confidence interval of 95% was used to determine statistical significance ($p<0.05$) via Student's t-test or ANOVA in conjunction with Tukey post-hoc-analysis. Significance was denoted by (*) for results relative to control conditions, while (#) was used to indicate specific pairwise comparisons. All data are represented as average ± standard deviation.

5.4 Results

5.4.1 Effect of integrin inhibition on IL-8 secretion

In conventional 2-D cultures on plastic, we found that pre-treatment with integrin monoclonal antibodies reduced overall cell numbers after 3 days of culture (Fig. 5.2A). This effect was observed with inhibition of both $\alpha_v\beta_3$ and β_1. β_1 inhibition had a stronger effect on the change in cell number, inducing a 36% decrease in cell number. Combined treatment with both integrin inhibitors showed a slight synergistic effect, causing a 50% decrease in cell number. Conversely, when IL-8 data was analyzed, it was found that $\alpha_v\beta_3$ inhibition had the stronger effect, leading to a 57% decrease in overall secretion (Fig. 5.2B). β_1 blocking did not significantly affect IL-8 secretion, and use of both antibodies did not produce an effect beyond

that observed for $\alpha_v\beta_3$ alone.

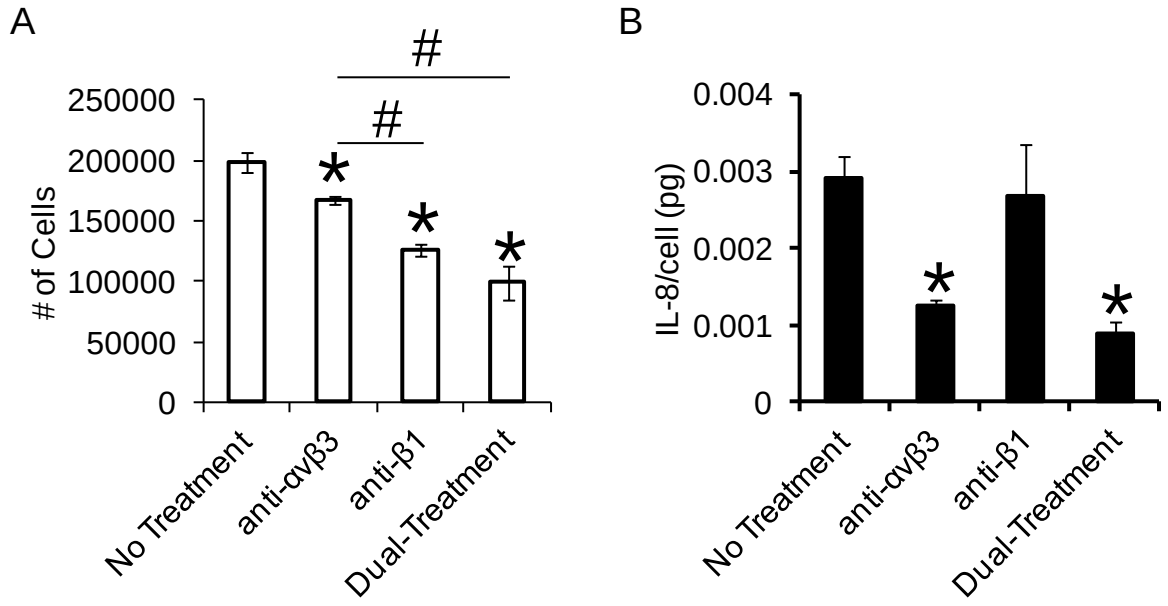

Figure 5.2: Effect of integrin inhibition on MDA-MB231 cell behavior
(A) Number of cells after 3 days of culture with integrin inhibitors as assessed through hemacytometer. Results indicate that treatment with inhibitor of β1 causes greatest decrease in cell growth. (B) IL-8 quantification via ELISA for same experiment shows that only inhibition of αvβ3 attenuates secretion of IL-8. (*$p<0.05$)

5.4.2 Effect of downstream signaling targets of integrins on IL-8 secretion

To determine if known downstream effectors of integrins potentially play a role in integrin-mediated IL-8 secretion, inhibitors against FAK (PF573228) and Ras (B581) were utilized. Initial studies on dose dependency indicated that neither molecule had a deleterious effect on cell health, though PF573228 did cause a slight decrease in cell growth over a 3 day period (data not shown). When averaged on a per cell basis, we found that IL-8 secretion is significantly reduced with administration of both inhibitors. B581 produced a sharper decrease of 40% in overall IL-8 levels (Fig. 5.3).

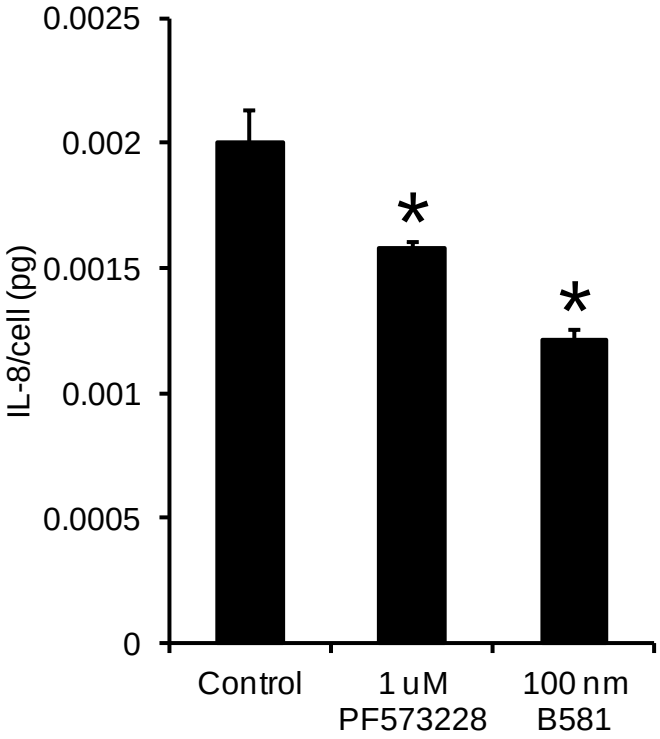

Figure 5.3: Inhibition of FAK and Ras and effects on IL-8 secretion
Inhibition of FAK phosphorylation (by PF573228) and Ras activation (B581) lead to decreased IL-8 IL-8 secretion as measured by ELISA. (*$p<0.05$)

5.4.3 Characterization of films

Since to our knowledge spin-casting of mineral containing polymer films had yet to be achieved, we began by attempting varying formulations to yield the ideal surface coating. Concentrations of both polymer and mineral were varied to obtain the most uniformly coated surface with minimized roughness. Using AFM, spin cast surfaces were microscopically inspected and roughness was quantified. Regardless of formulation, all mineral-containing films were relatively rough, especially when compared to smooth non-mineral-containing films. However, increasing HA content to 8% resulted in a notable decrease in roughness (Fig. 5.4A). This is due to less mound formation during spin-casting, as observed in AFM images (Fig. 5.4B). Tapping mode was used to calculate overall roughness on a single film initially (thus the lack of statistics in Fig. 5.4A). After initial roughness measurement, 8% HA films were selected for further evaluation. Film stability and adhesion to the underlying glass slide were evaluated by washing in PBS. Weaker film formulations would delaminate and break apart during the washing procedure. Increasing the PLG concentration in the original solution to 2% from 1% alleviated issues with loss of film integrity. In the end, 8% HA and 2% PLG (weight percentage) were found to provide the ideal balance of properties (termed MIN herein).

5.4.4 Effect of mineral on cell behavior

After obtaining preliminary evidence that integrin-based signaling could underlie cancer cell regulation of IL-8, we next investigated how mineral may further modulate these interactions. First, the basic effect of HA in 2-D culture was explored. Over 3 days, cells grew by nearly 67% on HA-containing films (MIN). Growth was much slower over the same time period on non-HA-containing films (125) at just under 30% (Fig. 5.5A). IL-8 secretion was also enhanced on MIN films relative to the NM controls (Fig. 5.5B).

5.4.5 Relationship between integrin engagement and HA in promoting IL-8 secretion

Since we had observed that blockade of the OPN-binding $\alpha_v\beta_3$ integrin attenuates (Fig. 5.2) and HA promotes IL-8 secretion (Fig. 5.5), the role of OPN in our system was next tested. First, the OPN adsorption capacity of HA was quantified. Examination of the amount of unbound protein after incubation with films indicated that MIN films were superior in terms of OPN adsorption. In fact, after 1 hour, over 99% of OPN was observed to be stably bound to MIN films (Fig. 5.6A). To test if integrin engagement with proteins such as OPN was enough to induce IL-8 secretion, cells were cultured for 24 hours on MIN films pre-adsorbed with OPN in serum-free medium. While culture with OPN did not lead to more IL-8 production than normal culture with serum, pre-incubation of cells with the LM609 blocker caused a nearly 4-fold decrease in secretion, similar the level of inhibition observed on tissue culture plastic (Fig. 5.6B). Use of LM609 in 3-D cultures in non-mineral-containing scaffolds (PLG) and mineral-containing scaffolds (PLG/HA) also resulted in a significant reduction in IL-8 secretion (Fig. 5.7).

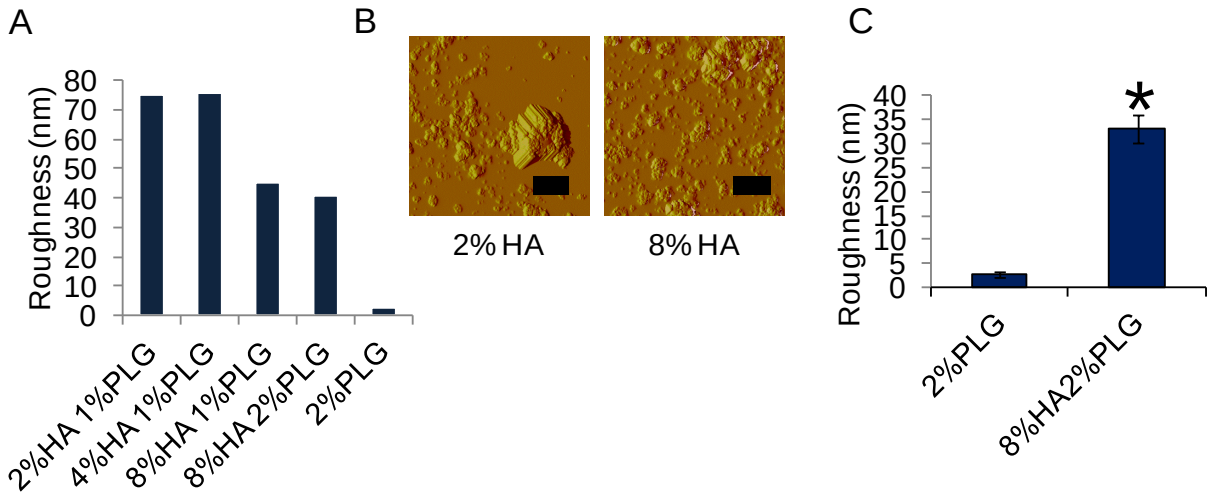

Figure 5.4: AFM characterization of films
(A) Initial testing with AFM revealed that increasing HA content in spin casting solution to 8% resulted in the smoothest films among mineral-containing group. (B) Representative AFM micrographs of films. With 2% HA, formation of large mounds was common. Scales bars represent 2 μm. (C) Further testing

with 8%HA and 2% PLG films revealed consistent roughness measurement, indicating acceptable batch-to-batch variation. (*p<0.05)

5.5 Discussion

Because mammary tumors are in the presence of HA both near microcalcifications in the breast and eventually in bone after metastasis, understanding the dynamics of their interactions might help to determine what drives and causes malignant progression. While HA-containing systems have been produced in the past, the role of ECM proteins in modulating cell-HA interactions has remained relatively unstudied. Thus, even though it is known that HA is a biomaterial that can actively dictate cell behavior (24), the mechanisms by HA directly interact with cells are still not totally clear. In this study, mineral-containing films have been employed in conjunction with simple inhibitory strategies to help develop a basic signaling model through which HA can instruct cellular behavior. Our data suggest that HA may affect cancer cells by modulating interactions with ECM proteins, inducing cells to secrete increased levels of pro-tumorigenic and pro-metastatic cytokines such as IL-8.

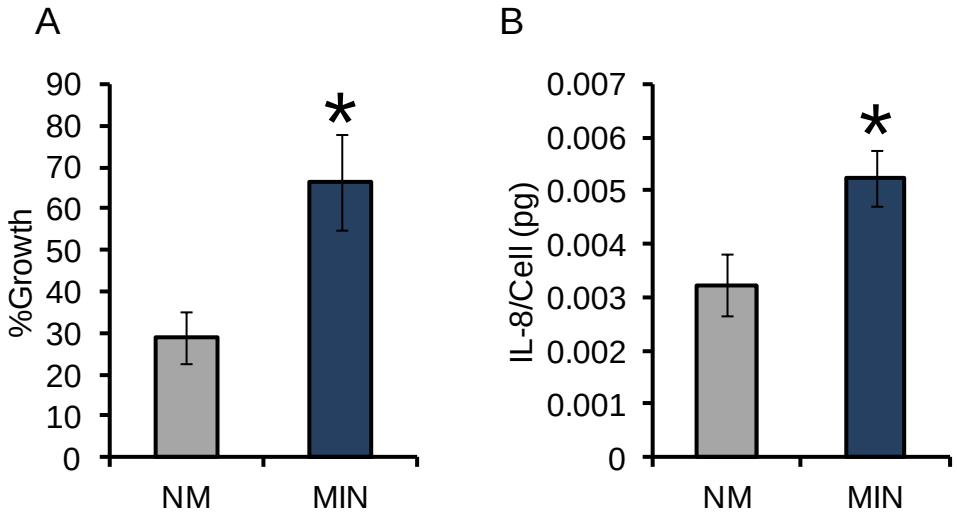

Figure 5.5: Cell behavior on films (A) Cell growth on films after 3 days in culture as measured by hemacytometer. Results show that MDA-MB231 cells grow more than twice as fast over this time frame

on mineral-containing films (MIN). (B) IL-8 ELISA further indicates that cells also secrete more IL-8 on mineral-containing films compared to controls (NM). IL-8 data was normalized on a per cell basis. (*$p<0.05$)

Cell-ECM interactions are an integral component of the tumor microenvironment. Integrins are utilized by cells to anchor to and receive signal inputs from ECM proteins. The activity and engagement properties of integrins are known to be dysregulated in a variety of cancers (195). In metastatic breast cancer, expression of integrin $\alpha_v\beta_3$ can be upregulated (196), and our findings here suggest that this upregulation may be related to enhanced IL-8 levels. Increased levels of IL-8 are clinically observed in a variety of cancers, and this is especially true in the case of cancer that exhibit tendency to metastasize to bone (114, 135). Taken together, these findings allow us to infer that IL-8 secretion may be microenvironmentally regulated by cell-ECM interactions and specifically integrin engagement.

Interestingly, while blocking $\alpha_v\beta_3$ with LM609 attenuated IL-8 secretion, β_1 inhibition did not generate similar results (Fig. 5.3). Physiologically, both of these sets of integrins bind to ECM proteins at RGD-sequences. It may be that despite engaging similar ECM proteins, the two types of integrins control fundamentally different signaling pathways. β_1 inhibition did hinder cell growth more effectively (Fig. 5.3), demonstrating that β_1 integrins were actively affecting overall cell phenotype. Taking this observation into account, our findings suggest that multiple integrins control various aspects of behavior that are relevant to tumor progression. In terms of inducing IL-8 signaling, we explored several downstream effectors of integrins that are associated with the clustering of proteins that takes places during focal adhesion formation. We used an inhibitor of FAK phosphorylation (P573228) and were able to show decrease in IL-8 secretion similar to that observed when using LM609. Furthermore, blocking activation of Ras, a protein that is known to be connected to pFAK and can induce transcriptional signals (197) also

produced a drop in IL-8 levels. The fact that blocking each of these signaling molecules produced the same effect in the context of IL-8 strongly suggests that they are involved in inducing its production. Indeed, Src, which has been shown in other studies to be heavily involved in IL-8 transcription (179, 198, 199), is part of a well-known signaling cascade that is initiated by FAK and involves Ras (200). While inhibition of Ras had a definite effect on IL-8, it did not alter cell growth, indicating that the pathway by which β_1 integrins might promote mitogenic activity is fundamentally different than the one proposed here for IL-8 production.

Microcalcifications are a common feature associated with mammary tumors. They represent one of the most important diagnostic markers used in contemporary medicine. While their presence has been used clinically, this utility has been limited to helping surgeons identify tumor margins (201). Past work from our studies and others indicates that HA may actually actively affect metastatic progression (23, 108). Clinical data further suggests that microcalcifications composed of highly crystalline HA have greater than 90% sensitivity in predicting metastasis to bone (27). Understanding how HA can instruct cell behavior might be important to determining how microcalcifications influence metastagenicity. Here, our findings implicate HA in promoting both tumor cell growth and IL-8 secretion (Fig. 5.5). These results corroborate studies with HA in other culture models (24, 63), but our studies further demonstrate that these effects are directly mediated by adsorption of RGD-containing proteins such as OPN (Fig. 5.6B). Comparison with a 3-D model indicates that integrin blockade similarly affects cells in scaffolds, ensuring that our findings are not an artifact of 2-D culture. 2-D culture may in fact be physiologically relevant for this case, because cellular interactions with mineral at the nanoscale are largely polarized and planar, as for example with osteoclasts (202). OPN has been found to be overexpressed in many mammary tumors, and high levels in the ductal structures are

correlated specifically with bone metastasis (31, 56, 203). As our data show, HA as presented in microcalcifications adsorbs OPN extremely effectively (Fig. 5.6A). Potentially, microcalcifications act as sinks for OPN, which is not typically found in non-lactating breast tissue, thereby providing a specific ECM motif that can stimulate production of IL-8 and help to initiate bone metastasis.

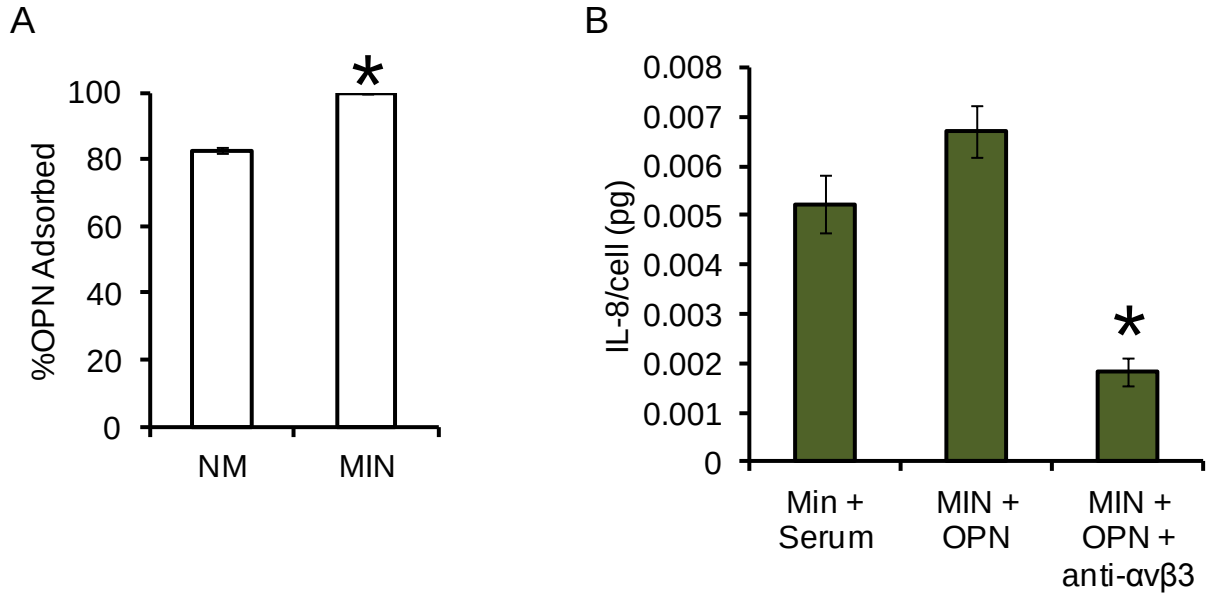

Figure 5.6: OPN adsorption on films and effect of αvβ3 inhition
(A) Bicinchonic assay (BCA) shows that OPN adsorption is enhanced on mineral-containing films. (B) Measurement of IL-8 by ELISA shows that OPN alone allows cells to secrete IL-8, and that blocking integrin αvβ3 causes decrease in this secretion. (*$p<0.05$)

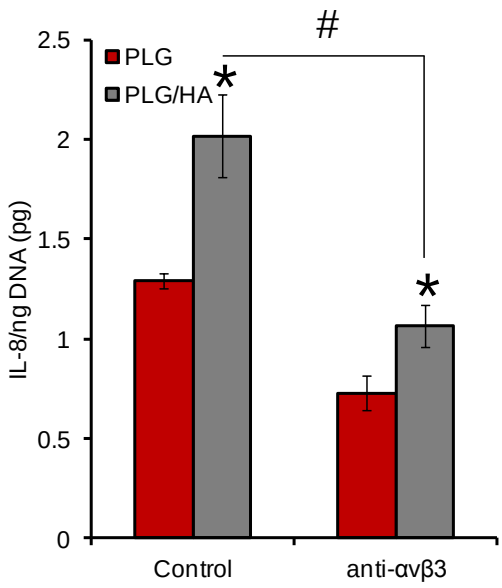

Figure 5.7: IL-8 secretion under integrin inhibition in 3-D
ELISA on 3-D conditioned media shows that blocking integrin αvβ3 reduces IL-8 production in mineral-containing scaffolds also.

Though this study helped to elucidate potential mechanisms by which HA in microcalcifications can influence malignant cell behavior, several limitations exist. The effect of HA properties on protein adsorption have been neglected, as commercial mineral has been used. Other studies have illustrated that adsorption capacity and even the types of proteins adsorbed may differ if mineral properties change (59). It is possible that changes in mineral properties could also affect protein folding. Given the distinct difference that we observed in cell behavior in response to blocking integrins $\alpha_v\beta_3$ and β_1, it is worth noting that preference for engagement could be modulated by changes in folding. β_1 integrins like $\alpha_5\beta_1$ require the proximity of a "synergy site" for effective engagement (204), while no such requirement exists for $\alpha_v\beta_3$. In both fibronectin, the predominant peptide found in serum, and osteopontin, the synergy site's proximity to the RGD-sequence is controlled by protein-folding (205). When proteins become unfolded, the synergy site can be too far from the RGD-sequence to allow effective integrin engagement. It is possible that this type of phenomenon affected our findings. Further, while MDA-MB231 cells represent an excellent model for aggressive breast cancers, integrin expression is extremely heterogeneous across cancer populations, making it difficult to definitively characterize a single integrin as being solely responsible for a response as important as IL-8 secretion. Still, since past studies have shown that HA promotes IL-8 response in a host of cell lines (63), it is likely that the findings here reflect an actively important mechanism for production of pro-metastatic cytokines.

The generation of systems that incorporate HA for presentation to cells is an emerging and growing research interest. It is increasingly apparent that cell-mineral interactions play a role in the pathogenesis of mammary and other tumors. By developing a film system that easily enables uniform protein adsorption, we have been able to gain basic insights into how cell

behavior can be dictated by mineral. Though 3-D systems offer an increased level of complexity for recapitulating physiological microenvironments, the film system enabled simpler evaluation of basic protein adsorption and its relationship to cell behavior. Because cell-HA interactions produced similar response in both 2-D and 3-D, and because planar systems are more amenable to a diversity of imaging techniques, there is strong potential for future implementation of the films for further study of cell-mineral interactions. With a stronger understanding of how specifically mineral drives the progression of cancer, the community is better equipped to identify new and potentially more efficacious targets for therapies.

CHAPTER 6: CONCLUSIONS

In total, the studies outlined herein show that HA can be deeply involved in the metastatic cascade that ensues when breast cancer advances to and colonizes the skeleton. Overall findings have provided insights that are valuable not just to cancer biology, but also to the fields of tissue engineering and biomaterials science in the context of tumor model development. Mammary tumor cell interactions with mineral and the factors facilitating and controlling these interactions were studied within engineered material systems to reveal biomolecular mechanisms and cytokine signaling networks that underlie bone metastasis. Furthermore, the relationship between HA materials properties and cellular activity was illuminated, and the vast potential for using carefully-defined synthetic HA in biomedical engineering was explored. Since breast cancer cells are exposed to mineral at both the primary and metastatic site in the form of microcalcifications and bone, respectively, the development of tools to specifically investigate how cells interface and respond to mineral may prove useful in the identification of novel therapeutic possibilities. Moreover, because tissue engineering principles were used to conceive the systems utilized in these studies and because HA has been identified as a bioactive material that is being increasingly employed in implants, the potential tumorigenic effects of mineral that were highlighted are especially crucial to understand. The overriding research plan was performed to specifically investigate three major concepts that as a whole aimed to confirm the original hypothesis that mammary tumor cell-mineral interactions essentially promote the directed formation of osteolytic metastases in bone. These three conceptual questions are specifically defined in section 1.6.

6.1 Mineral promotes osteoclastogenesis by enhancing tumor cell secretion of osteolytic factors

The phenomenological relationship between HA and MDA-MB231 cells was first studied. Changes in cell behavior were studies in terms of how they may functionally promote the osteolytic phenotype observed in skeletal metastases originating from mammary tumors. This was accomplished by using a biomaterials system that was designed based on tissue engineering principles. The fabrication of gas-formed/particulate leached HA-containing scaffolds and their use as platforms for research of cancer biology was described (Chapter 2). Initial investigations focused on confirming that cells were appropriately exposed to mineral within this scaffold system, and subsequently, a variety of assays was used to determine how cell behavior varied in mineral-containing scaffolds relative to non-mineral-containing controls. Specific increases in IL-8, a molecule established as having the capability to drive osteolytic activity, were observed for MDA-MB231 cells. Further evidence to corroborate these findings was presented in Chapter 3, where it was demonstrated that DCIS cell lines exhibited similar behavior in mineral-containing scaffolds. Taken together, these results suggest that cell-HA interactions certainly may promote osteoclast differentiation via soluble IL-8.

Initially, the surface presence of HA in scaffolds was assessed through a variety of physicochemical characterization techniques including EDS, microCT, and microscopic inspection (Fig. 2.1). More careful inspection with electron microscopy showed definitively that HA was available to cells within scaffold pores (Fig. 4.5-6). Observation of cell attachment to scaffolds revealed that HA enabled a pronounced adhesion advantage for breast cancer cells upon static seeding. Not only did quantitative analysis demonstrate more cells in the scaffold in total, histological analysis showed that cells were able to adhere in the innermost pores of only

mineral-containing scaffolds (Fig. 2.2). Cell growth and IL-8 secretion were also higher in mineral-containing scaffolds, and through use of conditioned media, we saw that this tumor-derived IL-8 did indeed cause a dramatic increase in differentiation of RAW 264.7 osteoclast precursor cells. Analysis on mineral-containing surfaces showed that resorptive activity was also increased in the presence of conditioned medium from mineral-containing cultures and that this effect was mediated by IL-8 at least in part (Fig. 2.4-5).

Though these studies taken together certainly provided evidence that HA altered breast cancer cell behavior in a functional manner, a molecular understanding of these phenomena was not yet developed. Other potential molecular players were still not identified, mediators of cell-HA interactions had not been studied, and the avidity for bone displayed by breast cancers was unexplored. Furthermore, the value of attempting to recapitulate bone with the scaffold was still undetermined, as skeletal mineral differs significantly in terms of distribution in tissue, composition, and material properties from the commercial HA we had used. Still, this initial work did demonstrate that the scaffold system was effective for probing cell-mineral interactions, and it was indicated that the model may be suited to study microcalcifications, a common feature in mammary tissue for metastatic breast cancer. With these limitations acknowledged, it was clear that further analysis with the scaffold system could help in elucidating how cell-HA interactions were pathologically relevant.

6.2 Exposure to microcalcifications/mineral primes mammary tumor cells for colonization of bone by stimulating MSC-driven recruitment

In studying pathological relevance, mineral-containing scaffold models were again utilized, this time to model tumor cell interactions with microcalcifications in the breast tissue (Chapter 3). A wider analysis on HA-regulated changes in gene expression was performed.

Functional consequences of alterations in breast cancer cell behavior as regulated by HA were also explored further, including effects on driving bone-directed migration through stimulation of MSCs. Studies on other cell types in scaffolds were carried out. Significantly, it was found that MCF10A-DCIS cells, a model representing breast cancer cells that are not fully committed to metastasis, were impacted by the presence of mineral similarly to MDA-MB231 cells. Beyond this, it was observed that metastatic site-specific subpopulations of MDA-MB231 cells all exhibited preference to colonize bone following exposure to HA. Finally, clinical insights were obtained by studying the correlation between mineral, molecular phenotype, and disease outcome in patient samples. The findings from all of these studies helped to demonstrate the validity of the second important concept of overriding hypothesis that the presence of HA could act in a pro-metastatic manner by initiating chemoattraction to stromal cells in bone.

From a disease perspective, DCIS cells are very relevant in study cell-mineral interactions, because microcalcifications are often found to be associated with DCIS cases. Further, comedo-type DCIS, which are most prone to progressing to invasive carcinoma, are frequently diagnosed through mammograms indicating the presence of microcalcifications. An elevation in secreted IL-8 by DCIS cells in the mineral-containing scaffolds helped to corroborate earlier findings with MDA-MB231 cells (Chapter 2), and also represented a major step in proving the physiological relevance of the model. More extensive molecular characterization of the scaffolds revealed that not only were IL-8 levels affected, but genes that had been identified as part of a genetic signature associated with bone metastasis were also upregulated in the presence of HA (Figure 3.3). This finding held true not just for parental MDA-MB231 cells, but also for subpopulations that had previously been identified as lung-specific (4175), indicating that, to some degree at least, expression of the bone metastasis gene signature

is microenvironmentally controlled. Additional confirmation of this was attained by injecting these cells into mice following culture in mineral-containing scaffolds, as they showed a tendency to colonize bone. In the bone, histological analysis provided evidence of osteolysis mediated by the colonizing 4175 cells. Along with the results presented in Chapter 2, there was now a strong suggestion that mineral promotes an overall metastatic and osteolytic phenotype.

Subsequent experiments involved understand the molecular mechanisms that might underlie HA-regulated metastasis to bone. These efforts demonstrated that tumor-derived IL-8 may play an additional role in eliciting SDF-1 secretion by MSCs, cells naturally found in the bone microenvironment. Through inhibition studies, we discovered that MSCs responded to IL-8 via the CXCR1 receptor and then dramatically increased their production of SDF-1 (Fig. 3.4A-B). In turn, it was found that these enhanced SDF-1 concentrations were capable of inducing breast cancer cell migration via chemoattraction. Transcriptional analysis had shown that upregulation of CXCR4 by breast cancer cells occurred in the presence of HA, and Western blot and immunofluorescence confirmed that surface presentation of the receptor also increased. Since CXCR4 is the cognate receptor for SDF-1, we postulated that migration may be taking place along the SDF-1/CXCR4 axis and that this cascade was initiated by IL-8 secretions. By separately inhibiting each of these, it was determined that this molecular model was valid (Fig. 3.4D). Mammary tumor cell interactions with HA cause increased secretion of IL-8, which drives SDF-1 production by MSCs. In this way, tumor cells are able to induce their own migration in response to HA. Additionally, HA stimulates increased concentrations of the SDF-1 receptor for tumor cells, thereby sensitizing their migratory reaction. While the scaffold system enabled the development of this fairly robust model, to truly evaluate its validity, these molecular players needed to be studied in a more pathologically relevant context. To this end, a panel of

clinical breast samples was assessed. Though only preliminary data was available, initial observations were promising. In localized analysis of individual ductal structures, there was a correlation between invasiveness and IL-8 level. Gross analysis was limited by lack of benign samples; however, there was at least marginal correlation between the appearance of microcalcifications and IL-8 levels. CXCR4 immunofluorescence also showed a correlation between the appearance of IL-8 and CXCR4 in ducts.

The overall findings presented in Chapter 3 presented an additional level of relevance to actual disease states by integrating the results from the scaffolds system with experiments in animal models and with clinical samples. The functional significance of results with IL-8 in Chapter 2 was explored, leading to the generation of a molecular model for HA-regulated metastasis to bone. To expand our understanding of how HA might initiate this complex cytokine signaling cascade underlying bone metastasis, the dynamics involved in mediating cell-mineral interactions needed to be studied in more detail.

6.3 Crystal properties modulate cell-ECM interaction to alter tumor cell behavior and regulate the malignant phenotype

Cell-mineral interactions in the tumor microenvironment need to be studied in two ways for a comprehensive understanding of how they affect disease. First, the downstream effects on cells need to be studied to understand how cell behavior is altered in terms of adhesion, proliferation, gene expression, secretory behavior, and other relevant properties that drive observed phenotypes. Much of this was studied in Chapters 2 and 3. Second, the fundamental mechanisms by which mineral can affect cells must be understood. Thus, the effects of changes in HA material properties and the modulation of cell-mineral interactions by ECM proteins was finally assessed (Chapters 4 and 5). In the concluding studies, techniques to synthesize well-

defined HA particles and incorporate these into 3-D culture platforms were used to show that changes in crystal properties strongly affected interactions with cells, altering growth and IL-8 secretion patterns (Chapter 4). A 2-D film system that allowed simpler analysis of how ECM proteins such as OPN controlled cell-HA interactions was also used, showing that integrin engagement likely plays a critical role in many of our IL-8 findings (Chapter 5).

Hydrothermal aging was used to synthesize HA with tunable crystallinity and particle size (Fig. 4.1). This novel process relied on separation of the precipitation and aging steps in creating HA. The stark contrast in monodispersity and crystal properties between our synthetic HA and commercially available HA can be observed in Fig. 4.2-3. A batch of HA particles with steadily increasing size and crystallinity was created and incorporated into the scaffold model. Significant differences in serum protein adsorption were found amongst the populations of crystals in scaffolds. Specifically, as HA crystallinity particle size decreased, protein adsorption increased (Fig. 4.6). Similar trends were observed for cell growth and adhesion on the scaffolds containing synthetic HA as well (Fig. 4.7). Conversely, IL-8 secretion increased with increasing size and crystallinity (Fig. 4.8). Highly crystalline HA is generally not found in bone, but microcalcifications sometimes contain this type of mineral. In fact, microcalcifications that are most crystalline and possess the least amount of carbonate substitution are associated with the greatest tendency to invasion in mammary tumors (27). In this context, our findings that highly crystalline stimulates the most IL-8 may be physiologically relevant. Furthermore, the observation that low crystallinity stimulates enhanced adhesion may be related to one advantage for tumor cells to metastasize to bone: because bone mineral is generally of low crystallinity, it would have high adhesive capacity and would be suitable for colonization by circulating tumor cells.

Given these first insights into how HA properties and protein adsorption affects tumor cell behavior, it was next important to understand how ECM proteins were involved in cell-HA interactions. The role of integrin engagement in IL-8 secretion was studied, revealing that integrin $\alpha_v\beta_3$ may be involved in stimulating IL-8 upon focal adhesion formation. Inhibition of downstream signaling targets (FAK and Ras) of this integrin further supported this idea (Fig. 5.2-3). The relationship of integrin binding to IL-8 secretion in conjunction with findings from the previous chapter that protein adsorption was a major determinant of cell behavior led us to use 2-D mineral-containing films for further studies. We observed that exposure to IL-8 enhanced cellular growth and secretion of IL-8 in 2-D, just as it did in 3-D (Chapter 2). It was also found that OPN was preferentially adsorbed on mineral-containing films and could stimulate IL-8 production via engagement of $\alpha_v\beta_3$ (Fig. 5.6). High levels of OPN are a defining feature of metastatic breast cancers, and our results had indicated that OPN upregulation occurs in the presence of HA (Chapter 3). In sum, it becomes clear that mineral properties and interactions with adhesive proteins like OPN are integral in driving bone metastasis.

This work demonstrated the need for understanding the dynamics of the relationship between HA and cells. Materials properties were found to play a major role in affecting how mammary tumor cells interact with mineral. Hydrothermal aging has emerged as a valuable tool to create well-defined HA that can be used to study biological phenomena. Since HA changes as a function of human development and disease, hydrothermally aged particles may be useful in a wide array of culture systems and biomedical applications. The underlying importance of protein adsorption and integrin engagement in dictating cell-material interactions was demonstrated with the use of the film system. Though integrins are already known to be extremely multifunctional,

these experiments have provided yet another context in which integrin engagement influences disease progression.

6.4 Future Directions

The total results of this work have several major implications. Firstly, the importance of biomaterials and scaffold systems for use as *in vitro* platforms to study cancer biology has been highlighted. By using tissue-engineering inspired techniques, we were able to study a range of phenomena, including cell-mineral interactions, that are not easily examined in conventional culture. HA has been identified as a major player in breast cancer metastasis, and our techniques to synthesize this mineral in a controlled manner and incorporate them into a scaffold culture system were highly successful. Secondly, this dissertation has provided fundamental evidence to support a thorough molecular model by which HA in microcalcifications can drive breast cancer metastasis to bone. OPN, which is observed in clinical breast tumors, was shown to be upregulated in response to HA and also to adsorb to HA and induce IL-8 secretion. IL-8 secretion was observed to stimulate production of SDF-1, which acts as a chemoattractant for breast cancer cells, and also to be involved in osteolysis at the metastatic site. HA was additionally found to stimulate expression of the SDF-1 receptor, CXCR4, making cancer cells even more sensitive to chemotactic effects and migration to bone. These findings are promising, but future work is needed to totally understand the role of HA in cancer pathogenesis and to translate insights gained in this thesis to practical use.

6.4.1 Genesis and characterization of microcalcifications

This thesis project has focused on the interactions that occur between mammary tumor cells and the pathological ramifications of their relationship. A comprehensive understanding of the role of mineral in breast cancer further requires insight into how microcalcifications form. In

the medical community, several potential explanation form microcalcifications exist, including adipose cell necrosis, tissue fibrosis, and sclerosing adenosis (206, 207). These phenomena are all passive effects associated with the hyperproliferative and potentially hypoxic microenvironment generated by the development of mammary tumors (208). However, given the active role that our results suggest for mineral in promoting metastasis, it is logical that tumor cells themselves may contribute to the genesis of microcalcifications. Future work should be directed at determining if active mineralization is a feature preceding metastasis. Preliminary work in our lab indicates that tumor-derived soluble factors can promote stromal cell-mediated tissue mineralization. MDA-MB231 subpopulations with previously established bone-specific metastatic phenotype, in particular, promoted enhanced mineralization. Further experiments should be aimed at identifying specific soluble factors that can promote stromal cell mineralization. Additionally, it will be important to determine how stromal cells can mineralize tissue. Knowledge gained in these endeavors will not only assist in learning about microcalcifications in breast cancer, but also in other diseases like atherosclerosis and valvular calcifications where ectopic mineralization is a key feature. If the mechanisms of the signaling pathways that drive ectopic calcification are elucidated, a range of new and innovative anti-mineralization therapies may also become viable.

Recent evidence has shown that the composition of microcalcifications is a valuable predictive factor for determining the likelihood of metastasis to bone (26, 27). Based on our findings showing that changes in mineral material properties actually alter cellular interactions, the effect of composition should be studied more extensively. Specifically, increasing levels of carbonate substitution in HA have been correlated with decreased risk for metastasis. With our ability to synthesize HA with tunable properties, altering carbonate concentrations is possible,

and a new series of particles should be synthesized and incorporated into the scaffold system. Effects on IL-8 secretion and expression of the bon metastasis genetic signature should be tested in the presence of these carbonated apatites. Calcium oxalate dihydrate is another mineral associated with non-malignant lesions of the breast (209, 210), and scaffolds incorporating this oxalate particles could be used as valuable controls for future studies. By completely understanding the role of mineral properties in modulating the molecular phenotype of tumor progression, it may become possible develop more effective and personalized treatment regimes earlier in the diagnostic process.

While creating particles with varying composition and phase for incorporation into the scaffold models is very important in revealing the molecular players that are associated with states of microcalcification, the reverse approach is also possible given the findings of this dissertation. With access to clinical samples, it is possible to in the future perform a robust battery of materials testing on human tissue to determine the specific characteristics of microcalcifications. Where past studies have shown preliminary data on the relation between mineral phase and composition and disease outcome, the work presented in this dissertation has equipped us with tools to develop a more comprehensive understanding of how crystals can affect disease. Using a combination of XRD, FTIR, and other characterization tools, it may be possible to translate our findings with hydrothermally aged particles to these clinical samples, testing the effects of particle size and overall crystallinity. Additionally, because we have used our mineral-containing scaffolds as a platform to develop an understanding of the molecular basis of bone metastasis, immunostaining and biomolecular techniques can be used to analyze human tissue for factors shown to be significant *in vitro*. By combining the materials approach with the biomiolecular approach, a truly comprehensive model of breast cancer metastasis to

bone with unprecedented detail can be developed, showing the connection between nanoscale material properties, molecular phenotype of cells, and patient outcome. Such a model would be of tremendous value for clinical treatment and diagnosis.

6.4.2 Mediators of cell-HA interactions

Experiments in this body of work provided strong evidence that RGD-containing ECM proteins such as OPN and fibronectin may dictate interactions between cells and HA. However, future work must clarify how these proteins are involved in changes of cell behavior with varying mineral properties. Current examinations were limited to experiments with commercially available HA, but use of our synthetic HA instead will provide a more complete understanding of these dynamics. A starting point for these future studies might involve investigating cell spreading and morphological changes as a function of changes in mineral properties. The development of a planar system, such as the one introduced in chapter 4, but incorporating synthetic well-defined HA, would facilitate such analyses. Similar approaches in terms of OPN adsorption and integrin blocking should be undertaken on these planar surfaces, and additional assessment of focal adhesion formation and colocalization of specific integrins with OPN will provide useful information on the interplay between RGD-containing proteins, HA, and breast cancer cells. Protein binding to the surface should also be studied in the absence of cells. While the studies presented in this dissertation showed differences in the quantity of protein adsorption, it will also be possible to explore how proteins fold differently as a function of mineral characteristics. For this, the single-molecule FRET technique can be employed, allowing quantification of protein folding for molecules like fibronectin (21). These proposed studies might reveal why different patterns and types of HA stimulate such stark differences in disease progression, potentially further increasing the diagnostic value of mammograms.

6.4.3 Role of native bone cells in pre-metastatic niche formation

The initial studies presented in this thesis demonstrated that tumor-derived soluble factors can have tangible effects on native bone cell function, including driving osteoclast activity and stimulating secretory function from hMSCs. It is also possible that hematopoietic stem cells (HSCs) are involved in priming the bone microenvironment for metastasis. Previous studies have shown that HSCs can also secrete SDF-1 and may act to induce cancer cell migration (55). Additionally, HSCs are the capable of generating osteoclasts through differentiation, and it has been observed that HSC mobilization is involved in the coordination of bone homeostasis (211). Future studies should focus on looking at how HA-regulated tumor-derived soluble factors affect HSC proliferation, differentiation, and secretion of pro-migratory factors in a manner similar to studies performed in this dissertation with MSCs. In terms of tumor-derived soluble factors promoting enhanced osteoclast activity, the possibility that these communications take place even before cancer cells leave the primary tumor should be investigated. For instance, future work might focus on understanding how cancer cell-mediated changes to the bone microenvironment may be part of the establishment of a pre-metastatic niche. If cancer cells are capable of altering osteoclast or osteoblast function in an endocrine manner, perhaps changes in bone ensue prior to colonization. Endocrine signaling by IL-8 may promote skeletal excavation by osteoclasts ahead of metastasis, enriching the bone microenvironment with growth factors, increasing trabecular surface area available for colonization, and generally creating conditions favorable for tumor growth. Xenograft studies in mice, where tumors will not colonize bone under normal conditions, may allow the examination of the effect of increased levels of IL-8 on bone degradation. MicroCT and histological analysis can be used to show changes in bone parameters such as trabecular geometry and bone volume fraction that are mediated by a distant

tumor. If osteolysis is a precursor to metastasis, it may additionally play a role in microcalcification formation: past studies have indicated that hypercalcaemia, which can be initiated by overactive osteoclasts, may play a role in facilitating ectopic calcifications during breast cancer (212, 213). Thus, the proposed mouse study could also entail measuring plasma levels of Ca^{2+}, and looking at the xenografts for the formation of microcalcifications through histopathological analysis.

6.4.4 Therapeutic targets

The contribution to the development of better therapeutic options is always on of the main goals for a dissertation in cancer-related fields. While the majority of the work here was performed primarily to develop fundamental insights into cancer biology and the utility of 3-D biomaterial culture systems, it is hoped that some of the findings can be translated into the generation of more efficacious treatments at some point in the future. In this work, the basic importance of IL-8 in promoting metastasis via the SDF-1/CXCR4 axis was highlighted. To truly cross-validate these findings with clinical models, a future extension of the clinical study described in Chapter 3 should be undertaken. Local correlations between microcalcifications, CXCR4 levels, and IL-8 should be explored. Concurrently, analyzing patient plasma samples to check SDF-1 levels would be insightful. Still, based on the current work, targeting IL-8, SDF-1 , or CXCR4 would be a promising strategy to curb breast cancer metastasis to bone. These approaches have been variously explored. Inhibitors of IL-8 signaling are currently in clinical trials (115) as is blockade of the SDF-1/CXCR4 axis by small molecule inhibition of the receptor (214). Given the heterogeneity of cancer, and the fact that IL-8 receptors can be bound by other ligands (215, 216), future work might also explore alternative mechanisms that can activate metastatic signaling.

Since therapies focused on the cytokine signaling network exist, future work may also involve investigating phenomena that may help to generate other types of therapies. One concept that needs to be understood further is the use of bisphosphonates. Currently, this class of drugs is prescribed universally for osteoporosis, but it has also been used in cases of osteolytic metastasis (35, 212). Bisphosphonates function by adsorbing to bone mineral by virtue of their phosphate groups and killing osteoclasts that take up the drug by interfering with biosynthesis. In Chapter 2, we showed that the bisphosphonate ibandronate preferentially targeted breast cancer cells in mineral-containing scaffolds for death. Future work should expand on this finding, to determine the mechanism by which bisphosphonates can kill cancer cells. Also, in the context of the hypothesis that osteoclastic activity is a necessary precursor for metastasis, the use of bisphosphonates in preventing metastasis may be an option. Since bisphosphonates prevent resorption, perhaps prophylactic administration to patients with non-disseminated DCIS or increased breast cancer risk factor will prevent colonization of bone. In the proposed future work with mice on investigating formation of a pre-metastatic niche, dosing with bisphosphonates as a bone protective drug could also be tested. While some recent clinical trials have indicated the prophylactic bisphosphonate treatment may indeed inhibit metastatic disease (217), long term use of bisphosphonates is not ideal; side effects include increased risk for pathological fracture (218), esophageal inflammation, and perhaps even esophageal cancer (219). Future work with our system could investigate the ability to inhibit osteoclast activity temporarily or through a specific molecular mechanism that does not completely de-regulate the entire system of skeletal turnover. For instance, inhibition of soluble IL-8 could work as a preventative measure against osteolysis-mediated pre-metastatic niche formation. Beyond this, by working with the mineral-containing culture system and osteoclast precursor cells further, molecular insights into how to

inhibit enhanced osteoclast activity in the presence of tumor-derived soluble factors without destroying this cellular population may be revealed.

One final therapeutic concept that might be explored could involve directly interfering with microcalcification formation. Future work that focuses on determining the origin of microcalcifications may uncover molecular factors that are crucial to the genesis of ectopic calcification in mammary tissue. Inhibitory strategies against these molecules may be effective in preventing mineralization and destroying the metastatic cascade described by our model. Since hypercalcaemia is also likely playing a role in formation of microcalcifications, therapies to scavenge extra plasma Ca^{2+} may be effective. These might include strategies such as calcium dialysis, which are usually employed for patients with renal-failure associate hypercalcaemia (220, 221). Overall, the breadth of strategies covered here is not a complete list, but the diversity of the proposed option reflects the potential practical utility of the work performed and the systems develop over the course of this thesis work.

REFERENCES

1. Mundy GR. Metastasis to bone: causes, consequences and therapeutic opportunities. Nat Rev Cancer. 2002;2(8):584-93. Epub 2002/08/03.
2. Siegel R, Naishadham D, Jemal A. Cancer statistics, 2012. CA Cancer J Clin. 2012;62(1):10-29. Epub 2012/01/13.
3. Guise TA. Antitumor effects of bisphosphonates: promising preclinical evidence. Cancer Treat Rev. 2008;34 Suppl 1:S19-24. Epub 2008/05/20.
4. Kozlow W, Guise TA. Breast cancer metastasis to bone: mechanisms of osteolysis and implications for therapy. J Mammary Gland Biol Neoplasia. 2005;10(2):169-80. Epub 2005/07/19.
5. Hanahan D, Weinberg RA. The hallmarks of cancer. Cell. 2000;100(1):57-70. Epub 2000/01/27.
6. Singletary SE, Connolly JL. Breast cancer staging: working with the sixth edition of the AJCC Cancer Staging Manual. CA Cancer J Clin. 2006;56(1):37-47; quiz 50-1. Epub 2006/02/02.
7. O'Shaughnessy J. Extending survival with chemotherapy in metastatic breast cancer. Oncologist. 2005;10 Suppl 3:20-9. Epub 2005/12/22.
8. Guise TA, Kozlow WM, Heras-Herzig A, Padalecki SS, Yin JJ, Chirgwin JM. Molecular mechanisms of breast cancer metastases to bone. Clin Breast Cancer. 2005;5 Suppl(2):S46-53. Epub 2005/04/06.
9. Society AC. Cancer Facts & Figures 2012. Atlanta: American Cancer Society. 2012.
10. Desmedt C, Sotiriou C, Piccart-Gebhart MJ. Development and validation of gene expression profile signatures in early-stage breast cancer. Cancer Invest. 2009;27(1):1-10. Epub 2009/02/05.
11. Sotiriou C, Pusztai L. Gene-expression signatures in breast cancer. N Engl J Med. 2009;360(8):790-800. Epub 2009/02/21.
12. Loi S, Haibe-Kains B, Desmedt C, Wirapati P, Lallemand F, Tutt AM, et al. Predicting prognosis using molecular profiling in estrogen receptor-positive breast cancer treated with tamoxifen. BMC Genomics. 2008;9:239. Epub 2008/05/24.
13. Hudis CA. Trastuzumab--mechanism of action and use in clinical practice. N Engl J Med. 2007;357(1):39-51. Epub 2007/07/06.
14. Hudis CA, Gianni L. Triple-negative breast cancer: an unmet medical need. Oncologist. 2011;16 Suppl 1:1-11. Epub 2011/02/10.
15. Coleman RE, Rubens RD. The clinical course of bone metastases from breast cancer. Br J Cancer. 1987;55(1):61-6. Epub 1987/01/01.
16. Paget S. The distribution of secondary growth in cancer of breast. Lancet. 1889;1:571-3.
17. Ribatti D, Mangialardi G, Vacca A. Stephen Paget and the 'seed and soil' theory of metastatic dissemination. Clin Exp Med. 2006;6(4):145-9. Epub 2006/12/28.
18. Kang Y, Siegel PM, Shu W, Drobnjak M, Kakonen SM, Cordon-Cardo C, et al. A multigenic program mediating breast cancer metastasis to bone. Cancer Cell. 2003;3(6):537-49. Epub 2003/07/05.
19. Correia AL, Bissell MJ. The tumor microenvironment is a dominant force in multidrug resistance. Drug Resist Updat. 2012;15(1-2):39-49. Epub 2012/02/18.

20. Kenny PA, Lee GY, Bissell MJ. Targeting the tumor microenvironment. Front Biosci. 2007;12:3468-74. Epub 2007/05/09.
21. Chandler EM, Saunders MP, Yoon CJ, Gourdon D, Fischbach C. Adipose progenitor cells increase fibronectin matrix strain and unfolding in breast tumors. Phys Biol. 2011;8(1):015008. Epub 2011/02/09.
22. Balasundaram G, Sato M, Webster TJ. Using hydroxyapatite nanoparticles and decreased crystallinity to promote osteoblast adhesion similar to functionalizing with RGD. Biomaterials. 2006;27(14):2798-805.
23. Morgan MP, Cooke MM, McCarthy GM. Microcalcifications associated with breast cancer: an epiphenomenon or biologically significant feature of selected tumors? J Mammary Gland Biol Neoplasia. 2005;10(2):181-7. Epub 2005/07/19.
24. Morgan MP, Cooke MM, Christopherson PA, Westfall PR, McCarthy GM. Calcium hydroxyapatite promotes mitogenesis and matrix metalloproteinase expression in human breast cancer cell lines. Mol Carcinog. 2001;32(3):111-7. Epub 2001/12/18.
25. Boskey AL. Biomineralization: an overview. Connect Tissue Res. 2003;44 Suppl 1:5-9. Epub 2003/09/04.
26. Bi X, Patil C, Morrissey C, Roudier MP, Mahadevan-Jansen A, Nyman J. Characterization of bone quality in prostate cancer bone metastases using Raman spectroscopy. Proceedings of SPIE. 2010;7548:75484L.
27. Haka AS, Shafer-Peltier KE, Fitzmaurice M, Crowe J, Dasari RR, Feld MS. Identifying microcalcifications in benign and malignant breast lesions by probing differences in their chemical composition using Raman spectroscopy. Cancer Res. 2002;62(18):5375-80. Epub 2002/09/18.
28. Elliott JC. Structure, crystal chemistry and density of enamel apatites. Ciba Found Symp. 1997;205:54-67; discussion -72. Epub 1997/01/01.
29. Boskey A. Mineral changes in osteopetrosis. Crit Rev Eukaryot Gene Expr. 2003;13(2-4):109-16. Epub 2003/12/31.
30. Weiner S, Wagner HD. THE MATERIAL BONE: Structure-Mechanical Function Relations. Annual Review of Materials Science. 1998;28(1):271-98.
31. Carlinfante G, Vassiliou D, Svensson O, Wendel M, Heinegard D, Andersson G. Differential expression of osteopontin and bone sialoprotein in bone metastasis of breast and prostate carcinoma. Clin Exp Metastasis. 2003;20(5):437-44. Epub 2003/10/04.
32. Boskey AL, Maresca M, Ullrich W, Doty SB, Butler WT, Prince CW. Osteopontin-hydroxyapatite interactions in vitro: inhibition of hydroxyapatite formation and growth in a gelatin-gel. Bone Miner. 1993;22(2):147-59. Epub 1993/08/01.
33. Giachelli CM. Ectopic calcification: gathering hard facts about soft tissue mineralization. The American journal of pathology. 1999;154(3):671.
34. Steitz SA, Speer MY, McKee MD, Liaw L, Almeida M, Yang H, et al. Osteopontin inhibits mineral deposition and promotes regression of ectopic calcification. The American journal of pathology. 2002;161(6):2035.
35. Diel IJ, Solomayer EF, Seibel MJ, Pfeilschifter J, Maisenbacher H, Gollan C, et al. Serum bone sialoprotein in patients with primary breast cancer is a prognostic marker for subsequent bone metastasis. Clin Cancer Res. 1999;5(12):3914-9. Epub 2000/01/13.
36. Ibrahim T, Leong I, Sanchez-Sweatman O, Khokha R, Sodek J, Tenenbaum HC, et al. Expression of bone sialoprotein and osteopontin in breast cancer bone metastases. Clin Exp Metastasis. 2000;18(3):253-60. Epub 2001/04/21.

37. Kohno N, Kitazawa S, Fukase M, Sakoda Y, Kanbara Y, Furuya Y, et al. The expression of parathyroid hormone-related protein in human breast cancer with skeletal metastases. Surgery today. 1994;24(3):215-20.
38. Hall JM, Lee MK, Newman B, Morrow JE, Anderson LA, Huey B, et al. Linkage of early-onset familial breast cancer to chromosome 17q21. Science. 1990;250(4988):1684-9. Epub 1990/12/21.
39. Bissell MJ, Hines WC. Why don't we get more cancer? A proposed role of the microenvironment in restraining cancer progression. Nature medicine. 2011;17(3):320-9. Epub 2011/03/09.
40. Calvo F, Sahai E. Cell communication networks in cancer invasion. Current opinion in cell biology. 2011;23(5):621-9. Epub 2011/05/17.
41. Beckermann BM, Kallifatidis G, Groth A, Frommhold D, Apel A, Mattern J, et al. VEGF expression by mesenchymal stem cells contributes to angiogenesis in pancreatic carcinoma. Br J Cancer. 2008;99(4):622-31. Epub 2008/07/31.
42. Hanahan D, Weinberg RA. Hallmarks of cancer: the next generation. Cell. 2011;144(5):646-74. Epub 2011/03/08.
43. Bendre MS, Gaddy-Kurten D, Mon-Foote T, Akel NS, Skinner RA, Nicholas RW, et al. Expression of interleukin 8 and not parathyroid hormone-related protein by human breast cancer cells correlates with bone metastasis in vivo. Cancer Res. 2002;62(19):5571-9. Epub 2002/10/03.
44. Fischbach C, Kong HJ, Hsiong SX, Evangelista MB, Yuen W, Mooney DJ. Cancer cell angiogenic capability is regulated by 3D culture and integrin engagement. Proc Natl Acad Sci U S A. 2009;106(2):399-404. Epub 2009/01/08.
45. Ferrara N, Hillan KJ, Novotny W. Bevacizumab (Avastin), a humanized anti-VEGF monoclonal antibody for cancer therapy. Biochemical and biophysical research communications. 2005;333(2):328-35. Epub 2005/06/18.
46. Varner JA, Cheresh DA. Integrins and cancer. Current opinion in cell biology. 1996;8(5):724-30. Epub 1996/10/01.
47. Goldberg HA, Warner KJ, Li MC, Hunter GK. Binding of bone sialoprotein, osteopontin and synthetic polypeptides to hydroxyapatite. Connective tissue research. 2001;42(1):25-37.
48. Helfrich MH, Nesbitt SA, Dorey EL, Horton MA. Rat osteoclasts adhere to a wide range of rgd (arg-gly-asp) peptide-containing proteins, including the bone sialoproteins and fibronectin, via a β3 integrin. Journal of Bone and Mineral Research. 2009;7(3):335-43.
49. Kaplan RN, Psaila B, Lyden D. Bone marrow cells in the 'pre-metastatic niche': within bone and beyond. Cancer Metastasis Rev. 2006;25(4):521-9. Epub 2006/12/23.
50. Huang S, Terstappen L. Lymphoid and myeloid differentiation of single human CD34+, HLA-DR+, CD38-hematopoietic stem cells. Blood. 1994;83(6):1515-26.
51. Bendre M, Gaddy D, Nicholas RW, Suva LJ. Breast cancer metastasis to bone: it is not all about PTHrP. Clin Orthop Relat Res. 2003(415 Suppl):S39-45. Epub 2003/11/06.
52. Guise TA, Yin JJ, Taylor SD, Kumagai Y, Dallas M, Boyce BF, et al. Evidence for a causal role of parathyroid hormone-related protein in the pathogenesis of human breast cancer-mediated osteolysis. J Clin Invest. 1996;98(7):1544-9. Epub 1996/10/01.
53. Singh A, Settleman J. EMT, cancer stem cells and drug resistance: an emerging axis of evil in the war on cancer. Oncogene. 2010;29(34):4741-51. Epub 2010/06/10.
54. Karnoub AE, Dash AB, Vo AP, Sullivan A, Brooks MW, Bell GW, et al. Mesenchymal stem cells within tumour stroma promote breast cancer metastasis. Nature. 2007;449(7162):557-63. Epub 2007/10/05.

55. Kucia M, Reca R, Miekus K, Wanzeck J, Wojakowski W, Janowska-Wieczorek A, et al. Trafficking of normal stem cells and metastasis of cancer stem cells involve similar mechanisms: pivotal role of the SDF-1-CXCR4 axis. Stem Cells. 2005;23(7):879-94. Epub 2005/05/13.
56. McAllister SS, Gifford AM, Greiner AL, Kelleher SP, Saelzler MP, Ince TA, et al. Systemic endocrine instigation of indolent tumor growth requires osteopontin. Cell. 2008;133(6):994-1005. Epub 2008/06/17.
57. Dar A, Kollet O, Lapidot T. Mutual, reciprocal SDF-1/CXCR4 interactions between hematopoietic and bone marrow stromal cells regulate human stem cell migration and development in NOD/SCID chimeric mice. Exp Hematol. 2006;34(8):967-75. Epub 2006/07/26.
58. Liu H, Chin T, Lai L, Chiu S, Chung K, Chang C, et al. Hydroxyapatite synthesized by a simplified hydrothermal method. Ceramics international. 1997;23(1):19-25.
59. Nagano M, Nakamura T, Kokubo T, Tanahashi M, Ogawa M. Differences of bone bonding ability and degradation behaviour< i> in vivo</i> between amorphous calcium phosphate and highly crystalline hydroxyapatite coating. Biomaterials. 1996;17(18):1771-7.
60. Kim SS, Sun Park M, Jeon O, Yong Choi C, Kim BS. Poly(lactide-co-glycolide)/hydroxyapatite composite scaffolds for bone tissue engineering. Biomaterials. 2006;27(8):1399-409. Epub 2005/09/20.
61. Freund A, Chauveau C, Brouillet JP, Lucas A, Lacroix M, Licznar A, et al. IL-8 expression and its possible relationship with estrogen-receptor-negative status of breast cancer cells. Oncogene. 2003;22(2):256-65. Epub 2003/01/16.
62. Heppner GH, Miller FR, Shekhar PM. Nontransgenic models of breast cancer. Breast cancer research : BCR. 2000;2(5):331-4. Epub 2001/03/16.
63. Pathi SP, Kowalczewski C, Tadipatri R, Fischbach C. A novel 3-D mineralized tumor model to study breast cancer bone metastasis. PLoS One. 2010;5(1):e8849. Epub 2010/01/29.
64. Kingsley LA, Fournier PG, Chirgwin JM, Guise TA. Molecular biology of bone metastasis. Molecular cancer therapeutics. 2007;6(10):2609-17. Epub 2007/10/17.
65. Minn AJ, Kang Y, Serganova I, Gupta GP, Giri DD, Doubrovin M, et al. Distinct organ-specific metastatic potential of individual breast cancer cells and primary tumors. J Clin Invest. 2005;115(1):44-55. Epub 2005/01/05.
66. Bendre MS, Montague DC, Peery T, Akel NS, Gaddy D, Suva LJ. Interleukin-8 stimulation of osteoclastogenesis and bone resorption is a mechanism for the increased osteolysis of metastatic bone disease. Bone. 2003;33(1):28-37. Epub 2003/08/16.
67. Mercer RR, Miyasaka C, Mastro AM. Metastatic breast cancer cells suppress osteoblast adhesion and differentiation. Clin Exp Metastasis. 2004;21(5):427-35. Epub 2005/01/28.
68. Bachelder RE, Crago A, Chung J, Wendt MA, Shaw LM, Robinson G, et al. Vascular endothelial growth factor is an autocrine survival factor for neuropilin-expressing breast carcinoma cells. Cancer Res. 2001;61(15):5736-40. Epub 2001/08/02.
69. Deckers MM, Karperien M, van der Bent C, Yamashita T, Papapoulos SE, Lowik CW. Expression of vascular endothelial growth factors and their receptors during osteoblast differentiation. Endocrinology. 2000;141(5):1667-74. Epub 2000/05/10.
70. Youngs SJ, Ali SA, Taub DD, Rees RC. Chemokines induce migrational responses in human breast carcinoma cell lines. Int J Cancer. 1997;71(2):257-66. Epub 1997/04/10.
71. Mitsuyama H, Kambe F, Murakami R, Cao X, Ishiguro N, Seo H. Calcium signaling pathway involving calcineurin regulates interleukin-8 gene expression through activation of NF-kappaB in human osteoblast-like cells. J Bone Miner Res. 2004;19(4):671-9. Epub 2004/03/10.

72. Logothetis CJ, Lin SH. Osteoblasts in prostate cancer metastasis to bone. Nat Rev Cancer. 2005;5(1):21-8. Epub 2005/01/05.
73. Tanaka Y, Abe M, Hiasa M, Oda A, Amou H, Nakano A, et al. Myeloma cell-osteoclast interaction enhances angiogenesis together with bone resorption: a role for vascular endothelial cell growth factor and osteopontin. Clin Cancer Res. 2007;13(3):816-23. Epub 2007/02/10.
74. Mizukami Y, Jo WS, Duerr EM, Gala M, Li J, Zhang X, et al. Induction of interleukin-8 preserves the angiogenic response in HIF-1alpha-deficient colon cancer cells. Nat Med. 2005;11(9):992-7. Epub 2005/08/30.
75. Kindle L, Rothe L, Kriss M, Osdoby P, Collin-Osdoby P. Human microvascular endothelial cell activation by IL-1 and TNF-alpha stimulates the adhesion and transendothelial migration of circulating human CD14+ monocytes that develop with RANKL into functional osteoclasts. J Bone Miner Res. 2006;21(2):193-206. Epub 2006/01/19.
76. Nagano M, Nakamura T, Kokubo T, Tanahashi M, Ogawa M. Differences of bone bonding ability and degradation behaviour in vivo between amorphous calcium phosphate and highly crystalline hydroxyapatite coating. Biomaterials. 1996;17(18):1771-7. Epub 1996/09/01.
77. Pezzatini S, Morbidelli L, Solito R, Paccagnini E, Boanini E, Bigi A, et al. Nanostructured HA crystals up-regulate FGF-2 expression and activity in microvascular endothelium promoting angiogenesis. Bone. 2007;41(4):523-34. Epub 2007/08/08.
78. Pampaloni F, Reynaud EG, Stelzer EH. The third dimension bridges the gap between cell culture and live tissue. Nat Rev Mol Cell Biol. 2007;8(10):839-45. Epub 2007/08/09.
79. Fischbach C, Chen R, Matsumoto T, Schmelzle T, Brugge JS, Polverini PJ, et al. Engineering tumors with 3D scaffolds. Nat Methods. 2007;4(10):855-60. Epub 2007/09/04.
80. Bissell MJ, Radisky D. Putting tumours in context. Nat Rev Cancer. 2001;1(1):46-54. Epub 2002/03/20.
81. Rao H, Tan J, Fewkes EJ. Corning Bone Cell Assay Surface. Bone. 2009;44(Supplement 1):S141-S.
82. Blank RD, Baldini TH, Kaufman M, Bailey S, Gupta R, Yershov Y, et al. Spectroscopically determined collagen Pyr/deH-DHLNL cross-link ratio and crystallinity indices differ markedly in recombinant congenic mice with divergent calculated bone tissue strength. Connect Tissue Res. 2003;44(3-4):134-42. Epub 2003/09/25.
83. Anselme K. Osteoblast adhesion on biomaterials. Biomaterials. 2000;21(7):667-81. Epub 2000/03/11.
84. Gilbert M, Shaw WJ, Long JR, Nelson K, Drobny GP, Giachelli CM, et al. Chimeric peptides of statherin and osteopontin that bind hydroxyapatite and mediate cell adhesion. J Biol Chem. 2000;275(21):16213-8. Epub 2000/04/05.
85. Khalili P, Arakelian A, Chen G, Plunkett ML, Beck I, Parry GC, et al. A non-RGD-based integrin binding peptide (ATN-161) blocks breast cancer growth and metastasis in vivo. Mol Cancer Ther. 2006;5(9):2271-80. Epub 2006/09/21.
86. Mundy GR. Mechanisms of bone metastasis. Cancer. 1997;80(8 Suppl):1546-56. Epub 1997/11/15.
87. Yin JJ, Selander K, Chirgwin JM, Dallas M, Grubbs BG, Wieser R, et al. TGF-beta signaling blockade inhibits PTHrP secretion by breast cancer cells and bone metastases development. J Clin Invest. 1999;103(2):197-206. Epub 1999/01/23.
88. Mailland M, Waelchli R, Ruat M, Boddeke HG, Seuwen K. Stimulation of cell proliferation by calcium and a calcimimetic compound. Endocrinology. 1997;138(9):3601-5. Epub 1997/09/01.

89. Casanovas O, Hicklin DJ, Bergers G, Hanahan D. Drug resistance by evasion of antiangiogenic targeting of VEGF signaling in late-stage pancreatic islet tumors. Cancer Cell. 2005;8(4):299-309. Epub 2005/10/18.
90. Koch AE, Polverini PJ, Kunkel SL, Harlow LA, DiPietro LA, Elner VM, et al. Interleukin-8 as a macrophage-derived mediator of angiogenesis. Science. 1992;258(5089):1798-801. Epub 1992/12/11.
91. Suda T, Nakamura I, Jimi E, Takahashi N. Regulation of osteoclast function. J Bone Miner Res. 1997;12(6):869-79. Epub 1997/06/01.
92. Bancroft CC, Chen Z, Yeh J, Sunwoo JB, Yeh NT, Jackson S, et al. Effects of pharmacologic antagonists of epidermal growth factor receptor, PI3K and MEK signal kinases on NF-kappaB and AP-1 activation and IL-8 and VEGF expression in human head and neck squamous cell carcinoma lines. Int J Cancer. 2002;99(4):538-48. Epub 2002/05/07.
93. Singhal H, Bautista DS, Tonkin KS, O'Malley FP, Tuck AB, Chambers AF, et al. Elevated plasma osteopontin in metastatic breast cancer associated with increased tumor burden and decreased survival. Clin Cancer Res. 1997;3(4):605-11. Epub 1997/04/01.
94. Boskey AL, Spevak L, Paschalis E, Doty SB, McKee MD. Osteopontin deficiency increases mineral content and mineral crystallinity in mouse bone. Calcif Tissue Int. 2002;71(2):145-54. Epub 2002/06/20.
95. Ducy P, Desbois C, Boyce B, Pinero G, Story B, Dunstan C, et al. Increased bone formation in osteocalcin-deficient mice. Nature. 1996;382(6590):448-52. Epub 1996/08/01.
96. Iafisco M, Palazzo B, Falini G, Foggia MD, Bonora S, Nicolis S, et al. Adsorption and conformational change of myoglobin on biomimetic hydroxyapatite nanocrystals functionalized with alendronate. Langmuir. 2008;24(9):4924-30. Epub 2008/04/01.
97. Paszek MJ, Zahir N, Johnson KR, Lakins JN, Rozenberg GI, Gefen A, et al. Tensional homeostasis and the malignant phenotype. Cancer Cell. 2005;8(3):241-54. Epub 2005/09/20.
98. Roderick HL, Cook SJ. Ca2+ signalling checkpoints in cancer: remodelling Ca2+ for cancer cell proliferation and survival. Nat Rev Cancer. 2008;8(5):361-75. Epub 2008/04/25.
99. Mastro AM, Vogler EA. A three-dimensional osteogenic tissue model for the study of metastatic tumor cell interactions with bone. Cancer Res. 2009;69(10):4097-100. Epub 2009/05/14.
100. Moreau JE, Anderson K, Mauney JR, Nguyen T, Kaplan DL, Rosenblatt M. Tissue-engineered bone serves as a target for metastasis of human breast cancer in a mouse model. Cancer Res. 2007;67(21):10304-8. Epub 2007/11/03.
101. Fischbach C, Mooney DJ. Polymers for pro- and anti-angiogenic therapy. Biomaterials. 2007;28(12):2069-76. Epub 2007/01/27.
102. Minn AJ, Gupta GP, Siegel PM, Bos PD, Shu W, Giri DD, et al. Genes that mediate breast cancer metastasis to lung. Nature. 2005;436(7050):518-24. Epub 2005/07/29.
103. Hartley JW, Evans LH, Green KY, Naghashfar Z, Macias AR, Zerfas PM, et al. Expression of infectious murine leukemia viruses by RAW264.7 cells, a potential complication for studies with a widely used mouse macrophage cell line. Retrovirology. 2008;5:1. Epub 2008/01/08.
104. Matsumoto M, Sudo T, Saito T, Osada H, Tsujimoto M. Involvement of p38 mitogen-activated protein kinase signaling pathway in osteoclastogenesis mediated by receptor activator of NF-kappa B ligand (RANKL). J Biol Chem. 2000;275(40):31155-61. Epub 2000/06/22.

105. Polek TC, Talpaz M, Darnay BG, Spivak-Kroizman T. TWEAK mediates signal transduction and differentiation of RAW264.7 cells in the absence of Fn14/TweakR. Evidence for a second TWEAK receptor. J Biol Chem. 2003;278(34):32317-23. Epub 2003/06/10.
106. Nakagawa N, Kinosaki M, Yamaguchi K, Shima N, Yasuda H, Yano K, et al. RANK is the essential signaling receptor for osteoclast differentiation factor in osteoclastogenesis. Biochem Biophys Res Commun. 1998;253(2):395-400. Epub 1999/01/08.
107. Tabar L, Chen HH, Duffy SW, Yen MF, Chiang CF, Dean PB, et al. A novel method for prediction of long-term outcome of women with T1a, T1b, and 10-14 mm invasive breast cancers: a prospective study. Lancet. 2000;355(9202):429-33. Epub 2000/06/07.
108. Pathi SP, Lin DD, Dorvee JR, Estroff LA, Fischbach C. Hydroxyapatite nanoparticle-containing scaffolds for the study of breast cancer bone metastasis. Biomaterials. 2011;32(22):5112-22. Epub 2011/04/22.
109. Kessar P, Perry N, Vinnicombe S, Hussain H, Carpenter R, Wells C. How significant is detection of ductal carcinoma in situ in a breast screening programme? Clinical radiology. 2002;57(9):807-14.
110. Kang Y, He W, Tulley S, Gupta GP, Serganova I, Chen CR, et al. Breast cancer bone metastasis mediated by the Smad tumor suppressor pathway. Proc Natl Acad Sci U S A. 2005;102(39):13909-14. Epub 2005/09/21.
111. Dranoff G. Cytokines in cancer pathogenesis and cancer therapy. Nature Reviews Cancer. 2004;4(1):11-22.
112. Joyce JA, Pollard JW. Microenvironmental regulation of metastasis. Nature Reviews Cancer. 2008;9(4):239-52.
113. Singh B, Berry JA, Vincent LE, Lucci A. Involvement of IL-8 in COX-2-mediated bone metastases from breast cancer. The Journal of surgical research. 2006;134(1):44-51. Epub 2006/05/09.
114. Lehrer S, Diamond EJ, Mamkine B, Stone NN, Stock RG. Serum interleukin-8 is elevated in men with prostate cancer and bone metastases. Technology in cancer research & treatment. 2004;3(5):411. Epub 2004/09/30.
115. Ginestier C, Liu S, Diebel ME, Korkaya H, Luo M, Brown M, et al. CXCR1 blockade selectively targets human breast cancer stem cells in vitro and in xenografts. J Clin Invest. 2010;120(2):485-97. Epub 2010/01/07.
116. Wang J, Loberg R, Taichman RS. The pivotal role of CXCL12 (SDF-1)/CXCR4 axis in bone metastasis. Cancer Metastasis Rev. 2006;25(4):573-87. Epub 2006/12/14.
117. Hirbe A, Morgan E, Weilbaecher K. The CXCR4/SDF-1 chemokine axis: a potential therapeutic target for bone metastases? Current pharmaceutical design. 2010;16(11):1284-90.
118. Singh RK, Lokeshwar BL. The IL-8–Regulated Chemokine Receptor CXCR7 Stimulates EGFR Signaling to Promote Prostate Cancer Growth. Cancer research. 2011;71(9):3268-77.
119. Schmeichel KL, Bissell MJ. Modeling tissue-specific signaling and organ function in three dimensions. Journal of cell science. 2003;116(Pt 12):2377-88. Epub 2003/05/27.
120. Pampaloni F, Reynaud EG, Stelzer EHK. The third dimension bridges the gap between cell culture and live tissue. Nature reviews Molecular cell biology. 2007;8(10):839-45.
121. Fischbach C, Seufert J, Staiger H, Hacker M, Neubauer M, Gopferich A, et al. Three-dimensional in vitro model of adipogenesis: comparison of culture conditions. Tissue Eng. 2004;10(1-2):215-29. Epub 2004/03/11.

122. Lescarbeau RM, Seib FP, Prewitz M, Werner C, Kaplan DL. In vitro model of metastasis to bone marrow mediates prostate cancer castration resistant growth through paracrine and extracellular matrix factors. PLoS One. 2012;7(8):e40372. Epub 2012/08/08.
123. Murphy WL, Kohn DH, Mooney DJ. Growth of continuous bonelike mineral within porous poly(lactide-co-glycolide) scaffolds in vitro. Journal of biomedical materials research. 2000;50(1):50-8. Epub 2000/01/25.
124. Minn AJ, Gupta GP, Siegel PM, Bos PD, Shu W, Giri DD, et al. Genes that mediate breast cancer metastasis to lung. Nature. 2005;436(7050):518-24.
125. Li Y, Reca RG, Atmaca-Sonmez P, Ratajczak MZ, Ildstad ST, Kaplan HJ, et al. Retinal pigment epithelium damage enhances expression of chemoattractants and migration of bone marrow-derived stem cells. Invest Ophthalmol Vis Sci. 2006;47(4):1646-52. Epub 2006/03/28.
126. Schmittgen TD, Livak KJ. Analyzing real-time PCR data by the comparative C(T) method. Nat Protoc. 2008;3(6):1101-8. Epub 2008/06/13.
127. Bellahcene A, Castronovo V. Expression of bone matrix proteins in human breast cancer: potential roles in microcalcification formation and in the genesis of bone metastases. Bulletin du cancer. 1997;84(1):17.
128. Chandler EM, Seo BR, Califano JP, Andresen Eguiluz RC, Lee JS, Yoon CJ, et al. Implanted adipose progenitor cells as physicochemical regulators of breast cancer. Proc Natl Acad Sci U S A. 2012;109(25):9786-91. Epub 2012/06/06.
129. Auclair-Daigle C, Bureau MN, Legoux JG, Yahia L. Bioactive hydroxyapatite coatings on polymer composites for orthopedic implants. J Biomed Mater Res A. 2005;73(4):398-408. Epub 2005/05/14.
130. Cooke MM, McCarthy GM, Sallis JD, Morgan MP. Phosphocitrate inhibits calcium hydroxyapatite induced mitogenesis and upregulation of matrix metalloproteinase-1, interleukin-1beta and cyclooxygenase-2 mRNA in human breast cancer cell lines. Breast Cancer Res Treat. 2003;79(2):253-63. Epub 2003/06/27.
131. Szabo-Moskal J, Lasek W, Kozlowska R, Sir J, Serafin Z. [The role of preoperative hooked-wire localization of occult lesions for early detection of breast cancer]. Ginekol Pol. 2005;76(1):15-9. Epub 2005/04/23. Rola przedoperacyjnego znakowania zmian niepalpacyjnych dla wczesnego wykrywania raka sutka.
132. Chambers AF, Groom AC, MacDonald IC. Dissemination and growth of cancer cells in metastatic sites. Nature Reviews Cancer. 2002;2:563-72.
133. Helbig G, Christopherson KW, Bhat-Nakshatri P, Kumar S, Kishimoto H, Miller KD, et al. NF-κ B promotes breast cancer cell migration and metastasis by inducing the expression of the chemokine receptor CXCR4. Journal of Biological Chemistry. 2003;278(24):21631-8.
134. Charafe-Jauffret E, Ginestier C, Iovino F, Wicinski J, Cervera N, Finetti P, et al. Breast cancer cell lines contain functional cancer stem cells with metastatic capacity and a distinct molecular signature. Cancer research. 2009;69(4):1302-13.
135. Benoy IH, Salgado R, Van Dam P, Geboers K, Van Marck E, Scharpé S, et al. Increased serum interleukin-8 in patients with early and metastatic breast cancer correlates with early dissemination and survival. Clinical cancer research. 2004;10(21):7157-62.
136. Miller L, Kurtzman S, Wang Y, Anderson K, Lindquist R, Kreutzer D. Expression of interleukin-8 receptors on tumor cells and vascular endothelial cells in human breast cancer tissue. Anticancer research. 1998;18(1A):77.
137. Verbridge SS, Chandler EM, Fischbach C. Tissue-engineered three-dimensional tumor models to study tumor angiogenesis. Tissue Eng Part A. 2010;16(7):2147-52. Epub 2010/03/11.

138. Shimoda M, Mellody K, Orimo A. The SDF-1-Rich Tumour Microenvironment Provides a Niche for Carcinoma Cells. Tumor-Associated Fibroblasts and their Matrix. 2011:245-55.
139. Kaplan RN, Riba RD, Zacharoulis S, Bramley AH, Vincent L, Costa C, et al. VEGFR1-positive haematopoietic bone marrow progenitors initiate the pre-metastatic niche. Nature. 2005;438(7069):820-7.
140. Liang Z, Wu T, Lou H, Yu X, Taichman RS, Lau SK, et al. Inhibition of breast cancer metastasis by selective synthetic polypeptide against CXCR4. Cancer research. 2004;64(12):4302-8.
141. Wong D, Korz W. Translating an antagonist of chemokine receptor CXCR4: from bench to bedside. Clinical cancer research. 2008;14(24):7975-80.
142. Rodrigues LR, Teixeira JA, Schmitt FL, Paulsson M, Lindmark-Mänsson H. The role of osteopontin in tumor progression and metastasis in breast cancer. Cancer Epidemiology Biomarkers & Prevention. 2007;16(6):1087-97.
143. Lu X, Wang Q, Hu G, Van Poznak C, Fleisher M, Reiss M, et al. ADAMTS1 and MMP1 proteolytically engage EGF-like ligands in an osteolytic signaling cascade for bone metastasis. Genes & development. 2009;23(16):1882-94. Epub 2009/07/18.
144. Vyborny CJ, Giger ML, Nishikawa RM. Computer-aided detection and diagnosis of breast cancer. Radiologic Clinics of North America. 2000;38(4):725-40.
145. Kilroy GE, Foster SJ, Wu X, Ruiz J, Sherwood S, Heifetz A, et al. Cytokine profile of human adipose-derived stem cells: Expression of angiogenic, hematopoietic, and pro-inflammatory factors. Journal of cellular physiology. 2007;212(3):702-9.
146. Elliott JC. Structure and chemistry of the apatites and other calcium orthophosphates. Amsterdam [The Netherlands]; New York: Elsevier; 1994.
147. Boskey A. Bone mineral crystal size. Osteoporosis Int. 2003;14:S16-S20.
148. Reichert JC, Quent VM, Burke LJ, Stansfield SH, Clements JA, Hutmacher DW. Mineralized human primary osteoblast matrices as a model system to analyse interactions of prostate cancer cells with the bone microenvironment. Biomaterials. 2010;31(31):7928-36. Epub 2010/08/07.
149. Kothapalli CR, Shaw MT, Wei M. Biodegradable HA-PLA 3-D porous scaffolds: Effect of nano-sized filler content on scaffold properties. Acta Biomaterialia. 2005;1(6):653-62.
150. Weiner S, Bar-Yosef O. States of Preservation of Bones from Prehistoric Sites in the near-East - a Survey. J Archaeol Sci. 1990;17(2):187-96.
151. Dorozhkin SV. Nanosized and nanocrystalline calcium orthophosphates. Acta Biomaterialia. 2010;6(3):715-34.
152. Boskey AL, van der Meulen MC, Wright TM. Guidelines for describing mouse skeletal phenotype. J Orthop Res. 2003;21(1):1-5. Epub 2003/01/01.
153. el Feki H, Rey C, Vignoles M. Carbonate ions in apatites: infrared investigations in the upsilon 4 CO3 domain. Calcif Tissue Int. 1991;49(4):269-74. Epub 1991/10/01.
154. Ruoslahti E. Fibronectin. J Oral Pathol. 1981;10(1):3-13. Epub 1981/02/01.
155. Green AR, Green VL, White MC, Speirs V. Expression of cytokine messenger RNA in normal and neoplastic human breast tissue: identification of interleukin-8 as a potential regulatory factor in breast tumours. Int J Cancer. 1997;72(6):937-41. Epub 1997/11/05.
156. Conz MB, Granjeiro JM, Soares GdA. Physicochemical characterization of six commercial hydroxyapatites for medical-dental applicatons as bone graft. scielo; 2005. p. 136-40.

157. Cai YR, Tang RK. Calcium phosphate nanoparticles in biomineralization and biomaterials. J Mater Chem. 2008;18(32):3775-87.
158. Cunniffe GM, O'Brien FJ, Partap S, Levingstone TJ, Stanton KT, Dickson GR. The synthesis and characterization of nanophase hydroxyapatite using a novel dispersant-aided precipitation method. J Biomed Mater Res Part A. 2010;95A(4):1142-9.
159. Martins MA, Santos C, Almeida MM, Costa MEV. Hydroxyapatite micro- and nanoparticles: Nucleation and growth mechanisms in the presence of citrate species. J Colloid Interf Sci. 2008;318(2):210-6.
160. Murray CB, Kagan CR, Bawendi MG. Synthesis and characterization of monodisperse nanocrystals and close-packed nanocrystal assemblies. Annual Review of Materials Science. 2000;30:545-610.
161. Sawyer AA, Hennessy KM, Bellis SL. The effect of adsorbed serum proteins, RGD and proteoglycan-binding peptides on the adhesion of mesenchymal stem cells to hydroxyapatite. Biomaterials. 2007;28(3):383-92. Epub 2006/09/06.
162. Woo KM, Seo J, Zhang R, Ma PX. Suppression of apoptosis by enhanced protein adsorption on polymer/hydroxyapatite composite scaffolds. Biomaterials. 2007;28(16):2622-30. Epub 2007/02/27.
163. Lundqvist M, Stigler J, Elia G, Lynch I, Cedervall T, Dawson KA. Nanoparticle size and surface properties determine the protein corona with possible implications for biological impacts. Proc Natl Acad Sci U S A. 2008;105(38):14265-70. Epub 2008/09/24.
164. Redey SA, Razzouk S, Rey C, Bernache-Assollant D, Leroy G, Nardin M, et al. Osteoclast adhesion and activity on synthetic hydroxyapatite, carbonated hydroxyapatite, and natural calcium carbonate: relationship to surface energies. Journal of biomedical materials research. 1999;45(2):140-7. Epub 1999/07/09.
165. Yang Y, Cavin R, Ong JL. Protein adsorption on titanium surfaces and their effect on osteoblast attachment. J Biomed Mater Res A. 2003;67(1):344-9. Epub 2003/10/01.
166. Cukierman E, Pankov R, Yamada KM. Cell interactions with three-dimensional matrices. Current opinion in cell biology. 2002;14(5):633-9. Epub 2002/09/17.
167. Garcia AJ, Vega MD, Boettiger D. Modulation of cell proliferation and differentiation through substrate-dependent changes in fibronectin conformation. Mol Biol Cell. 1999;10(3):785-98. Epub 1999/03/09.
168. Sun JS, Tsuang YH, Liao CJ, Liu HC, Hang YS, Lin FH. The effects of calcium phosphate particles on the growth of osteoblasts. Journal of biomedical materials research. 1997;37(3):324-34. Epub 1997/11/22.
169. Lange T, Schilling AF, Peters F, Haag F, Morlock MM, Rueger JM, et al. Proinflammatory and osteoclastogenic effects of beta-tricalciumphosphate and hydroxyapatite particles on human mononuclear cells in vitro. Biomaterials. 2009;30(29):5312-8. Epub 2009/07/07.
170. Detsch R, Mayr H, Ziegler G. Formation of osteoclast-like cells on HA and TCP ceramics. Acta Biomaterialia. 2008;4(1):139-48.
171. Addadi L, Rubin N, Scheffer L, Ziblat R. Two and three-dimensional pattern recognition of organized surfaces by specific antibodies. Acc Chem Res. 2008;41(2):254-64. Epub 2008/01/26.
172. Park EJ, Park K. Oxidative stress and pro-inflammatory responses induced by silica nanoparticles in vivo and in vitro. Toxicol Lett. 2009;184(1):18-25. Epub 2008/11/22.

173. Morgan MP, Cooke MM, Christopherson PA, Westfall PR, McCarthy GM. Calcium hydroxyapatite promotes mitogenesis and matrix metalloproteinase expression in human breast cancer cell lines. Molecular Carcinogenesis. 2001;32(3):111-7. Epub 2001/12/18.
174. Thomas RJ, Guise TA, Yin JJ, Elliott J, Horwood NJ, Martin TJ, et al. Breast cancer cells interact with osteoblasts to support osteoclast formation. Endocrinology. 1999;140(10):4451-8. Epub 1999/09/28.
175. Boyan BD, Lossdorfer S, Wang L, Zhao G, Lohmann CH, Cochran DL, et al. Osteoblasts generate an osteogenic microenvironment when grown on surfaces with rough microtopographies. Eur Cell Mater. 2003;6:22-7. Epub 2003/10/25.
176. Geblinger D, Addadi L, Geiger B. Nano-topography sensing by osteoclasts. Journal of cell science. 2010;123(Pt 9):1503-10. Epub 2010/04/09.
177. Ramankulov A, Lein M, Kristiansen G, Loening SA, Jung K. Plasma osteopontin in comparison with bone markers as indicator of bone metastasis and survival outcome in patients with prostate cancer. The Prostate. 2006;67(3):330-40.
178. Singhal H, Bautista DS, Tonkin KS, O'Malley FP, Tuck AB, Chambers AF, et al. Elevated plasma osteopontin in metastatic breast cancer associated with increased tumor burden and decreased survival. Clinical cancer research. 1997;3(4):605-11.
179. Zhang XH, Wang Q, Gerald W, Hudis CA, Norton L, Smid M, et al. Latent bone metastasis in breast cancer tied to Src-dependent survival signals. Cancer Cell. 2009;16(1):67-78. Epub 2009/07/04.
180. Rangaswami H, Bulbule A, Kundu GC. Osteopontin: role in cell signaling and cancer progression. Trends in cell biology. 2006;16(2):79-87.
181. Prince CW, Dickie D, Krumdieck CL. Osteopontin, a substrate for transglutaminase and factor XIII activity. Biochemical and biophysical research communications. 1991;177(3):1205-10.
182. Wai PY, Kuo PC. The role of osteopontin in tumor metastasis. Journal of Surgical Research. 2004;121(2):228-41.
183. Bellahcene A, Castronovo V. Increased expression of osteonectin and osteopontin, two bone matrix proteins, in human breast cancer. The American journal of pathology. 1995;146(1):95.
184. Weiner S, Traub W, Wagner HD. Lamellar bone: structure–function relations. Journal of structural biology. 1999;126(3):241-55.
185. Giachelli CM, Steitz S. Osteopontin: a versatile regulator of inflammation and biomineralization. Matrix Biology. 2000;19(7):615-22.
186. Goldberg HA, Hunter GK. The Inhibitory Activity of Osteopontin on Hydroxyapatite Formation In Vitroa. Annals of the New York Academy of Sciences. 2006;760(1):305-8.
187. Bautista DS, Xuan J, Hota C, Chambers AF, Harris JF. Inhibition of Arg-Gly-Asp (RGD)-mediated cell adhesion to osteopontin by a monoclonal antibody against osteopontin. Journal of Biological Chemistry. 1994;269(37):23280-5.
188. Shin H, Zygourakis K, Farach-Carson MC, Yaszemski MJ, Mikos AG. Attachment, proliferation, and migration of marrow stromal osteoblasts cultured on biomimetic hydrogels modified with an osteopontin-derived peptide. Biomaterials. 2004;25(5):895-906.
189. Boskey AL, Moore DJ, Amling M, Canalis E, Delany AM. Infrared analysis of the mineral and matrix in bones of osteonectin-null mice and their wildtype controls. J Bone Miner Res. 2003;18(6):1005-11. Epub 2003/06/24.

190. Reinholt FP, Hultenby K, Oldberg A, Heinegård D. Osteopontin--a possible anchor of osteoclasts to bone. Proceedings of the National Academy of Sciences. 1990;87(12):4473-5.
191. Liaw L, Skinner MP, Raines EW, Ross R, Cheresh DA, Schwartz SM, et al. The adhesive and migratory effects of osteopontin are mediated via distinct cell surface integrins. Role of alpha v beta 3 in smooth muscle cell migration to osteopontin in vitro. Journal of Clinical Investigation. 1995;95(2):713.
192. Kumar CC. Signaling by integrin receptors. Oncogene. 1998;17(11 Reviews):1365-73. Epub 1998/10/21.
193. Butler SM, Tracy MA, Tilton RD. Adsorption of serum albumin to thin films of poly(lactide-co-glycolide). Journal of controlled release : official journal of the Controlled Release Society. 1999;58(3):335-47. Epub 1999/04/01.
194. Daly SM, Przybycien TM, Tilton RD. Adsorption of poly(ethylene glycol)-modified ribonuclease A to a poly(lactide-co-glycolide) surface. Biotechnol Bioeng. 2005;90(7):856-68. Epub 2005/04/21.
195. Juliano R. Signal transduction by integrins and its role in the regulation of tumor growth. Cancer Metastasis Rev. 1994;13(1):25-30. Epub 1994/03/01.
196. Liapis H, Flath A, Kitazawa S. Integrin alpha V beta 3 expression by bone-residing breast cancer metastases. Diagnostic molecular pathology: the American journal of surgical pathology, part B. 1996;5(2):127.
197. Ruoslahti E. Fibronectin and its integrin receptors in cancer. Advances in cancer research. 1999;76:1-20.
198. Yeh M, Gharavi NM, Choi J, Hsieh X, Reed E, Mouillesseaux KP, et al. Oxidized phospholipids increase interleukin 8 (IL-8) synthesis by activation of the c-src/signal transducers and activators of transcription (STAT) 3 pathway. Journal of Biological Chemistry. 2004;279(29):30175-81.
199. Liu R, Aupperle K, Terkeltaub R. Src family protein tyrosine kinase signaling mediates monosodium urate crystal-induced IL-8 expression by monocytic THP-1 cells. Journal of leukocyte biology. 2001;70(6):961-8.
200. Mitra SK, Schlaepfer DD. Integrin-regulated FAK–Src signaling in normal and cancer cells. Current opinion in cell biology. 2006;18(5):516-23.
201. Graham RA, Homer MJ, Sigler CJ, Safaii H, Schmid CH, Marchant D, et al. The efficacy of specimen radiography in evaluating the surgical margins of impalpable breast carcinoma. American Journal of Roentgenology. 1994;162(1):33-6.
202. Takahashi N, Ejiri S, Yanagisawa S, Ozawa H. Regulation of osteoclast polarization. Odontology. 2007;95(1):1-9.
203. Ibrahim T, Leong I, Sanchez-Sweatman O, Khokha R, Sodek J, Tenenbaum HC, et al. Expression of bone sialoprotein and osteopontin in breast cancer bone metastases. Clinical and Experimental Metastasis. 2000;18(3):253-60.
204. Krammer A, Craig D, Thomas WE, Schulten K, Vogel V. A structural model for force regulated integrin binding to fibronectin's RGD-synergy site. Matrix Biology. 2002;21(2):139-47.
205. Yokosaki Y, Tanaka K, Higashikawa F, Yamashita K, Eboshida A. Distinct structural requirements for binding of the integrins αvβ6, αvβ3, αvβ5, α5β1 and α9β1 to osteopontin. Matrix Biology. 2005;24(6):418-27.

206. Dershaw DD, McCormick B, Cox L, Osborne M. Differentiation of benign and malignant local tumor recurrence after lumpectomy. American Journal of Roentgenology. 1990;155(1):35-8.
207. Hogge JP, Robinson RE, Magnant CM, Zuurbier RA. The mammographic spectrum of fat necrosis of the breast. Radiographics. 1995;15(6):1347-56.
208. Bussolati G, Bongiovanni M, Cassoni P, Sapino A. Assessment of necrosis and hypoxia in ductal carcinoma in situ of the breast: basis for a new classification. Virchows Archiv. 2000;437(4):360-4.
209. Haka AS, Volynskaya Z, Gardecki JA, Nazemi J, Lyons J, Hicks D, et al. In vivo Margin Assessment during Partial Mastectomy Breast Surgery Using Raman Spectroscopy [? Q1: Running head: Raman Margin Assessment at Partial Mastectomy. Short title OK? Q1]. Cancer research. 2006;66(6):3317-22.
210. Going J, ANDERSON T, CROCKER P, LEVISON D. Weddellite calcification in the breast: eighteen cases with implications for breast cancer screening. Histopathology. 1990;16(2):119-24.
211. Kollet O, Dar A, Shivtiel S, Kalinkovich A, Lapid K, Sztainberg Y, et al. Osteoclasts degrade endosteal components and promote mobilization of hematopoietic progenitor cells. Nature medicine. 2006;12(6):657-64.
212. Fleisch H. Bisphosphonates. Pharmacology and use in the treatment of tumour-induced hypercalcaemic and metastatic bone disease. Drugs. 1991;42(6):919.
213. Bundred N, Walls J, Ratcliffe WA. Parathyroid hormone-related protein, bone metastases and hypercalcaemia of malignancy. Annals of the Royal College of Surgeons of England. 1996;78(4):354.
214. Burger J, Peled A. CXCR4 antagonists: targeting the microenvironment in leukemia and other cancers. Leukemia. 2008;23(1):43-52.
215. Murphy PM. Chemokines and the molecular basis of cancer metastasis. New England Journal of Medicine. 2001;345(11):833-5.
216. Strieter RM, Belperio JA, Phillips RJ, Keane MP, editors. CXC chemokines in angiogenesis of cancer. Seminars in cancer biology; 2004: Elsevier.
217. Michaelson MD, Smith MR. Bisphosphonates for treatment and prevention of bone metastases. Journal of clinical oncology. 2005;23(32):8219-24.
218. Shane E. Evolving Data about Subtrochanteric Fractures and Bisphosphonates. New England Journal of Medicine. 2010;362(19):1825-7.
219. Green J, Czanner G, Reeves G, Watson J, Wise L, Beral V. Oral bisphosphonates and risk of cancer of oesophagus, stomach, and colorectum: case-control analysis within a UK primary care cohort. BMJ. 2010;341:c4444. Epub 2010/09/04.
220. Trimarchi H, Lombi F, Forrester M, Elizondo C, Sawinski D, Pereyra H, et al. Disodium pamidronate for treating severe hypercalcemia in a hemodialysis patient. Nature Clinical Practice Nephrology. 2006;2(8):459-63.
221. Stewart AF. Hypercalcemia associated with cancer. New England Journal of Medicine. 2005;352(4):373-9.